# NUMERICAL SIMULATION OF FLOW AND HEAT TRANSFER IN MELTING-SOLIDIFICATION PROBLEMS IN DIFFERENT CAVITIES

*Thesis submitted by*

**Debasree Ghosh**

**Doctor of Philosophy**
**(Engineering)**

**DEPARTMENT OF CHEMICAL ENGINEERING**

**FACULTY OF ENGINEERING & TECHNOLOGY**

**JADAVPUR UNIVERSITY**

**2019**

**JADAVPUR UNIVERSITY**
**KOLKATA-700032, INDIA**

**INDEX NO. 179/13/E**

1. **Title of the Thesis**:

   **Numerical Simulation of Flow and Heat Transfer in Melting-Solidification Problems in Different Cavities**

2. **Name, Designation & Institution of the Supervisor:**

   **Prof. Chandan Guha**
   Professor, Chemical Engineering Department,
   Jadavpur University, Kolkata-700032

3. **List of Publications:**

   **1. Ghosh, D.** & Guha, C., (2019). Numerical and experimental investigation of paraffin wax melting in spherical cavity. *Heat and Mass Transfer* 55:1427-1437. *DOI: 10.1007/s00231-018-2522-0.*

4. **List of Patents:** Nil

5. **List of Presentations in National / International Conferences:**

   1. **Ghosh, D**., Guha, C. & Ghose. J. Numerical simulation on heat transfer analysis in zinc solidification process using enthalpy porosity method. National Conference on Computational Modeling Of Fluid Dynamics Problems (CMFDP-2019)(NITW).
   2. **Ghosh, D.,** Guha, C. Numerical simulation of solidification process in spherical Aluminium cavity. ICEAPM2016 (BIT Mesra).

# CERTIFICATE

This is to certify that the thesis entitled "**Numerical Simulation of Flow and Heat Transfer in Melting-Solidification Problems in Different Cavities**" submitted by *Smt. Debasree Ghosh,* who got her name registered on *07.05.2013* for the award of Ph.D. (Engineering) degree of Jadavpur University is absolutely based upon her own work under the supervision of Prof. Chandan Guha and that neither her thesis nor any part of the thesis has been submitted for any degree/ diploma or any other academic award anywhere before.

(Prof. Chandan Guha)
Signature of the Supervisor
and date with Official Seal

# *About the Author*

Mrs **Debasree Ghosh** was born in Asansol, West Bengal in the year 1980. She did her secondary schooling from Sodepur Colliery High School, Asansol, West Bengal and higher secondary from Bidhan Chandra Institution for Girls', Durgapur, West Bengal. After that, she joined the B.E. program in Chemical Engineer at Regional Engineering College Durgapur. She did M.E. in the Mechanical Engineering from Birla Institute of Technology, Mesra, Ranchi, Jharkhand. After M.E., She joined at BIT, Mesra as Lecturer in 2009. She is currently employed as Assistant Professor in Department of Chemical Engineering, Birla Institute of Technology, Mesra, Ranchi.

# *Acknowledgement*

I would like to express my gratitude to my advisors, Dr Chandan Guha, Professor, Chemical Engineering Department, Jadavpur University, Kolkata for his guidance, inspiration and encouragement throughout my PhD program at Jadavpur University. I have benefitted from their profound knowledge, enormous enthusiasm, and keen insight into the field of chemical and mechanical engineering. I am also indebted to him to give me sufficient freedom to pursue my own ideas and develop myself as an independent researcher. It is my honour to have the opportunity of working under his supervision.

I am very much thankful to all the Departmental Review Committee (DRC) members of Jadavpur University for selecting me for the PhD program, providing time to review my dissertation, and for their valuable suggestions during the review.

I would like to extend my deepest thanks to BIT, Mesra administration including the Vice-Chancellor and the Registrar to allow me to pursue my PhD at Jadavpur University, Kolkata. Furthermore, I would like to thank the former Head of Department, Dr. (Mrs.) Mandira Mukherjee, for her kind permission to use departmental facilities at Chemical Engineering and Technology department, BIT, Mesra. I also want to thank all my colleagues in the Chemical Engineering Department of BIT, Mesra. I am also thankful to BIT administration for allowing me to use Computer Aided Design (CAD) lab at BIT, Mesra. I want to thank all the CAD lab officials of BIT, Mesra.

Finally, I would like to thank my family. My parents, Shri Biswanath Ghosh and Smt. Rupali Ghosh, who instilled in me the values of life and responsibility, was my inspiration throughout the PhD program. I would also like to acknowledge the help and support of my parents-in-law, Shri Nirod Kumar Ghose and Smt. Aparna Ghosh. Last but not least, I thank my husband, Joyjeet Ghose and my daughter, Spriha and son, Shrijeet; without their love, support and help, it would have become difficult for me to complete my thesis successfully.

Place: Kolkata, India

Date: **Debasree Ghosh**

*Dedicated To*

*My family*

# *Table of Contents*

# *List of Figures*

# *List of Tables*

# *List of Symbols and Nomenclature*

| Symbols and Nomenclature | Description | Unit |
|---|---|---|
| C | Mushy zone constant | |
| $C_p$ | Specific heat constant | J/kg.K |
| $C_{pl}$ | Specific heat constant of liquid PCM | J/kg.K |
| g | Gravitational acceleration | $m/s^2$ |
| $h$ | Enthalpy of fluid mixture in computational cell. | J/kg |
| L | Latent heat of solid-liquid phase change | J/kg |
| $k$ | Thermal conductivity of fluid mixture in the computational cell | W/m.K |
| $k_{PCM}$ | Thermal conductivity of PCM mixture in the computational cell | W/m.K |
| $k_{air}$ | Thermal conductivity of air mixture in the computational cell | W/m.K |
| $k_{PCM,liq}$ | Thermal conductivity of liquid phase PCM in the computational cell | W/m.K |
| $k_{PCM,solid}$ | Thermal conductivity of solid phase PCM in the computational cell | W/m.K |
| m | Mass of PCM | kg |
| mf | Meltfraction of PCM in heat exchanger | |
| N,W,E,S | Neighbouring nodes of control volume | |
| n,w,e,s | Neighbouring faces of control volume | |
| p | Pressure | $N/m^2$ |
| $S_i$ | Momentum source | |
| t | Time | Second |
| $T$ | Temperature | K |
| $T_w$ | Cavity wall temperature | K |
| $T_s$ | Solidus temperature of PCM | K |

| | | |
|---|---|---|
| $T_l$ | Liquidus temperature of PCM | K |
| $u_i$ | Velocity component in i th node | m/s |
| | | |
| α | Thermal diffusivity | $m^2/s$ |
| $\alpha_n$ | the $n^{th}$ fluid's volume fraction in the computational cell | - |
| $\alpha_{air}$ | volume fraction of air in the computational cell | - |
| β | Coefficient of volume expansion | 1/K |
| $\rho$ | Density of fluid mixture in the computational cell | $Kg/m^3$ |
| $\rho_{PCM}$ | Density of PCM in the computational cell | $Kg/m^3$ |
| $\rho_{air}$ | Density of air in the computational cell | $Kg/m^3$ |
| $\rho_{PCM,liq}$ | Density of liquid phase PCM in the computational cell | $Kg/m^3$ |
| $\rho_{PCM,solid}$ | Density of solid phase PCM in the computational cell | $Kg/m^3$ |
| $\mu$ | Viscosity of fluid mixture in the computational cell | Kg.m/s |
| $\mu_{PCM}$, $\mu_{PCM,liq}$ | Viscosity of liquid phase PCM in the computational cell | Kg.m/s |
| $\mu_{air}$ | Viscosity of air in the computational cell | Kg.m/s |
| γ | Liquid fraction of PCM | |
| $\gamma_{mix}$ | Liquid fraction of PCM and air | |

# *List of Abbreviations*

| | |
|---|---|
| 2D | Two-dimensional |
| 3D | Three-dimensional |
| CFD | Computational fluid dynamics |
| Fo | Fourier number |
| Gr | Grasshof number |
| HTF | High temperature fluid |
| htc | Heat transfer coefficient |
| LHS | Latent heat storage |
| Nu | Nusselt number |
| PCM | Phase change material |
| PRESTO | Pressure staggered option |
| Pr | Prandlt number |
| RT27 | Paraffin wax |
| RT50 | Paraffin wax |
| SHS | Sensible heat storage |
| SIMPLE | semi-implicit method for pressure-linked equation |
| St | Stefan number |
| TES | Thermal Energy Storage |
| VOF | Volume-of-fluid |

# *ABSTRACT*

The solid-liquid phase change processes are one of the important areas of energy transfer processes. These melting and solidification processes are classified as moving boundary problems. It involves changes in the thermo-physical properties of phase change material (PCM). The progress of phase change processes is very different from one another. In this thesis, the flow and heat transfer involved in melting-solidification processes are analyzed for various boundary conditions. Since the experimental study of transient solid-liquid phase processes is very difficult the numerical simulation is adopted for detailed phase change study. Commercial software Ansys-fluent is used for simulation. The phase change model used is enthalpy-porosity model. This model helps to identify the solid-liquid interface of PCM. A source term is used in the momentum balance equation to include the velocity suppression of solid phase. The numerical model is validated with the experimental result. The experimentation is done for melting of PCM (RT 27) in a spherical cavity. The image analysis tool is used to compare the experimental and numerical results. The deviation of numerical results from experimental results is within the permissible limit. The deviation is due to the difficulty involved in the identification of semi-solid and solid phase. This validated model is used for simulation of melting and solidification processes in different cavities for different boundary conditions. The simulation results include the effect of thermal diffusivity of cavity material on the melting process in spherical cavity. The different cavity materials are aluminium, copper, and glass. The thermal diffusivity of copper is highest and for glass, it is very low. It shows the shape of solid PCM is very different for glass cavity than that of aluminium and copper cavity. The melting time is lowest for highest thermal diffusivity cavity material. The effect of wall temperature of the cavity is also studied. Stefan number is defined to express the wall temperature in dimensionless form. For both spherical and rectangular shape, the melting time is inversely proportional to Stefan number. It is also found that though the size of spherical cavity is higher than the rectangular cavity for same Stefan number

melting time is not much more different. The dependency of meting time on Stefan number and area of the cavity is derived. The effect of initial shape of PCM in the rectangular cavity is studied and found that the distance between PCM and cavity wall controls the phase change process. After melting, solidification processes are simulated in spherical and rectangular cavity for different Stefan number. The solidification process is much slower than melting process the simulations are done with copper cavity to minimize the computational time. For both the shapes a detailed discussion on flow and heat transfer involved is phase change processes are discussed in the thesis. The casting or solidification of pure metal like zinc and aluminium are also simulated. Since the thermal conductivity of metals and very high and surrounding temperature is very less compared to the solidus temperature of metals the solidification process is very fast. The process is even a little fast for high thermal conductivity material aluminium. On the other hand, density of metals is not affected by the solidification process. The melting is repeated with flow boundary conditions. The charging or melting of PCM in heat exchanger for different flow rates and temperatures of high-temperature fluid (HTF) are studied to suggest an effective range of flow rate and temperature of HTF.

# CHAPTER 1
# INTRODUCTION

# CHAPTER 1
# INTRODUCTION

## 1.1 Introduction to phase change process

Phase change processes are very common in nature as well as in industries. The phase change process results in change in thermo-physical properties of phase change material (PCM). Melting of ice and freezing of water, ground freezing (the uppermost surface layer), solidification of volcanic lava and the melting processes that evolve deep under the earth surface are the natural occurring solid-liquid phase change processes(Jan Taler 2006). The freezing of foods, the thermal energy storage, casting processes are the engineering applications of phase change phenomena (Hill JM 1983; SM 1998; M. Janik 2004; Jan Taler 2006). During solidification of alloys, or energy storage using organic phase change material (PCM) does not occur at constant temperature but in a range of temperature. In such phase-change process, three different phases like, the mushy zone, solid phase and liquid phase coexist. The mushy zone consists of both the liquid and solid phases. The latent heat is released/absorbed during continuous formation of solid/liquid in the mushy zone. The latent heat transfer can be treated as considered as heat generation/absorption within the mushy zone. Phase change involves heat transfer, super-cooling, transfer of latent heat and changes in thermo-physical properties. The molecules vibrate around the fixed equilibrium positions in the solid phase, while in a liquid the molecules may skip from the equilibrium position. This vibration energy is called heat or thermal energy and the measure of which is temperature. The molecules of liquid phase contain more thermal energy than solid phase and other properties remain approximately constant. Therefore, before melting, a solid must attain a certain level of energy to overcome the intermolecular forces between molecules that form the solids structure and this energy is known as latent heat (Vasilios Alexiades 1993). The phase change is very irregular in nature. The small change in thermal boundary condition makes significant change in solid shape after solidification. Due to the complex nature of phase change process, the shape of PCMs are very irregular

in intermediate steps of melting and solidification. The irregularities are shown in Fig 1.1. It is observed that, the shape of unmelt structure are very irregular in nature. The liquid phase formed are not similar around each side of the solid phase.

**Fig 1.1: Unconstrained phase change processes**

It is difficult to predict the nature of melting and solidification stochastically or experimentally. A numerical simulation is a tool which helps to predict the shape of PCM in an intermediate step. It also helps to calculate the processing time and the melt fraction at any time in the control volume.

## 1.2 Industrial application of phase change process

### 1.2.1 Phase change in metal casting process

The phase change process plays a crucial role in metal processing also. The heat transfer or cooling rate decides the grain structure and hence the properties of the product. For example, vacuum continuous casting (VCC) is used for manufacturing of copper rod (D.C. Tsai 2012). The use of Copper is very common used in electrical

wiring. The desired electrical and thermal properties, excellent formability, and anticorrosive nature make it suitable for electrical application. Advancements in technology demands for thinner and smaller electronic devices which are more delicate wiring systems. Solidification phenomenon in VCC is very significant. The formation of the bulk microstructure depends on solidification rate, which determines the chemical and mechanical properties. The casting speed is one such casting parameter, which subsequently controls the thermal energy gradient and growth rate of the solid structure. Therefore, for controlled growth of solid microstructure during solidification and for improvement of the specified properties casting speed and casting or solidification period should be manipulated. Twin-roll strip casting processes are widely used by steel makers all over the world. This casting process is significant for low energy consumption which improves the process efficiency and enhances mechanical properties of the product. In this casting process, solidification must be completed when the liquid touches the kissing point (minimum clearance point) between the rolls. If the solidification occurs before kissing point results in distortion of the solid when operating with fixed openings, and visco-plastic strains arise in the casting strip. The lower range of solidification completion temperature or solidus temperature is set above the kissing point. The interior of the strip must be solidified totally as it meets the rolls, not below the kissing point. The large un-solidified region at the middle may result in breaking of casting strip. Therefore, temperature plays an important for controlling the quality of strip (Yu-Chuan Mia 2006). The continuous casting of steel is performed in water-cooled mould. The layer of solidified steel of desired thickness and strength are attained from the mould. The selection of mould is very important to avoid absconding and flow out of molten steel (M. Janik 2004). The Ferro-static pressure results in breakout of mould. The mould acts as a support for the newly solidified steel. If billet parting the mould is too weak, the Ferro-static forces beat the material strength and cause the flow out of liquid steel. Therefore, successful production of final product needs proper control on casting speed, cooling rate, and poured temperature of liquid metal. The control of mentioned parameters requires a critical understanding of melting and solidification processes.

### 1.2.2 Phase change in food industries

The food industry is another area where phase change is seen frequently. Chocolate industry is one of them. The sensitive properties of this complex food product are controlled mainly by the crystal structure and the polymorphism of cocoa butter. The different polymorph structure of cocoa butter makes the manufacturing of chocolate complex (Wille 1966; Ollivon 2004). The simulation of phase change process considers the change in structure of PCMs and helps to predict the intermediate conditions of PCM.

### 1.2.3 Phase change in energy storage equipment

The non-stop rise in the level of greenhouse gas discharges and the climb in fuel prices are the key driving forces for use of various sources of renewable energy (Atul Sharma 2009). The experts of this area are concentrating in search of novel renewable energy sources. The development of energy storage devices is very important along with developing novel sources of energy. The energy should be stored in a form which is easily recoverable. Therefore, the design of such energy storage is a challenging job for the engineers. Energy storage helps to reduce the discrepancy in chain of supply and demand and improves the efficiency and dependability on energy storing systems. Many energy sources are intermittent in nature where energy storage plays vital roles in storing available energy and refining its application. The energy storage time can vary from few hours to few months as per the availability and requirement of energy. Solar energy is available only during the day, and hence, the thermal energy collected during sunshine hours and stored using efficient thermal energy storage for later use during the night. Similarly, the waste heat availability and consumption periods are different in heat recovery systems which requires some thermal energy storage. In extremely cold and hot climate countries the electrical energy demand varies significantly throughout the day. The major part of the energy variation is due to air conditioning and domestic space heating. The energy requirement is generally low after midnight until early morning which is called off-peak period. Power stations are designed so that it can fulfil the energy requirement during peak load as well as in the off-peak period. A very efficient power distribution grid would be required for such situations.

Thermal energy storage is a probable solution for management of power generation by shifting some of the peak load to the off-peak load period. Hence, the fruitful application of load shifting and storage of solar energy demands an effective method of energy storage (Mohammed M. Farid 2004). Energy can be stored in different ways as shown in Fig 1.2.

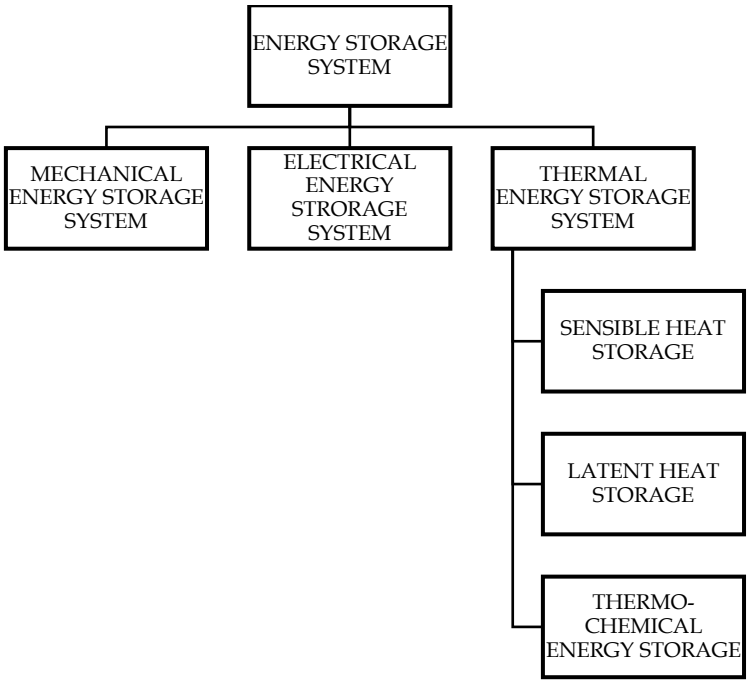


**Fig 1.2: Classification of energy storage system**

**Mechanical energy storage system**

The compressed air energy storage (CAES) and flywheels, pumped hydropower storage (PHPS) or gravitational storage of energy, is the example of mechanical energy storage systems. Energy storage is required when reasonable off-peak power is existing, especially, at sleeping or non-working hours. The energy stored is supplied during inadequate power supply from the base-load plant.

**Electrical storage system**

The energy can be stored in batteries. In a battery, charging is done by connecting it to a source of direct electric current and the stored as chemical energy. The chemical energy stored is converted into electrical energy at the time of discharge. These batteries are used in off-peak power periods, for load leveling, and storing the electrical energy generated by photovoltaic plants or wind turbine. The most common batteries used for storage are lead acid and Ni–Cd.

**Thermal energy storage (TES) system**

Thermal energy can be stored as sensible heat, latent heat and thermo-chemical or combination of these. These energies stored are nothing but change in internal energy of a material as per first law of thermodynamics. Fig 1.3 shows the change in energy level in melting process. Initially with an increase in temperature the energy is stored as sensible heat in the material. After reaching the melting point temperature the energy stored is increased sharply. This energy is stored as latent heat and the temperature is constant during the process. The completion of melting once again sensible heat transfer occurs in the liquid phase.

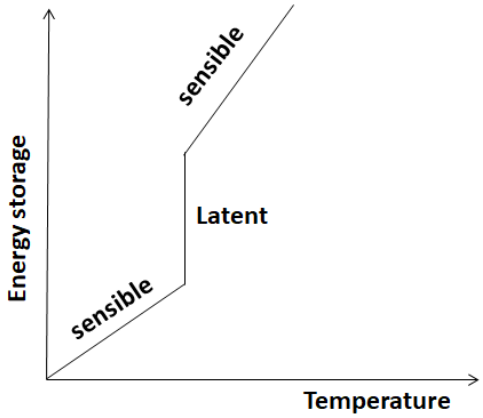


**Fig 1.3: Change in energy level during pure substance melting**

***Sensible heat storage system***

The thermal energy stored by increasing the temperature of storage medium is called sensible heat storage (SHS). The energy stored in such process is proportional to the specific heat and change in temperature of the storage system. The sensible heat method is very common for thermal energy storage. In solar heating systems, liquid-based systems use water for sensible heat storage, while a rock bed is used for air-based systems. The design of sensible heat storage units is explained in textbooks (Duffie JA 1980; Garg HP 1985). Refractory bricks used as energy storage heaters in the application of load equalization is called a night storage heater (SM 1998). The night storage heaters are storing heat at night and supplying stored heat for the space heating at day time from the stored heat during the night. These units are very heavy and huge in size.

*Latent heat storage system*

A huge amount of energy is transferred as latent heat during phase change from gas to liquid or liquid to solid and vice versa. The Latent heat storage (LHS) is constructed on this concept of large heat absorption or release by PCM. The PCM is having energy storage density with a smaller temperature swing compared to sensible heat storage. However, practically the phase change materials have several limitations like low-density change, low thermal conductivity, and lack of stability of properties under prolonged cycling of phase change. Sometimes phase segregation and sub-cooling of the PCMs affects the stability of the PCM used in thermal energy storage unit.

*Thermo-chemical energy storage system*

The energy absorbed and released in a completely reversible chemical reaction is stored as thermo-chemical energy. The energy evolved or released due to breaking and reforming molecular bonds during the reversible chemical reaction. In such condition, the amount of heat stored is function of the mass of phase change material used for energy storage, the heat of reaction, and the degree of conversion.

## 1.3 Types of PCMs and their properties used for energy latent heat storage

The phase change materials (PCM) are organic and inorganic. Inorganic PCMs have higher latent heat values, higher thermal conductivity, inflammable and more economical compared to organic PCMs and are inexpensive and readily available. On the other hand; inorganic PCMs are unstable; improper re-solidification; undergoes decomposition which affects their phase change proper (Karthikeyan S. 2006). To overcome the shortcoming of inorganic materials, organic materials are considered under the study of phase change materials. Organic PCMs are non-corrosive and chemically more stable than inorganic PCMs. The high latent heat per unit weight is also very high for organic PCMs over inorganic PCMs. they are recyclable, they melt consistently, and subcooling is not required for initiation of crystallization (SOCACIU 2012).

**Table: 1.1 List of some commercially used PCM and their properties (E. Assis 2007; A. A. Rabinataj Darzi 2015; Majid Gorzin 2018)**

| PCM Name | Type of Product | Solid-liquid phase change temperature [°C] | latent heat of fusion [kJ/kg] |
|---|---|---|---|
| RT26 | Paraffin | 24-26 | 232 |
| RT27 | Paraffin | 28-30 | 179 |
| RT50 | Paraffin | 45-50 | 168 |
| PEG10000 | Polyethylene glycol | 69.7 | 191 |
| Capric acid | Fatty acid | 32 | 152 |
| $CaCl_2.6H_2O$ | Salt Hydrate | 29 | 190 |
| $Ba(OH)_2.8$ $H_2O$ | Salt Hydrate | 48 | 266 |

The desirable properties of PCM should be:

- Thermodynamic properties:
    - High value of latent heat with respect to the volume of the storage unit;
    - High change in internal energy near the phase change temperature;
    - High latent heat of fusion per unit mass is desirable in order to store more energy in less amount of PCMs;
    - The phase change temperature should be fixed in the desired operating temperature range and known;
    - Consistent melting temperature to avoid segregation;
    - Volume expansion coefficient should be low during phase change;
    - High-density PCMs are required to keep the cavity volume minimum;
    - The charging and discharging of the energy storage depends on higher thermal conductivity of PCMs.
- Kinetic properties:
    - No sub-cooling during the freezing process;
    - Sufficient crystallization rates.
- Chemical properties

- Chemically stable without chemical decomposition and life of energy storage system is assured;
- Less corrosiveness to construction material;
- Chemically stable for long time;
- Non-explosive in nature;
- Inflammable.

- Physical properties:
  - Changes in density during the phase change is low to protect the storage tank;
  - The compact size of storage units;
  - Low vapour pressure;
  - Favourable phase equilibrium.
- Economic properties:
  - Should be available easily;
  - Cost is low to make the system economical.

## 1.4 Motivation for the research work

The application of phase change processes needs the information of different parameter like temperature, heat flux, change in volume, location of moving boundary, time required for completion of processes etc. Experimental measurement of all those parameters is very difficult. The simulation of phase change can predict melt fraction, temperature with using any measuring device. This saves the cost involved for installation of the experimental setup. In case of energy storage process, the total charging and discharging time can be calculated practically but, actual initiation of phase change cannot be measured experimentally. During different casting processes cooling rate plays an important role to yield a perfect product. Generally scanning electron microscopy (SEM) or optical microscopy images of final product obtained from casting processes is required to investigate the quality of the product. It is very difficult to measure the actual time required for complete solidification for different cooling rate. Computation fluid dynamics (CFD) is a very useful tool to overcome the above-mentioned shortcomings of experimental process.

Such shortcomings are complicated and expensive instrumentation system. The process can run safely with prior simulated knowledge of the process.

Aim of numerical studies is to gain an understanding of the process without actual experimentation. Numerical studies make the process cost-effective and safe. Computation fluid dynamics (CFD) can be treated as a useful technique for the simulation process. Simulation is very much important for moving boundary problem. In the phase change process, the solid-liquid interface changes its position with time which is known as a moving boundary. During the process of phase change, no parameter is measurable for intermediate step within the control volume. Complex sensors can be used to measure the process parameters real time during the process, however, installation of such sensors in the control volume affects the thermal process and hence the measured results. In the $19^{th}$ century, J. Stefan formulated the problem to calculate the temperature distribution and freezing front during solidification of water in a rectangular cavity. Such problem named after him, the Stefan problem, is one which takes the researchers slightly into the world of non-linearity. To the computational scientist, modelling of phase change processes leads beyond intuition and needs advanced graphics and computing tools. In the same vein, the engineers also deal with even more complex processes arising from dynamically growing technological challenges(Vasilios Alexiades 1993).

CFD is a tool to solve the continuity, momentum and energy equations associated with a process having given boundary conditions. Therefore, the understanding of the problem is very important to achieve the correct result of the problem. CFD involves three major steps – preprocessing, solver and post-processing. Preprocessing requires the generation of the control volume, the solver needs the boundary conditions to solve the governing equations and post-processing helps to represent the results of given problem. Preprocessing step needs proper attention in grid generation and the reason is convergence of numerical method applied in solver step is dependent on it. The solid-liquid or liquid-vapour moving interface between phases has been investigated in the literature with interface-tracking and interface-capturing methods (Giuseppe Labonia 1998). The interface-capturing methods can determine the details of the structure of the interface. The modelled interface extends

the actual physical discontinuity to someplace near the middle of the temperature gradient. Very finer meshing is required to locate the interface accurately. The enthalpy method considers both phases together in the solution of governing equation, and the properties of phase change material are either changed discretely at the interface or continuously over a range near the interface. It is a one-domain method. In this method, interface is not tracked explicitly. Methods of interface tracking are different from interface-capturing and classified into front-tracking and volume-tracking approaches. In front tracking the interface is recognized by an ordered set of indicator points located on the interface or moving boundary, and is represented by the distance between the points and some reference surface. The front is represented by a line connecting the indicator points, usually a piecewise polynomial. An unstructured grid is used in the interface.

The irregular shape, complex instrumentation arrangement, safety demand numerical simulation of phase change processes prior to experimentation and practical application of phase change process. Visualization or graphics is the important feature of CFD tool which explains process very efficiently.

**References**

A. A. Rabinataj Darzi, H. H. A., M. Khaki, M. Abbasi (2015). "Unconstrained melting and solidification inside rectangular enclosure." Journal of Fundamental and Applied Sciences **7**(3): 436-451.

Atul Sharma, V. V. T., C.R. Chen, D. Buddhi (2009). "Review on thermal energy storage with phase change materials and applications." Renewable and Sustainable Energy Reviews **13**: 318-3345.

D.C. Tsai, W. S. H. (2012). "Numerical simulation of the solidification processes of copper during vacuum continuous casting." Journal of Crystal Growth(343): 45-54.

Duffie JA, B. W., Ed. (1980). Solar energy thermal processes. New York, USA, John Wiley.

E. Assis, L. K., G.Ziskind, R.Letan (2007). "Numerical and Experimental Study of Melting in a Spherical Shell." International Journal of Heat and Mass Transfer **50**: 1790–1804.

Garg HP, M. S., Bhargava AK. , Ed. (1985). Solar thermal energy storage. Holland, Reidel Publishing Company.

Giuseppe Labonia, V. T., James E. Simpson, Suresh V. Garimella, Eddie Leonardi & Graham de Vahl Davis (1998). "Reconstruction and advection of a moving interface in three dimensions on afixed grid." Numerical Heat Transfer,Part D **34**: 121-138.

Hill JM, K. A. (1983). "Freezing a saturated liquid inside a sphere." International Journal of Heat and Mass Transfer **26**(11): 1631-1638.

Jan Taler, P. D. (2006). Melting and Solidification (Freezing). In: Solving Direct and Inverse Heat Conduction Problems. Springer, Berlin, Heidelberg 799-829.

Karthikeyan S., M. S. S., Prashanth R. (2006). "Energy conservation through phase change material based thermal energy storage system-a project report."

M. Janik, H. D. (2004). "Modelling of three-dimensional temperature field inside the mould during continuous casting of steel." Journal of Materials Processing Technology **157-158**: 177-182.

Majid Gorzin, M. J. H., Ali A. Ranjbara, Rasool Bahrampoury (2018). "Investigation of PCM charging for the energy saving of domestic hot water system." Applied Thermal Engineering **137**: 659-668.

Mohammed M. Farid, A. M. K., Siddique Ali K. Razack, Said Al-Hallaj (2004). "A review on phase change energy storage: materials and applications." Energy Conversion and Management **45**: 1597-1615.

Ollivon, M. (2004). "Chocolate,a mysteriously appealing food." European Journal of Lipid Science and Technology **106**: 205-206.

SM, H. (1998). "Review on sustainable thermal energy storage technologies, Part 11: Heat storage materials and techniques." Energy Convers Mgmt. **39**: 1127-1138.

SOCACIU, L. G. (2012). "Thermal Energy Storage with Phase Change Material." Leonardo Electronic Journal of Practices and Technologies(20): 75-98.

Vasilios Alexiades, A. D. S., Ed. (1993). Mathematical Modeling and Freezing Processes, Hemisphere Publishing Corporation.

Wille, R. L., Lutton,E.S. (1966). "Polymorph of mofcocoa butter." Journal of the American Oil Chemists' Society **43**: 491–496.

Yu-Chuan Mia, X.-M. Z., Hong-Shuang Di, Guo-Dong Wang (2006). "Numerical simulation of the fluid flow, heat transfer, and solidification of twin-roll strip casting." Journal of Materials Processing Technology **174**: 7-13.

# CHAPTER 2
# LITERATURE SURVEY AND SCOPE OF WORK

# CHAPTER 2

# LITERATURE SURVEY AND SCOPE OF WORK

## 2.1 Introduction

The liquid-solid phase change phenomena are important in many areas of science and engineering, particularly in the metal and food processing industries. For pure materials, phase change occurs at a fixed temperature resulting in an interface which separates distinct solid and liquid phases, e.g. freezing of water or rapid solidification of metals. In contrast, for multi-component substances, phase change occurs over a temperature range and the solid and liquid phases are separated by a 'mushy' region which is characterized by solids suspended in a liquid region, e.g. solidification of wax or polymers, thawing of foods, metal processing, casting etc. Various numerical methods have been developed to solve phase change problems for pure as well as multi-component substances. Initially, studies based on finite element formulations were carried out using the temperature method (B. Rubinsky 1981; J. Yoo 1983). In the temperature method, strictly applicable for pure substances, the energy balance equation is solved separately for both solid and liquid phases and the moving phase change front is tracked with the appropriate interface conditions. Solutions based on the temperature method, which involve remeshing of the computational domain, become cumbersome for multidimensional problems or in situations where multiple fronts appear e.g. phase change under the influence of microwaves.

Accurate simulation of moving boundary flows is a difficult and demanding task, because computing a succession of transient states may require reconstruction of the mesh several times as the flow domain changes in shape and size. The coupling between the instantaneous location of the interface and the field variables introduces additional non-linearity through the boundary conditions imposed there. This may be the reason that the full dynamics of the processes have not been examined thoroughly. The available numerical approaches can be classified as Lagrangian, Eulerian, and mixed Lagrangian-Eulerian based on the method generating the computational grid. Only Eulerian techniques provide easy handling of large

interfacial distortions because the grid points remain stationary or move in a predetermined manner, whereas the fluid moves in and out the computational cells. This is achieved at the expense of an interface that is not ''sharply'' defined and, consequently, the boundary conditions on it are not as accurately approximated as the rest of the field equations. Instead, the interface is calculated based on the values of the ''colour function'' by interpolating between cells, which requires very fine meshes to achieve certain accuracy and makes the computations very expensive, especially when the density ratio between the two fluids is different from unity. The surface tracking method is a significant improvement for Eulerian methods because it determines the interface explicitly using a separate unstructured grid (S.O. Unverdi 1992).

In the Lagrangian approach, the grid and the interface move with the local fluid velocity, this requires frequent remeshing, but provides a sharp definition of the interface even at large deformations and irrespective of the fluid properties. Finally, arbitrary Lagrange–Euler methods, kinematic descriptions combine the two previous approaches, but still, need a detailed technique for the mesh movement. The Lagrangian aspect of the method involves interpolation of the solution from the old to the new mesh, which is a nontrivial and diffusive operation. This difficulty is alleviated by employing a curvilinear coordinate system that conforms to the moving boundary. The evolving physical domain is mapped onto a simple and time-independent computational one in which the moving boundary coincides with one of the coordinate surfaces and in which it is trivial to generate the mesh. It is fairly easy to perform this boundary conforming mapping using simple algebraic relations (A.J. Poslinski 1991; A.J. Poslinski 1991). However, this technique is restricted to relatively simple initial shapes and small deformations and requires that the mapping function is single-valued. In this thesis, the following literature surveys to select the numerical model for the study of phase change process.

### 2.1.1 Melting phase change process in different geometry

Many studies of phase change processes in spherical cavity have been reported in the literature (T.S. Saitoh 1996; T.S. Saitoh 1997; K.A.R. Ismail 2000; E. Assis 2007; Tan 2008; E. Assis 2009; F.L. Tan 2009; M.Z.M. Rizan 2012; S.F. Hosseinizadeh 2012;

W. Zhao 2013; P. Chandrasekaran 2014). The phase change process depends on the mechanism of heat transfer. For conduction dominated gravity assisted melting process, the solid phase will not move and in the case of natural convection, the solid phase will sink at the bottom of the cavity.

A detailed study on the works carried out on solid-liquid phase change processes is presented in Table 2.1. It is evident from Table 2.1 that the numerical simulations of phase change processes are performed using finite volume method. Volume of fluid (VOF) method is applied to locate the solid-liquid interface in the cavity and enthalpy-porosity is applied to define the effect of phase change in momentum balance equation. The phase change processes in spherical cavity for paraffin wax with different boundary conditions show that the location of solid-liquid interface is different and also time required for complete phase change are different. In case of spherical cavity, no significant change in shape of solid fraction is observed if the wall boundary condition is uniform through the process (E. Assis 2007; E. Assis 2009; F.L. Tan 2009; M.Z.M. Rizan 2012). The case is different in rectangular cavity. The melting rate and the energy stored in heating, from vertical side, are much higher than that of heating from below or horizontal wall heating, due to enhanced natural convection effect (A.V. Arasu 2012). The rate of phase change in rectangular cavity also depends on the orientation of cavity. Babak and Hamid simulated the melting process of Lauric acid in horizontal rectangular cavity where the heating was supplied from bottom wall and all other walls were insulated and in case of vertical rectangular cavity the heating was supplied from right wall and all other walls were insulated (Babak Kamkaria 2017). It has been observed that phase change of lauric acid shows melting time is minimum for a horizontal rectangular cavity than vertical rectangular cavity. The effect of thermo-physical properties of PCM also plays an important role during phase change process. The thermo-physical properties of paraffin wax and n octadecane are almost similar, so the phase change process is same for those materials. On the other hand, the phase change of paraffin wax and n octadecane are very much different from that of water. The reason is due to melting the volume of water decreases and the solid phase of water floats on the liquid phase (T.S. Saitoh 1996; T.S. Saitoh 1997; E. Assis 2007; E. Assis 2009; M.Z.M. Rizan 2012).

The thermo-physical properties of liquid metals are very different from water and other organic PCM like paraffin wax and n octadecane. The thermal conductivity of metal is very high, and thermal expansion coefficient is very low which results in a decrease in natural convection effect. The thermal conductivity is thus important property for rapid completion of melting process (N. K. Kund 2010; A.V. Arasu 2012).

The literature has reported the work carried out with different PCMs, with different boundary conditions, various shape of cavity and for different orientation of cavity. However, the thermo-physical properties of cavity material are also an important parameter which needs to be studied numerically in order to understand the phase change process properly. This study tries to investigate the effect of thermo-physical properties of cavity material on phase change process. In order to investigate the same, the melting process of paraffin wax is simulated in a spherical cavity for various cavity materials having different thermal properties and for different thermal boundary conditions. The experimental investigation included visualization of shape of solid fraction which is used to validate the numerical approach of this computational study.

Ibáñez M et al. studied the phase change of sodium acetate trihydrate in aluminium bottles using TRANSYS model (Ibáñez M 2006). The phase change of Lauric acid and Liquid aluminium alloy (A356) in inclined rectangular cavity were analyzed experimentally and numerically (N. K. Kund 2010; Babak Kamkaria 2017). Many phase change analysis are also available for paraffin wax in a rectangular cavity with different boundary conditions (Piia Lamberg 2004; V. Dubovsky 2008; S. Lorente 2014). The potential of ice, gallium and paraffin wax as energy storage PCM has been studied by Annabelle et al. (Annabelle Joulin 2009). The study reveals that paraffin wax is most frequently used as PCM for thermal energy storage. During phase change of paraffin wax, the density of PCM changes which results in conduction-convection heat transfer process. The thermal conductivity of paraffin wax is very low which decreases the energy storage capacity of PCM. To improve the thermal energy storage capacity of paraffin wax, alumina with paraffin wax and paraffin wax

in aluminium foam are used as a thermal energy storing element (A.V. Arasu 2012; Xin Hua 2014). The phase change of a silicon rod was studied using floating zone method (Tanahashi 2005). In this simulation radiation heat transfer was considered as controlling heat transfer process between the surface of the rod and surroundings. In case of metal or metal alloys, the higher phase change temperature causes the radiation heat transfer. Therefore, it is observed that phase change processes are studied for different PCM with different boundary condition and orientation. The phase change processes in spherical cavity are also studied with different PCMs and for different boundary conditions. The empirical equations are developed to relate melt fraction with dimensionless numbers like Grashof number, Fourier number, Stefan number (E. Assis 2007; E. Assis 2009; S.F. Hosseinizadeh 2013). Empirical correlations are very important when a process is controlled by several factors. These correlations are used to estimate the process output in terms of dimensionless numbers. In Fundamental studies of convection heat transfer, heat exchanger a number of empirical relations were developed depending on the velocity of fluid flow, boundary conditions, the orientation of cavity etc. such correlations are like Sieder-Tate equation, Ditus-Bolter equation (J.P. Holman 2008). Various relations are also developed by Mc. Admas et al., Zuber, Sun and Lienhard for calculating the heat flux for boiling state (J.P. Holman 2008). In the case of solid-liquid phase change, the process is influenced by conduction, convection, thermal expansion coefficient, and change in thermo-physical properties of PCM.

The review of phase change processes shows that the development of empirical correlations for phase change processes in rectangular cavity is not studied as much as phase change processes in spherical condition. In this study, the melting phase change of paraffin wax in the rectangular cavity is studied for different wall temperature of the cavity. A detailed heat transfer analysis study is presented to propose an empirical relation. The variations of heat flux with time are estimated to analyze the mechanism and heat transfer during phase change process. The presence of air during phase change process is also considered in development of empirical relation which is not considered so far.

**Table 2.1: Literature survey on phase change processes**

| PCM | Shape of cavity | Boundary condition | Cavity material | Model used in simulation | Reference |
|---|---|---|---|---|---|
| Paraffin wax | Spherical | Constant temperature at cavity wall | glass | Enthalpy porosity model for free surface | (E. Assis 2007) |
| Paraffin wax | Spherical | Constant temperature at cavity wall and constrained melting | glass | Enthalpy porosity model for free surface | (F.L. Tan 2009) |
| Water | Spherical | Constant cavity wall temperature | | Boundary Fixing Method | (T.S. Saitoh 1996; T.S. Saitoh 1997) |
| Paraffin wax | Spherical | Constant temperature at cavity wall and unconstrained solidification | glass | Enthalpy porosity model for free surface | (E. Assis 2009) |
| n octadecane | Spherical | Uniform heat flux at outer shell | Pyrex | Boundary Fixing Method | (M.Z.M. Rizan 2012) |
| Paraffin wax + alumina | Square cavity | 1.Heated from bottom side and<br>2. vertical side | Not mentioned | Enthalpy porosity model | (A.V. Arasu 2012) |
| Lauric acid | Inclined rectangular enclosure | Constrained melting with the right wall of the cavity is set at a constant temperature and the other walls are adiabatic. | Not mentioned | Enthalpy porosity model | (Babak Kamkaria 2017) |
| Liquid aluminium alloy A356 | Pipe with slope | Cooling slope and no-slip boundary condition | Not mentioned | VOF and continuum surface force (CSF) model | (N. K. Kund 2010) |

| PCM | Shape of cavity | Boundary condition | Cavity material | Model used in simulation | Reference |
|---|---|---|---|---|---|
| Paraffin wax | Cylinder | Constant temperature at cavity wall and unconstrained solidification | Not mentioned | Enthalpy porosity model for free surface | (V. Dubovsky 2008) |
| sodium acetate trihydrate. | cylinder | Cooling and reheating | | TRANSYS | (Ibáñez M 2006) |
| Liquid aluminium alloy A356 | Pipe with slope | Cooling slope and no-slip boundary condition | | VOF and continuum surface force (CSF) model | (N. K. Kund 2010) |
| Paraffin wax | Rectangular cavity | Heating or cooling from side walls | | Enthalpy model and effective enthalpy method | (Piia Lamberg 2004) |
| Paraffin wax | Cylindrical enclosure | Vertical heated pipe on its axis | | Effective heat capacity method | (S. Lorente 2014) |
| Ice, gallium and Paraffin wax | Rectangular enclosure | Heated from a vertical wall | | Enthalpy porosity model | (Annabelle Joulin 2009) |
| Paraffin wax + alumina | Square cavity | 1.Heated from bottom side and<br>2. vertical side | | Enthalpy porosity model | (A.V. Arasu 2012) |
| Paraffin wax in aluminium foam structure | Cubic | Heated from top surface and other faces are insulated | | Direct numerical simulation method | (Xin Hua 2014) |
| Silicon | 2D Rod | Radiation heat transfer | | Floating zone method | (Tanahashi 2005) |

### 2.1.2 Solidification phase change process in different geometry

The determination of solidification characteristics of metals and alloys are very important and thermal analysis is a widely used method for it. Computer-aided

cooling curve analysis is such a low-cost technique. D. Emadi et al. descried the computer-aided cooling curve analysis method to determine the quality of cast iron, copper and aluminium alloys (D. Emadi 2005).

Solidification is the other side of melting process. Many researchers worked with solidification of different PCMs with different boundary conditions. K.A.R. Ismail and J.R. Henriquez numerically studied solidification in spherical cavity. The numerical model considered only conduction heat transfer for constant cavity wall temperature (K.A.R. Ismail 2000). In another study by K.A.R. Ismail et al. a curved surface is taken for solidification of phase change. In this geometry also the natural convection is neglected and constant wall temperature is assumed as boundary condition. K.A.R. Ismail et al. repeated the solidification of PCM: water in long horizontal with same assumption and i.e. Pure conduction no natural convection (K.A.R. Ismail 2014). M. Taghiloua and F. Talati solved the solidification process in rectangular cavity with time-dependent boundary condition (M.Taghiloua 2018). The results of the simulation are in good agreement with Lattice Boltzmaan Model (LBM) results and in both the models only conduction is the limitation. I. Jmal and M. Baccar considered natural convection in numerical model for studying solidification of finned PCM-air heat exchanger (I. Jmal 2015). Y. Hong et al. studied the effect of inverted cavity during the solidification in rectangular cavity. The paraffin wax (RT 47) is used for numerical simulation of mentioned solidification. The thermal behaviour is improved for inverting the cavity (Yuxiang Hong 2018). Sharma et al. compared the solidification time pure copper and copper-water nano-fluid under controlled temperature and concentration. The effect of wall inclination is also shown in the research article. They also considered the upper and lower walls of the cavity are insulated. S. Chakraborty et al. Simulated the solidification of binary alloy which solidified or cooled from the top and side wall rectangular cavity is insulated (S. Chakraborty 2003). They used turbulence k-€ model for this study which is used for other metal alloys (W. Shyy 1992). M.A. Ezan, M. Kalf used Consistent-Update-Technique algorithm for two-dimensional simulation of solidification of water in rectangular cavity. During freezing of water, cooling is provided only in one side at time (M. A. Ezan 2016). M.T. Stickland et al.

experimentally studied the solidification of water in a differentially heated cavity. This study is very important to validate numerical models. These observations are also limited to upper and lower insulated wall (M.T. Stickland 2007).

The solidification phase change studied so far has some limitations. In case of spherical cavity, the solidification study mostly limited to conduction model and for rectangular cavity, the opposite walls are adiabatic or insulated. In practical situations like casting or discharging of PCM or freezing in refrigerator the cooling is from the total outer surface. Therefore, the numerical simulation with uniform boundary condition from outer surface is required for analysis of actual transport process. The natural convection is also considered in mechanism of solidification process. The solidification results of spherical and rectangular cavity are compared to discuss the shape effect. The comparison of solidification in two different shape cavity is the another novality of the thesis.

### 2.1.3 Phase-change process in PCM heat exchanger

PCMs can be used for recovery of waste heat. This type of latent storage units is of different types like direct and indirect type shell and tube heat exchanger, plate and packed heat exchanger. Shell and tube heat exchanger is most common type PCM heat exchanger because of simple shape. Considerable research is done on performance study of the PCM heat exchanger. These studies include theoretical, numerical and experimental investigation of phase change process. F. Rosler and D. Bruggemann performed the analysis of PCM heat exchanger numerically and experimentally(Fabian Rosler 2011). Y. Pahamliet al. studied the performance PCM melting double pipe heat exchanger(Y. Pahamli 2018). They have shown that the time of melting of PCM is affected by the position of the inner pipe. The downward movement of inner pipe enhances the rate of heat transfer and minimizes the time of melting. The study also revealed that the charging or melting can be decreased by increasing the inlet temperature and mass flow rate of the high-temperature fluid.S. Riahi et al. investigated the solidification and melting processes in PCM shell and tube heat (Soheila Riahi 2017). They have shown the effect of a different configuration of the heat exchanger (HE): the parallel flow vertical HE, the parallel

flow horizontal HE, the counter flow vertical HE, the counter flow horizontal HE with top and bottom inlet. The melting time is maximum for counterflow vertical heat exchanger with natural convection and minimum for parallel flow horizontal heat exchanger. The study has also shown that solidification time is approximately same for different configurations of the heat exchanger. W. Youssef et al. presented a similar study for spiral-wired tubes PCM heat exchanger (W. Youssef 2018). M. Gorzin et al. simulated the phase change of PCM in heat exchanger (Majid Gorzin 2018). They proposed a system in which the surface area of PCM and HTF is increased to reduce the energy loss. The result shows the time of melting is minimum for 60:40 ratios (weight) of PCM in outer and inner tube respectively. Li et al. optimized the time of charging by varying the eccentricity and diameter of inner tube(Saiwei Li 2017). Hamid AitAdine and Hamid El Qarnia designed a composite PCM heat exchanger having maximum thermal storage efficiency (Hamid Ait Adine 2009). Wang et al. studied the performance of vertical shell and tube heat exchanger using erythritol as PCM (Yifei Wang 2016). The analysis focuses on effect of temperature, pressure and flow rate of high-temperature fluid (HTF) during charging and discharging cycle. The overall heat transfer coefficient is considered as a function of time, though the actually it is the function of both time and position. Y. Wang et al. investigated experimentally the phase change in a flat heat pipe. They also derived a correlation for volume of melt fraction from the measured temperature distribution (Y. Wang 1999).

### 2.1.4 Solidification of Pure Metals

A detailed literature review on solid-liquid phase change with different PCMs and different boundary conditions are presented. The phase change temperature of metals is very and referred to as high-temperature PCM. The castings of such metals are very important to get appropriate strength and crystalline structure of product. Bermudez and Otero compared the solidification of aluminium slab using direct chill casting and electromagnetic casting. The two-phase Stefan problem is considered for numerical simulation the solidification processes. The limitation of the proposed numerical model is fixed grid method (A. Bermudez 2006). Chakraborty studied the solidification of pure substance water using enthalpy

porosity model (Chakraborty 2017). The study considered the variation in specific heat in both the phase and showed a good agreement with the prediction made by Kowalewski and Rebow (Rebow 1999). Bot and Arquis simulated the one dimensional model of deposition and solidification of successive metal layers on a cold surface (Cedric Le Bot 2009). The model used for simulation not considered the convective phenomena because of negligible flow time. Tian et. al studied the effect of cooling rate in polymorph selection during solidification of zinc (Ze-an TIAN 2015). The study showed the effect of polymorph selection is different at different stage of cooling. Wenyi Hu optimized the casting of AZ31 magnesium slab using direct chill method with different cooling speed (Wenyi Hu 2013). Solidification studies are presented for different metals and alloys like Nickel (B.T. Bassler 2003), tin (Hwang 1997). The solidification of materials like Zirconia materials (Hz) used in refractory materials are also important (Cedric Patapy 2013). Tomasz and Ewa simulated the solidification of Copper using finite element method. They used front tracking method to locate the solid-liquid interface (Tomasz Skrzypczak 2012). Similar numerical studies are also presented by several authors with different boundary conditions (Zabaras N 1989; Zabaras N 1990; Zabaras N 1995; Slota 2011). Lewis and Ravindran simulated filling and solidification of molten aluminium in spiral and spillage wheel type cavity (R. W. Lewis 2000). They used finite element method with fixed grid for the solidification study. Fixed grid method is advantageous over moving grid. Fixed grid considers the total materials as a single phase and for moving grid the control volume is treated as two phase. In case of alloys more number of materials is present and using moving grid the calculation is complicated. In such situation the fixed grid method is more effective. During casting of metals the impurities are always present in optimum amount and fixed grid method is appropriate in such cases.

In this study, the authors focused on the fixed grid method for simulation of solidification of pure zinc under different thermal boundary conditions. Volume of fluid (VOF) method is used to describe the interface of air and zinc and enthalpy porosity model is adopted to locate the solid-liquid interface of phase changing material. The proposed model is widely applicable for different thermal boundary

conditions as well as different inorganic/organic PCMs, high/low phase change temperature materials.

**Table 2.2: Literature survey on phase change processes in PCM heat exchanger**

| Process | PCM | Model | Process characteristics | Reference |
|---|---|---|---|---|
| Energy storage using two PCMs in shell & tube heat exchanger | P116 and n-octadecane | Enthalpy method | Different flow rates and temperature of HTF | (Hamid Ait Adine 2009) |
| Melting of PCM in double pipe heat exchanger | RT50 | Enthalpy porosity model | 1.Different flow rates and temperature of HTF 2. Different position of inner pipe | (Y. Pahamli 2018) |
| PCM heat exchanger for Domestic water heat system | RT50 | Enthalpy porosity model | Different PCM mass distribution | (Majid Gorzin 2018) |
| Melting of PCM inside horizontal annulus | RT 27 | Enthalpy porosity model and volume of fluid (VOF) model | Different eccentricity and diameter of inner tube | (Saiwei Li 2017) |
| Energy storage using spiral-wired tubes PCM heat exchanger | A16 | Enthalpy porosity model | Charging and discharging at different flow rate and inlet temperature of HTF. | (W. Youssef 2018) |

## 2.2 Scope of work

In literature survey, it is found that a large number of works are done on solid-liquid phase change. The studies are on both experimental and simulation process. Phase change in spherical cavity is very common for studying melting and solidification. The different thermal boundary conditions and PCM materials are taken for phase change. In this study the cavity material is varied or effect of thermal properties of cavity materials on phase change is studied. No researchers are so far considering the effect of thermal properties of cavity material. Rectangular cavity is also very common for studying phase change. In this thesis, phase change is not only studied

for different thermal boundary conditions but also studied for initial shape of solid phase in cavity. The study of phase with different initial shape is another novelty of this work. For application studies, the performance PCM heat exchanger during charging process and casting of metals are considered. The empirical correlations are also proposed based on the effect of HTF temperature and flow rate. The simulation helps to analyze the process parameter at each and every step of time and position.

The fixed grid enthalpy-porosity model is chosen for the study of phase change processes. The details of simulated work are presented in Fig 2.1. The simulated model is experimentally validated for melting of paraffin wax (RT27) in 80 mm.

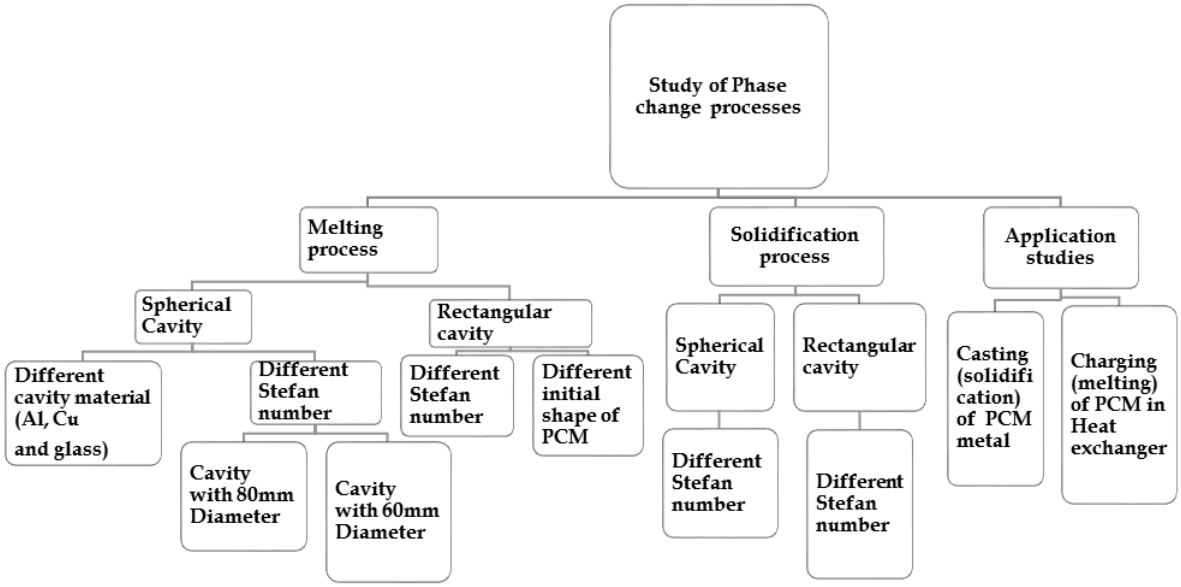


**Fig 2.1 Details of research layout**

## 2.3 Objective of the study

1. **To study the heat and flow analysis for melting process of paraffin wax in spherical and rectangular cavity**
2. **To study the heat and flow analysis for solidification process of paraffin in spherical and rectangular cavity**
3. **To study the charging of process of PCM in double pipe heat exchanger for different flow rate and temperature of high-temperature fluid (HTF) at inlet.**
4. **To study the heat and flow analysis for solidification process of high-temperature pure metals in rectangular cavity.**

**Reference**

A. Bermudez, M. V. O. (2006). "An existence result for a two-phase Stefan problem arising in metal casting in metal casting." Mathematical methods in applied sciences 29: 325-350.

A.J. Poslinski, D. O., J.A. Tsamopoulos (1991). "Inflation dynamics of fluid annular menisci inside a mold cavity-II. Deformation driven by large gas pressure." Chemical Engineering Science 46(2): 597-608.

A.J. Poslinski, J. A. T. (1991). "Inflation dynamics of fluid annular menisci inside a mold cavity-I. Deformation driven by small gas pressure." Chemical Engineering Science 46(1): 215-232.

A.V. Arasu, A. S. M. (2012). "Numerical study on melting of paraffin wax with Al2O3 in a square enclosure." International Communications in Heat and Mass Transfer 39: 8–16.

Annabelle Joulin , Z. Y., Laurent Zalewski , Daniel R. Rousse & Stéphane Lassue (2009). "A numerical study of the melting of phase change material heated from a vertical wall of a rectangular enclosure." International Journal of Computational Fluid Dynamics 23: 553–566.

B. Rubinsky, E. G. C. (1981). "A finite element method for the solution of one-dimensional phase change problems." International journal of Heat Mass Transfer 24: 1987-1989.

B.T. Bassler, W. H. H., R.J. Bayuzick (2003). "The solidification velocity of pure Nickel." Material Science & Engineering A 342: 80-92.

Babak Kamkaria, H. J. A. (2017). "Numerical simulation and experimental verification of constrained melting of phase change material in inclined rectangular enclosures." International Communications in Heat and Mass Transfer 88: 211-219.

Cedric Le Bot, E. A. (2009). "Numerical study of the solidification of successive thick metal layers." International Journal of Thermal Sciences 48: 412-420.

Cedric Patapy, M. H., René Guinebretière, Nathalie Gey, Michel Humbert, Alain Hazotte, Thierry Chotard (2013). "Solidification structure in pure zirconia liquid molten phase." Journal of the European Ceramic Society 33: 259-268.

Chakraborty, P. R. (2017). "Enthalpy porosity model for melting and solidification of pure-substance with large difference in phase specific heats." International Communication in Heat and Mass Transfer 81: 183-189.

D. Emadi, L. V. W., S. Nafisi, R. Ghomashchi (2005). "Applications of thermal analysis in quality control of solidification processes." Journal of Thermal Analysis and Calorimetry 81: 235-242.

E. Assis, G. Z., R. Letan (2009). "Numerical and experimental study of solidification in a spherical shell." Journal of heat transfer 131: 1-5.

E. Assis, L. K., G.Ziskind, R.Letan (2007). "Numerical and Experimental Study of Melting in a Spherical Shell." International Journal of Heat and Mass Transfer 50: 1790–1804.

F.L. Tan, S. F. H., J.M. Khodadadi, L. Fan (2009). "Experimental and computational study of constrained melting of phase change materials (PCM) inside a spherical capsule." International Journal of Heat and Mass Transfer 52: 3464–3472.

Fabian Rosler, D. B. (2011). "Shell-and-tube type heat thermal energy storage: numerical analysis and comparison with experiments." Heat Mass Transfer 47: 1027-1033.

Hamid Ait Adine, H. E. Q. (2009). "Numerical analysis of the thermal behaviour of a shell-and-tube heat storage unit using phase change materials." Applied Mathematical Modelling 33: 2132-2144.

Hwang, K.-Y. (1997). "Effects of density change and natural convection on the solidification process of a pure metal." Journal of Materials Processing Technology 71: 466-476.

I. Jmal, M. B. (2015). "Numerical study of PCM solidification in a finned tube thermal storage including natural convection." Applied Thermal Engineering 84(320-330).

Ibáñez M, C. L., Solé C, Roca J, Nogués M (2006). "Modelization of a water tank including a PCM module." Applied Thermal Engineering 26: 1328–33.

J. Yoo, B. R. (1983). "Numerical computation using finite elements for the moving interface in heat transfer problems with phase transformation." Numerical Heat Transfer 6: 209-222.

J.P. Holman, S. B., Ed. (2008). Heat Transfer, Tata MaGraw-Hill Publishing Company Limited.

K.A.R. Ismail, F. A. M. L., R.C.R. Silva, A. B. Jesus, L.C. Paixão (2014). "Experimentally validated two dimensional numerical model for the solidification of PCM along a horizontal long tube." International Journal of Thermal Sciences 75: 184-193.

K.A.R. Ismail, J. R. H. (2000). "Solidification of pcm inside a spherical capsule." Energy Conversion & Management 41: 173-187.

K.A.R. Ismail, J. R. H. q. (2000). "Solidification of pcm inside a spherical capsule." Energy Conversion Management 41: 173–187.

M. A. Ezan, M. K. (2016). "Numerical investigation of transient natural convection heat transfer of freezing water in a square cavity." International Journal of Heat and Fluid Flow 61: 438-448.

M.T. Stickland, T. J. S., J. MacKenzie (2007). "An experimental investigation of natural convection with solidification in a differentially heated cavity." International Journal of Heat and Mass Transfer 50: 36-44.

M.Taghiloua, F. T. (2018). "Analytical and numerical analysis of PCM solidification inside a rectangular finned container with time-dependent boundary condition." International Journal of Thermal Sciences 133: 69-81.

M.Z.M. Rizan, F. L. T., C.P. Tso (2012). "An experimental study of n-octadecane melting inside a sphere subjected to constant heat rate at surface." International Communications in Heat and Mass Transfer 39: 1624-1630.

Majid Gorzin, M. J. H., Ali A. Ranjbara, Rasool Bahrampoury (2018). "Investigation of PCM charging for the energy saving of domestic hot water system." Applied Thermal Engineering 137: 659-668.

N. K. Kund, P. D. (2010). "Numerical simulation of solidification of liquid aluminum alloy flowing on cooling slope." Trans. Nonferrous Met. Soc. China 20: 898-905.

P. Chandrasekaran, M. C., V. Kumaresan, R. Velraj (2014). "Enhanced heat transfer characteristics of water based copper oxide nanofluid PCM in a spherical capsule during solidification for energy efficient cool thermal storage system." Energy 72: 636–642.

Piia Lamberg, R. L., Anna-Maria Henell (2004). "Numerical and experimental investigation of melting and freezing processes in phase change material storage." International Journal of Thermal Sciences 43: 277-287.

R. W. Lewis, K. R. (2000). "Finite element of metal casting." International Journal for Numerical Methods in Engineering 47: 29-59.

Rebow, T. A. K. M. (1999). "Freezing of water in a differentially heated cubic cavity." International journal of computational fluid dynamics 11: 193-210.

S. Chakraborty, N. C., P. Kumar, P. Dutta (2003). "Studies on turbulent momentum, heat and species transport during binary alloy solidification in a top-cooled rectangular cavity." International Journal of Heat and Mass Transfer 46: 1115-1137.

S. Lorente, A. B., J.L. Niu c (2014). "Phase change heat storage in an enclosure with vertical pipe in the center." International Journal of Heat and Mass Transfer 72(329-335).

S.F. Hosseinizadeh, A. A. R. D., F.L. Tan (2012). "Numerical investigations of unconstrained melting of nano-enhanced phase change material (NEPCM) inside a spherical container." International Journal of Thermal Sciences 51: 77–83.

S.F. Hosseinizadeh, A. A. R. D., F.L. Tan, J.M. Khodadadi (2013). "Unconstrained melting inside a sphere." International Journal of Thermal Sciences 63: 55-64.

S.O. Unverdi, G. T. (1992). "A front-tracking method for viscous, incompressible, multi-fluid flows." Journal of Computational Physics 100.

Saiwei Li, Y. C. a. Z. S. (2017). "Numerical simulation and optimization of the melting process of phase change material inside horizontal annulus." Energies 10(1249).

Slota, D. (2011). "Restoring boundary conditions in the solidification of pure metals." Computers and Structures 89: 48-54.

Soheila Riahi, W. Y. S., Frank Bruno, Martin Belusko, N.H.S. Tay (2017). "Comparative study of melting and solidification processes in different configurations of shell and tube at high temperature latent heat storage." Solar Energy 150: 363-374.

T.S. Saitoh, H. H., K. Yamada (1997). "Theoretical analysis and experiment on combined close-contact and natural convection melting in thermal energy storage spherical capsule." Proc. Energy Conversion Engineering Conference 3 IEEE: 1656-1661.

T.S. Saitoh, H. K., H. Hoshina (1996). "Theoretical analysis for combined closecontact and natural convection melting in ice storage spherical capsule." Proc. Energy Conversion Engineering Conference 3IEEE: 2104-2108.

Tan, F. L. (2008). "Constrained and unconstrained melting inside a sphere." International Communications in Heat and Mass Transfer 35: 466–475.

Tanahashi, H. K. T. (2005). "Numerical analysis of thermal melt flow and melt/ solid interface shapes in the floating zone method." International Journal of Computational Fluid Dynamics 19: 243-251.

Tomasz Skrzypczak, E. W. g.-S. (2012). "Mathematical and numerical model of solidification of pure metals." International Journal of Heat and Mass Transfer 55: 4276-4284.

V. Dubovsky, E. A., E. Kochavi, G. Ziskind, R. Letan (2008). "study of solidification in vertical cylindrical shells." European Thermal-Sciences Conference 5.

W. Shyy, Y. P., G.B. Hunter, D.Y. Wei, M.H. Chen (1992). "Modeling of turbulent transport and solidification during continuous ingot casting." International Journal of Heat and Mass Transfer 35: 229-1245.

W. Youssef, Y. T. G., S.A. Tassou (2018). "CFD modelling development and experimental validation of a phase change material (PCM) heat exchanger with spiral-wired tubes." Energy Conversion and Management 157: 498-510.

W. Zhao, A. F. E., A. Oztekin, S. Neti (2013). "Heat transfer analysis of encapsulated phase change material for thermal energy storage." International Journal of Heat and Mass Transfer 63: 323–335.

Wenyi Hu, Q. L., Zhiqiang Zhang, Lei Bao, Jianzhong Cui (2013). "Numerical simulation of DC casting of AZ31 magnesium slab at different casting speeds." Journal of magnesium and Alloys 1: 88-93.

Xin Hua, S. S. P. (2014). "Modeling phase change material in micro-foam under constant temperature condition." International Journal of Heat and Mass Transfer 68: 677-682.

Y. Pahamli, M. J. H., A .A. Ranjbar, R. Bahrampoury (2018). "Inner pipe downward movement effect on melting of PCM in a double pipe heat exchanger." Applied Mathematics and Computation 316: 30-42.

Y. Wang, A. A., K. Vafai (1999). "An experimental investigation of the melting process in a rectangular enclosure." International Journal of Heat and Mass Transfer 42: 3659-3672.

Yifei Wang, L. W., Ningning Xie, Xipeng Lin, Haisheng Chen (2016). "Experimental study on the melting and solidification behavior of erythritol in a vertical shell-and-tube latent heat thermal storage unit." International Journal of Heat and Mass Transfer 99: 770-781.

Yuxiang Hong , W.-B. Y., Si-Min Huang, Juan Dua (2018). "Can the melting behaviors of solid-liquid phase change be improved by inverting the partially thermal-active rectangular cavity?" International Journal of Heat and Mass Transfer 126: 571-578.

Zabaras N (1990). "Inverse finite element techniques for the analysis of solidification processes." International Journal for Numerical Methods in Engineering 29: 1569-1587.

Zabaras N, N. T. (1995). "Control of the freezing interface morphology in solidification processes in the presence of natural convection." International Journal for Numerical Methods in Engineering 38: 1555-1578.

Zabaras N, R. Y. (1989). "A deforming finite element method analysis of inverse Stefan problem." International Journal for Numerical Methods in Engineering 28: 295-313.

Ze-an TIAN, L.-l. Z., Yun-fei MO, Yong-chao LIANG, Rang-su LIU (2015). "Cooling rate dependence of polymorph selection during rapid solidification of liquid metal zinc." Transactions of Nonferrous Metals Society of China 25: 4072-4079.

# CHAPTER 3

# MATHEMATICAL MODELLING AND EXPERIMENTAL VALIDATION

# CHAPTER 3

# MATHEMATICAL MODELLING AND EXPERIMENTAL VALIDATION

## 3.1 Introduction

The mathematical models help to explain a process. To overcome the limitations of the experimental process the mathematical model is needed. The application of mathematical models for numerical simulation minimises the cost of experimentation. On the other hand, the mathematical models are proposed on the basis of assumptions therefore, the validation of model through experimental results is the need for the research process. Experimental results ensure the authenticity of model assumptions. The knowledge of transport processes is used to develop or select the model for a specific process. The heat and flow processes in PCM control the progress of the solid-liquid phase change process. The theory of phase change indicates the temperature during phase change is constant for pure materials. A mathematical model is needed which can enable to explain the transition of solid and liquid phases. This model will be helpful to correlate the process parameters with time. The mathematical model is important to study the effect of the process of controlling parameters. In case of melting and solidification process, the mathematical model evaluates the effect of change of temperature, cavity material, size, and shape. The effect of flow of PCM materials also helps to control the phase change process.

In this chapter, the detail of the mathematical model is discussed and the results obtained from simulation are validated with lab experimental results. The gridindependency tests are also shown for different cavity shape.

### 3.1.1 Mathematical modelling

Melting and solidification processes need special attention during the simulation. This is because the physical properties change significantly. Viscosity is one such property. This viscosity term distinguishes the solid and fluid phases. In solid phase,

the heat transfer occurs by conduction only. The mechanism of conduction says that in this mode of heat transfer molecules vibrate only with respect to the equilibrium position, no permanent displacement of molecules observed. On the other hand in convection driven heat transfer process in fluid phase the molecules of fluid start moving after overcoming the intermolecular force of attraction. These characteristics need some source term in basic conservation equations. This source term differentiates solid and liquid phase. The model used in the thesis for simulation of melting and solidification process is called enthalpy porosity model. The overview of the model is discussed below:

1. The model is used for laminar, incompressible fluid or PCM.
2. The model is applicable to the melting and solidification of pure metal or binary alloys.
3. The phase change should occur at a constant temperature or over a range of temperatures.
4. The solid-liquid interface is not tracked explicitly. In this model solid-liquid interface treated as a porous mushy zone where the porosity of pure liquid phase is one and that of solid phase is zero.
5. A suitable source term is introduced to the momentum equation to calculate the effect of pressure drop due to the presence of solid material.
6. In this thesis, the multiphase volume-of-fluid (VOF) model is used locate the non-penetrating PCM and air phase.

The governing equations are explained below:

Continuity equation:

$$\frac{\partial \alpha_n}{\partial t} + u_i \frac{\partial \alpha_n}{\partial x_i} = 0 \qquad (3.1)$$

Where n is secondary material PCM

$\alpha_n$ denotes the $n^{th}$ fluid's volume fraction in the computational cell. If $\alpha_n$=0 the cell does not contain the $n^{th}$ fluid and $\alpha_n$ =1 implies the cell contains only the $n^{th}$ fluid. The cell contains mixture of $n^{th}$ fluid and other fluids if $\alpha_n$ value is in between zero and one. More specifically, the value of $\alpha_n$ is one at solid-liquid PCM interface (n is the PCM) and at PCM-air interface, the value of $\alpha_n$ lies between zero and one. The

volume fraction in Eqn. 3.1 will not be solved for the primary phase (air); the primary-phase volume fraction will be computed based on the following constraint

$$\alpha_{air} = 1 - \alpha_n \tag{3.2}$$

Here VOF model is chosen to locate PCM-air interface. Shrinkage in volume is observed in solidification process and the empty space in cavity is filled by air. This air and PCM are not penetrating each other and location of PCM-air interface is simulated by VOF model.

Momentum equation:

$$\frac{\partial}{\partial t}(\rho u_i) + \frac{\partial}{\partial x_i}(\rho u_j u_i) = \mu \frac{\partial^2 u_i}{\partial x_j \partial x_j} - \frac{\partial p}{\partial x_j} + (\rho - \rho_{ref})g + S_i \tag{3.3}$$

$\rho_{ref}$ is the density of cell at reference temperature $T_{ref}$.

Energy balance equation:

$$\frac{\partial}{\partial t}(\rho h) + \frac{\partial}{\partial x_i}(\rho u_i h) = \frac{\partial}{\partial x_i}\left(k \frac{\partial T}{\partial x_i}\right) \tag{3.4}$$

Where ρ is the density, k is the thermal conductivity, μ is the dynamic viscosity, $S_i$ is the momentum source term, $u_i$ is the velocity component, $x_i$ is a cartesian coordinate, and h is the specific enthalpy of both the air and PCM respectively in specified region. The Eqn. 3.3 and Eqn. 3.4 are applicable for air, PCM and their interface. The thermo physical properties like density, thermal conductivity and viscosity are calculated as follows:

$$\left.\begin{aligned} \rho &= \alpha_n \rho_{PCM} + (1 - \alpha_n)\rho_{air} \\ k &= \alpha_n k_{PCM} + (1 - \alpha_n) k_{air} \\ \mu &= \alpha_n \mu_{PCM} + (1 - \alpha_n)\mu_{air} \end{aligned}\right] \tag{3.5}$$

Where,

$$\left.\begin{aligned} \rho_{PCM} &= \gamma \rho_{PCM,liq} + (1 - \gamma)\rho_{PCM,solid} \\ k_{PCM} &= \gamma k_{PCM,liq} + (1 - \gamma) k_{PCM,solid} \\ \mu_{PCM} &= \mu_{PCM,liq} \end{aligned}\right] \tag{3.6}$$

Also, expression for change in enthalpy is defined as: $h = h_{ref} + \int_{T_{ref}}^{T} C_p dT + \gamma L$ . $h_{ref}$ is enthalpy at reference temperature $T_{ref}$. L is the specific enthalpy of melting (latent-heat of the material), and γ is the liquid fraction during the phase-change which occurs over a range of temperatures and defined by the following relations:

$$\left.\begin{array}{c} \gamma = 0\ at, T < T_s \\ \gamma = \frac{T-T_s}{T_l-T_s}, at T_s < T < T_l \\ and\ \gamma = 1\ at T > T_l \end{array}\right] \quad (3.7)$$

In enthalpy-porosity model, an additional momentum source term is added to define the velocity of solid and liquid phase of PCM. The velocity suppression of solid phase during the phase change process helps to identify the solid and liquid phase. This enthalpy-porosity method for fixed-grid meshing successfully modelled the velocity suppression because the solid phase is static. The two-phase domain is assumed as porous medium to define the source term in momentum equation. The momentum source term for flow through porous media is described with the help of the Kozeny-Carman equation and the source is defined as (Assis 2007):

$$S_i = -C\frac{(1-\gamma)^2}{\gamma^3+\varepsilon}u_i \quad (3.8)$$

Epsilon is a small non zero term, its value is 0.001. To keep the source term defined at complete solid phase (γ=0) epsilon has assigned this value. At complete liquid phase, γ=0 and source term will vanish and Eqn. 3.3 is normal fluid flow equation. In presence of solid phase, the mixture of solid-liquid phase acts as porous media and movement of solid in liquid follows Kozeny-Carman equation, which is defined by the source term given in Eqn 3.8. C in Eqn, 3.8 is called mushy zone constant. This mushy zone constant measures the damping nature of the phase change process. The mushy zone constant is taken as $10^5$ from the previous study for the PCM paraffin wax (RT27). The literature survey shows the mushy zone constant is varied from $10^3$ to $10^8$ for different melting and solidification studies (A.R. Archibold 2014; J.Vogel JF 2016; Y. Pahamli 2016; H. Niyas 2017; Y. Kozak 2017; Z.N. Meng 2017). The semi-solid region exists at the interface of solid and liquid phase is known as mushy region. The heat transfer is conduction dominated in solid phase and convection dominated in liquid. Therefore, heat transfer in semi-solid or mushy region is influenced by both conduction and convection. The high value of mushy zone constant indicates a lower convection effect hence the process is slower (Mathura Kumar 2017; Simone Arena 2017; Mohamed Fadl 2019).

Therefore, the enthalpy of control volume is calculated using energy balance equation given in Eqn. 3.4 and melt fraction or liquid fraction is calculated using

Eqn. 3.7. The calculated liquid fraction is updated in momentum Eqn. 3.3 or more specifically the liquid fraction value is update in source term defined in Eqn. 3.8. The negative sign refers that it is a sink term. As already mentioned the solid phase is static and it need velocity suppression in solid phase and this sink term is satisfying that criteria.

### 3.1.2 Numerical scheme

The enthalpy porosity model described above is solved in Ansys-fluent commercial software. The commercial software package has three main parts: pre-processor, solver and post-processing. In pre-processor, the geometry or computation domain is defined. The appropriate grid generation is done to obtain accurate results from the simulation. The fluid properties and boundary conditions are defined. Therefore, in the pre-processor step, all the inputs are fed. The next step is solver. In solver, the governing differential equations are discretised to convert to algebraic equations and solved by iterative methods. Finite element, finite difference, spectral method and finite volume are methods used for discretization. In this study, the finite volume method is applied for discretization. The control volume is considered as a staggered grid is to store the variable. The scalar properties are stored at ordinary node and velocities are stored at face centred node. The discretization of the governing equations can be illustrated most easily by considering the unsteady conservation equation for transport of a scalar quantity ϕ. This is demonstrated by the following equation written in integral form for an arbitrary control volume $V$ as follows:

$$\int \frac{\partial \rho \phi}{\partial t} dV + \oint \rho \phi \vec{v} \,.\, d\vec{A} = \oint \Gamma_{\phi} \nabla \phi . d\vec{A} + \int S_{\phi} dV \tag{3.9}$$

$$\text{or } \frac{\partial \rho \phi}{\partial t} V + \sum_{f}^{N_{faces}} \rho_f \phi_f \vec{v}_f \,.\, \overrightarrow{A_f} = \sum_{f}^{N_{faces}} \Gamma_{\phi} \nabla \phi_f \,.\, \overrightarrow{A_f} + S_{\phi} V \tag{3.10}$$

Where,

$N_{faces}$= number of faces enclosing cell

$\phi_f$= value of ϕ convected through face f

$\Gamma_{\phi} \nabla_{\phi,f} . \overrightarrow{A_f}$ = mass flux through the face

$\overrightarrow{A_f}$= area of the face

$\nabla\phi_f$= gradient of $\phi$ at face f

V = cell volume

The details of numerical scheme used for discretization are given in Table 3.1.

**Table 3.1: Discretization scheme**

| Equations | Discretization scheme |
|---|---|
| Pressure-velocity coupling equations | SIMPLE |
| Pressure equations | PRESTO |
| Momentum equations | First order Upwind |
| Volume fraction equations | Geo-construct |
| Energy equations | First order Upwind |

### 3.1.2.1 Pressure staggered option (PRESTO)

The finite volume method required special attention for storing the scalar and vector properties along with discretization. If the velocity and pressure are stored at same node at highly non-uniform pressure field starts acting as uniform pressure field in discretized momentum equation. The mentioned problem is explained with help of checker-board. The staggered grid can give the solution of it. In staggered grid as shown in Fig 3.1, the pressure, temperature and other scalar are stored at ordinary nodal points (marked by •) and velocity components are stored at staggered grids centred on cell faces (marked by → for u velocities and ↑ for v velocities). Scalar nodes are defined by capital letters (P, N, W, E and S) and node numbers by (I, J). Similarly cell nodes at face of control volume are defined by small letters (n, w, e, s) and node numbers (i, j). The scalar properties at point P is calculated from the known scalar properties of previous time step at neighbouring points N, S, W and E. The vectors or velocity components are calculated at face centre points (n, s, w, e) of P centred control volume. Discretization of momentum equation for velocity is:

$$a_P u = \sum_{nb} a_{nb} u_{nb} + \sum p_f A.\hat{\imath} + S \qquad (3.11)$$

Where, $a_P$ is the coefficient of velocity at point P and $a_{nb}$ is that at its neibouring points. $p_f$ is the corrected pressure field and S is the source term.

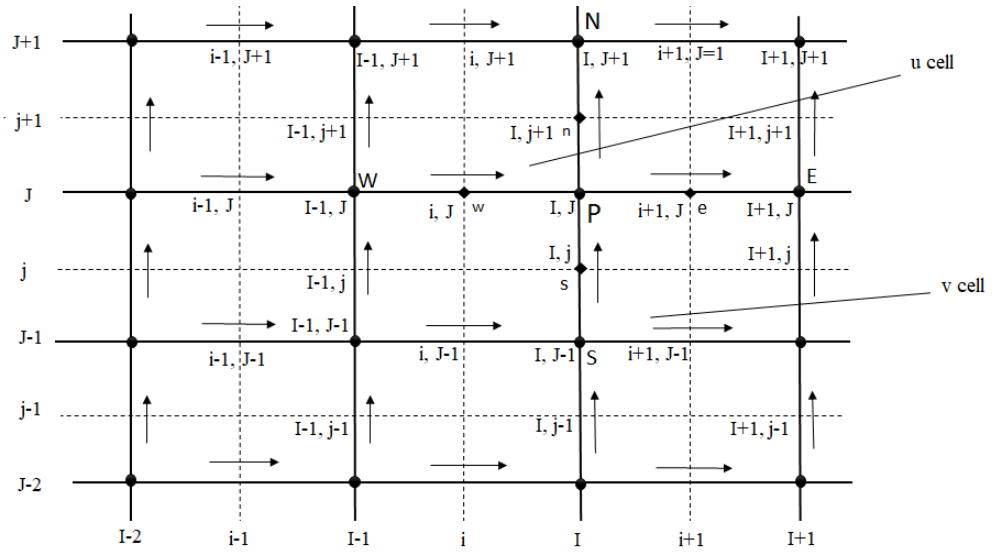


**Fig 3.1: Staggered grid**

### 3.1.2.2 Geometric reconstruction scheme (Geo reconstruct)

The geo reconstruct scheme is used to discretize the continuity equation for VOF model. A piecewise linear relation is assumed between two phases (air and PCM). This linear relation is used for calculation of the advection of fluid through the cell faces. The geo reconstruct scheme is used for calculating the volume fraction time-dependent solution and steps are as follows:

- The position of the linear interface relative to the centre of each partially-filled cell is calculated from the volume fraction and its derivatives in the cell.
- The advected amount of fluid through face are calculated from the above mentioned linear relation and normal and tangential velocity on the face.
- Calculation of the volume fraction in each cell using the balance of fluxes calculated during the previous step.
- The Standard finite difference interpolation schemes to the volume fraction

$$\frac{\alpha_n^{t+\Delta t}\rho_n^{t+\Delta t}-\alpha_n^t\rho_n^t}{\Delta t}V+\sum_{face}\rho_n U_{face}^t\alpha_{n,face}^t=\left[\sum_{n=1}^{N}(\dot{m}_{pn}-\dot{m}_{np})+S_{\alpha_n}\right]V \qquad (3.12)$$

$t+\Delta t$ = current time step

$t$ = previous time step

$\alpha_{n,face}$ = face value of the n$^{th}$ volume fraction

V =volume of cell

$U_{face}$ = volume flux through the face, based on normal velocity

N = total number of phases

$S_{\alpha_n}$= source term for n$^{th}$ volume fraction

$\dot{m}_{pn}, \dot{m}_{np}$= mass fraction from phase p to phase n and mass fraction from phase n to phase p

$$\sum_{n=1}^{N} \alpha_n = 1 \qquad (3.13)$$

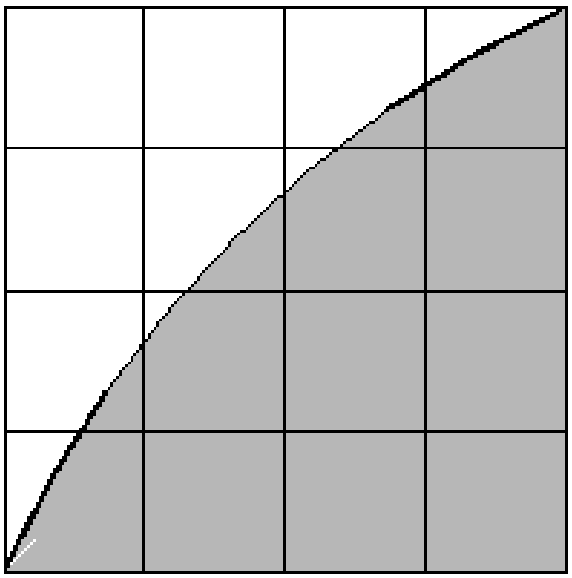

(a)

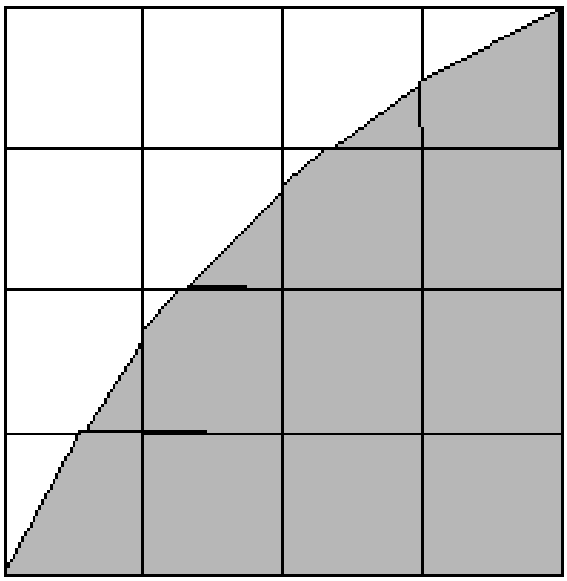

(b)

**Fig 3.2: (a) Actual interface shape, (b) Interface by using Geo reconstruct scheme**

### 3.1.2.3 First order upwind scheme

The first order upwind discretization is applied to energy and momentum equation. Different discretization scheme can be used for different terms like unwind scheme is suitable for advection terms and central differencing scheme is best for diffusion terms. In this section, the first ordered upwind differencing scheme is used. First order unwind scheme considers the direction of flow. For example, a convective flow from west to east (shown if Fig 3.3) is considered. This differencing scheme say that $u_w$ is more affected by properties at W than P. Similarly for negative flow direction east to west $u_e$ is more influenced by properties at E than P. Numerical study shows that the refined grids give more accurate results than courser grid. It important to mention in this differencing scheme flow should align with the grid line for successful implementation.

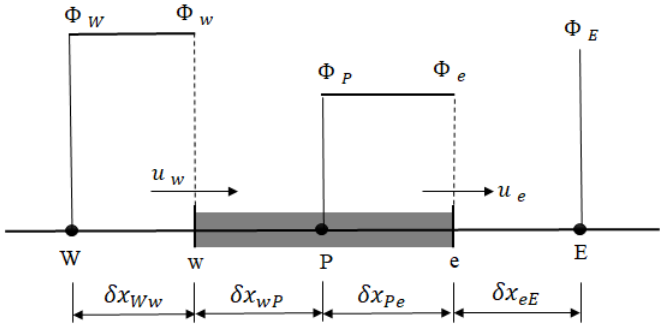


**Fig 3.3: Nodes for upwind scheme**

### 3.1.2.4 Pressure-velocity coupling

The solutions of momentum equation for incompressible fluid need special attention. For incompressible fluids density not changes with change in pressure therefore, the solution of different velocity components, pressure and other scale properties cannot be solved simultaneously. Different models are proposed for fluids like for steady state problems artificial compressibility factor method, stream-vorticity method for 2D irrational and pressure correction method for staggered grid. In this study the proposed model is solved using semi-implicit method for pressure-linked equation (SIMPLE) which is pressure correction method. The under-

relaxation factors are for pressure 0.3, for density, energy and body force 1, for momentum 0.7 and for liquid fraction update 0.95. The flow sheet for semi-implicit method for pressure-linked equation (SIMPLE) is given Fig 3.4.

**Flow sheet for transient SIMPLE algorithm**

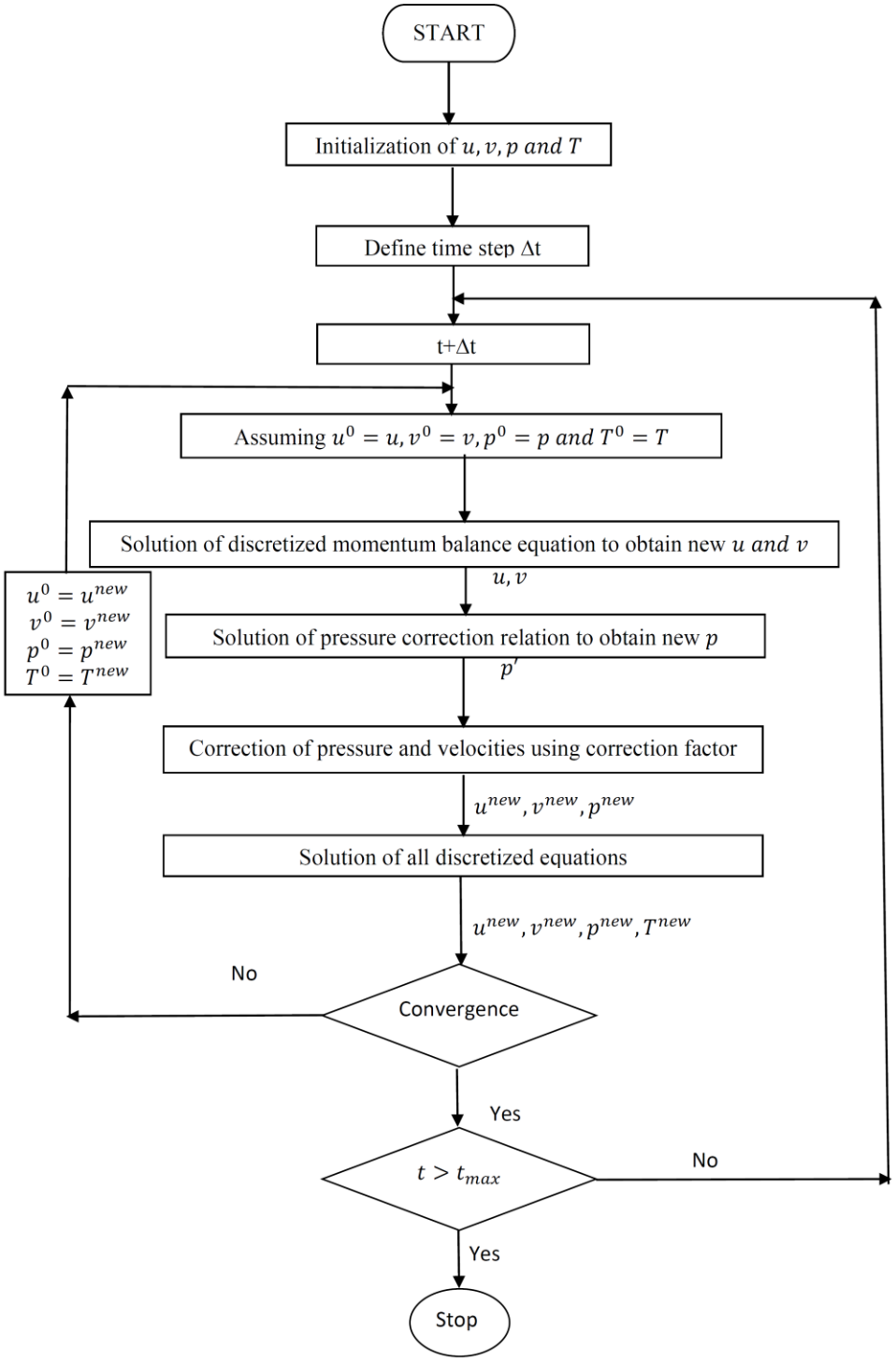


**Fig 3.4: Flow sheet for transient SIMPLE algorithm**

The post-processing helps to store and analyses the plots or results stored. The graphics is the most important feature of this computational fluid dynamics (CFD) package. In this thesis the volume average properties are calculated. The simulation steps in Ansys-Fluent process are given in Fig 3.5.

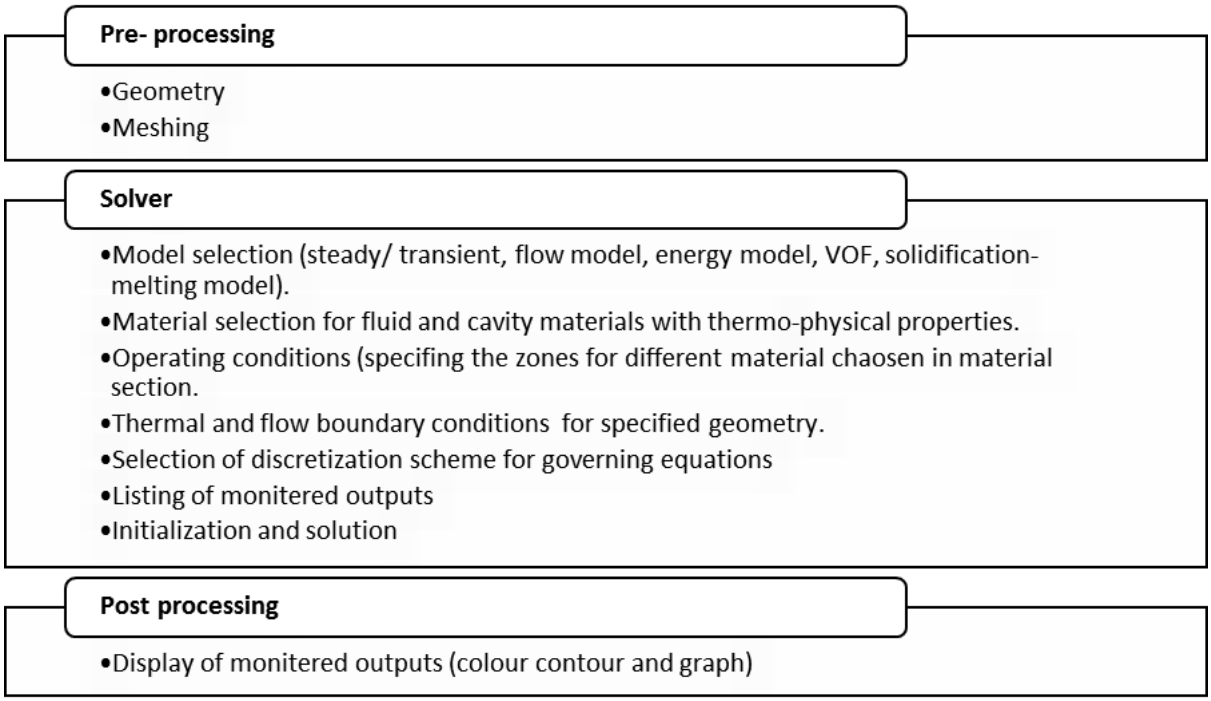


**Fig 3.5: Simulation steps in Ansys-fluent**

## 3.2 CFD packaged used for simulation

Ansys-fluent 15.0 and 16.2 are used for simulation of solid-liquid phase change method. The first step of simulation or pre-processing is done in Gambit and Ansys workbench. The computers used for simulation have following configuration**:** Intel® Xenon® CPU E3-1241 v3 @ 3.5 GHz. 16GB RAM. It took few days for some simulation and for some it took few weeks. In case glass cavity material the simulation took almost one month time for complete phase. The simulation time for solidification is much more than the time required for melting.

## 3.3 Experimental process and validation of the numerical model

### 3.3.1 Experimental Procedure

The experimental setup is shown in and Fig 3.6(a) and (b). The schematic diagram of setup is also shown in Fig 3.7. The experiment has been performed in a transparent tank, filled with water. The level of water is kept constant during the time of experimentation. An electrical heater is used to heat the water and PID (proportion-integral-derivative) controller is used to maintain constant temperature of the water bath. A spherical shell filled with the solid PCM is placed into the constant temperature water bath. The initial temperature of the phase change material inside the cavity is 300K (1K less than the solidus temperature of the PCM) and the experiment continues until the PCM has melted completely. The PCM will expand during its melting and the increased volume will be accommodated by replacing the air through the neck of the cavity. Images obtained during the melting process are recorded by a high-speed digital camera at various stages of the process. These images are analyzed using digital image processing technique, and the experimental values of the melt fraction are calculated at various time instants. The results are used for validation of the numerical approach, as reported in the next section. The properties of PCM are given in Table 3.2.

**Table 3.2: Thermo-physical properties of paraffin wax (RT27)**

| | |
|---|---|
| Density | 870 kg/m$^3$ (solid phase)<br>760kg/m$^3$ (liquid phase) |
| Specific heat | 1800 J/kg.K |
| Thermal conductivity | 0.15 W /m.K |
| Viscosity | 3.42×10$^{-3}$ kg/m.s |
| Solidus temperature | 301K |
| Liquidus temperature | 303K |
| Latent heat of fusion | 179 kJ/kg |

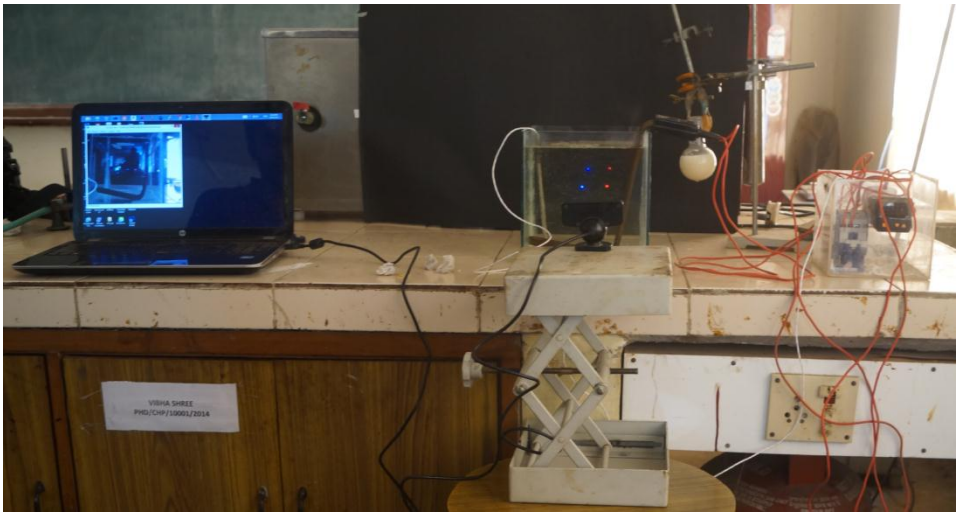

**(a)**

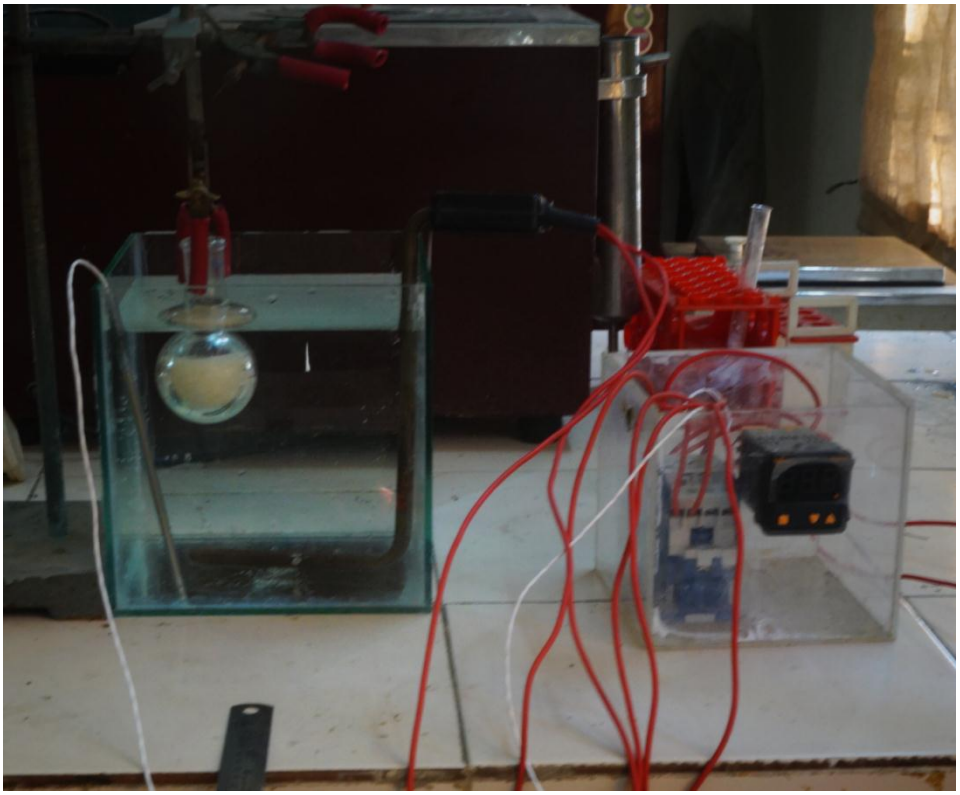

**(b)**

**Fig 3.6(a) & (b): Experimental setup**

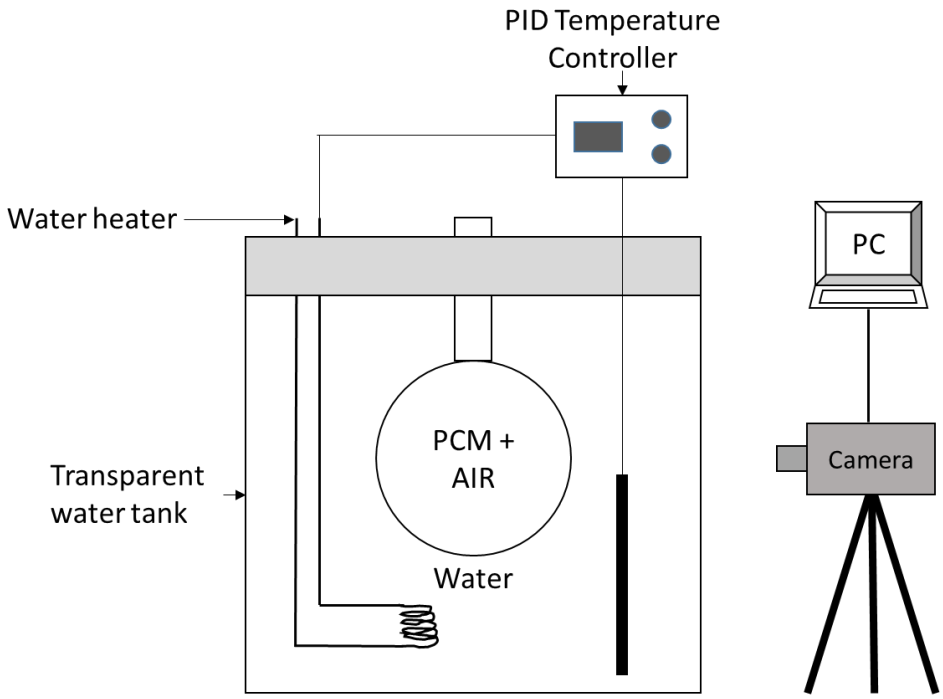


**Fig 3.7: Schematic diagram of the experimental setup**

### 3.3.2 Model validation

The images are captured during the experiment of melting of PCM in spherical cavity (80mm diameter) with water-bath at temperature 47°C.The melt fraction (air and liquid PCM) in the cavity are estimated from the images using digital image analysis. The melt fraction (air and liquid PCM) obtained from images were used to validate the numerical method. Melt fraction (air and liquid PCM) with time is shown in Fig 3.8(a). Melt fraction (air and liquid PCM) is average-volume fraction of fluid in air and paraffin wax mixture. The melt fraction (air and liquid PCM) is calculated using the following relation:

$$melt\ fraction = \gamma_{mix} = (1 - \alpha_n) + \alpha_n \gamma_{PCM} \quad (3.9)$$

The deviation of experimental result from simulated result at the initial stage of melting is because of presence of mushy zone. The estimation of exact melt fraction in mushy zone using digital image analysis technique is difficult because of similar colour contrast. In digital image analysis the volume of fluid is estimated from the colour of different zone. In this case, air and liquid wax are colourless and solid wax is white in colour. During initial stage of melting, as the volume fraction of liquid is very low in mushy zone, the colour remains white. Thus, the estimated melt fraction

differs from simulation at the initial stage of melting process. Figure 3.8(b) shows the experimental images and density contours at different instant of time are almost similar. In Fig 3.8(b) the red colour zone is complete solid phase and light orange is semi-solid or mushy zone and yellow colour is complete liquid phase. In digital images, complete liquid phase is identified but solid and semi-solid phases are not perfectly distinguishable. In Fig 3.8(b) the interface between semi-solid region and liquid region of experimental and simulation can be compared. The image validation is very much important for unconstrained melting as no other parameter like temperature inside the cavity, or melt-fraction of PCM are measurable during the continuous process. Due to this reason, the experiments are performed in transparent glass cavity and PCM is also chosen such that the colour of solid and liquid phase is distinguishable. The validated numerical model is applied to simulate phase change process inside a non-transparent cavity, which are used in practical cases.

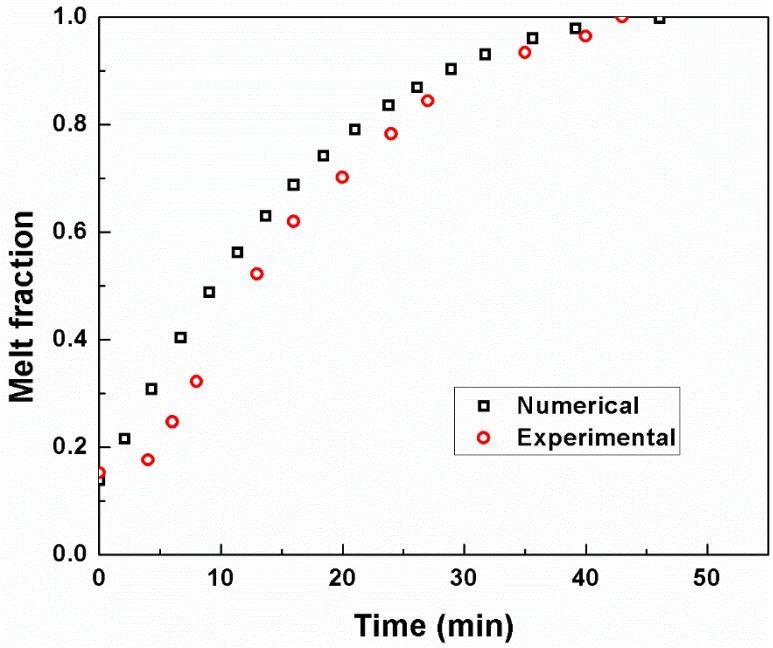


**Fig 3.8(a): Comparison of the experimental and numerical melt fraction (air +liquid PCM)**

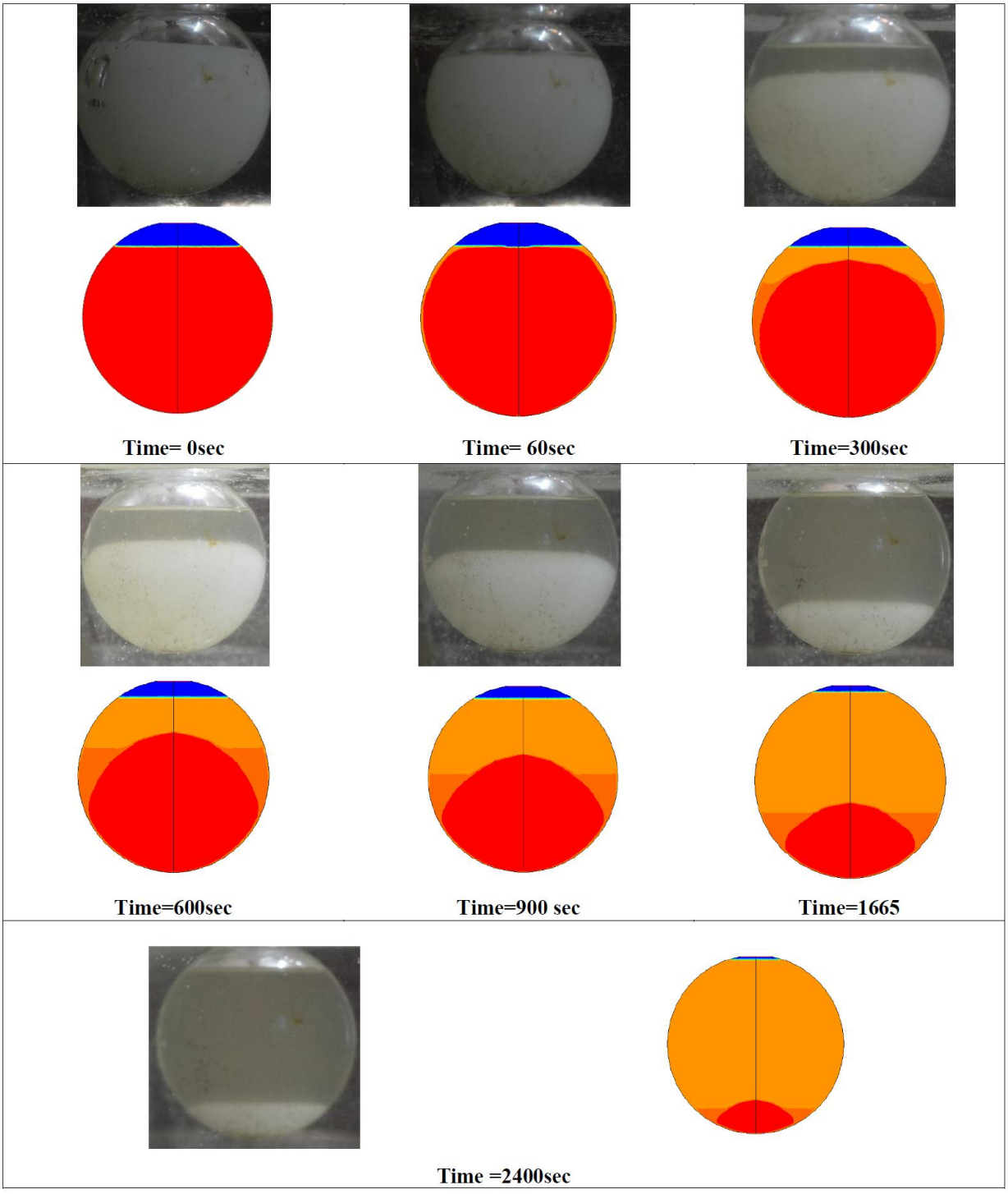


**Fig 3.8 (b): Experimental images matched with density contours of simulated result**

The physical model and computation domain of spherical cavity and rectangular cavity are shown in Fig 3.9. The simulation was done for 0.00001 sec, 0.0001sec, and 0.001 sec time step sizes and the results obtained are similar. In this study, results are

shown for 0.001 sec time step and 22320 numbers of cells. The simulations are repeated with 34612 and 15336 numbers of cells to prove the grid independency of the phase change model. An 80mm diameter spherical shape glass cavity is chosen for the grid independency study. To minimize the time of simulation a higher Stefan number (St = 0.21) is considered to check the grid independency. Figure 3.10 shows that the melt fraction is independent of number of cells. The grid independency for rectangular cavity is shown for solidification process and given in Fig 3.11.

The validated numerical model is applied for study of melting and solidification in spherical and rectangular cavity with different thermal boundary conditions of cavity wall. The same model is also used for study of solidification of metal PCM zinc having high phase change temperature. To study the phase change behaviour of PCM in heat exchanger the same enthalpy porosity is used with Boussinesq approximation.

### 3.3.3 Validation of Numerical model with standard phase change problem

The enthalpy-porosity model used in this thesis is validated with Neumann one dimenstional melting problem(Chin-Yuan Li 2003). In this validation the melting of ice is simulated. Since the process is one-dimentional, the vertical sides of the rectangular cavity are maintained at adiabatic condition. The bottom side of the cavity is kept at higher temperature which is 12 K higher than the melting temperature of ice and the top wall is maintained at 2 K less than the melting temperature of ice. The corresponding Stefan number calculated is 0.18. It is also assumed that the thermo-physical properties of ice remains constant during the melting process. The rectangular geometry contains 5112 rectangular elements. The contour of meltfraction is compared with the bench mark Neumann melting problem in Fig 3.12 (a) & (b). The position of the interface is observed to be similar in both the cases. Therefore, enthalpy-porosity model is appropriate for simulation of melting and solidification processes.

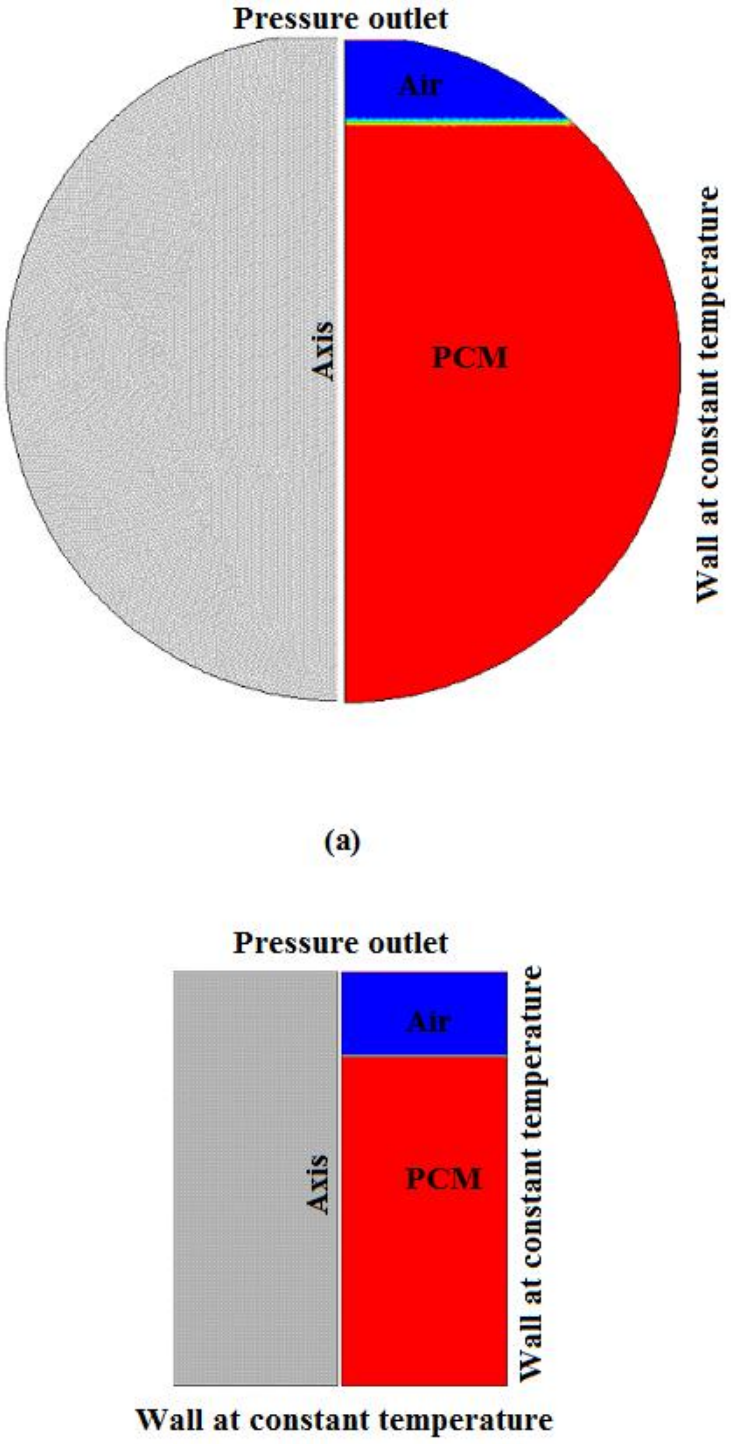


**Fig 3.9: Computational domain of the cavities**

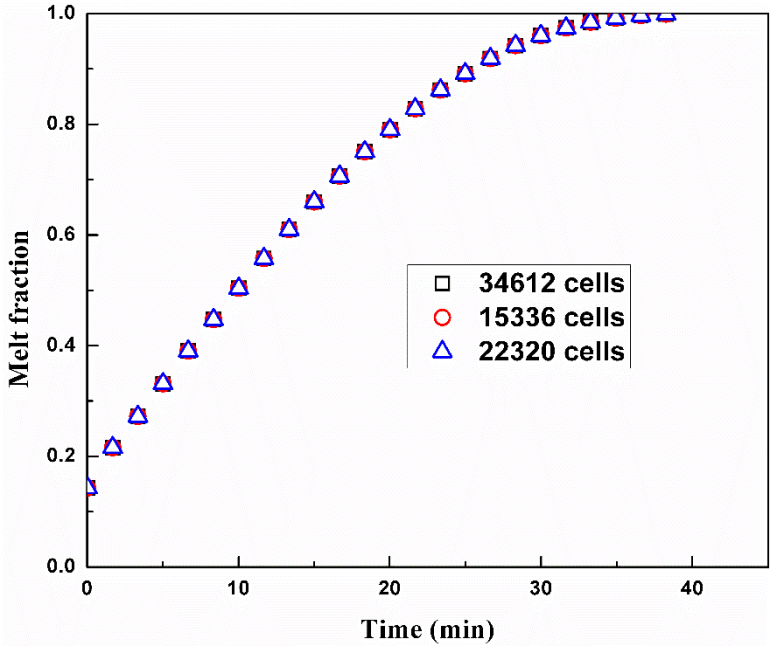


**Fig 3.10: Grid independency for the melting process in spherical cavity**

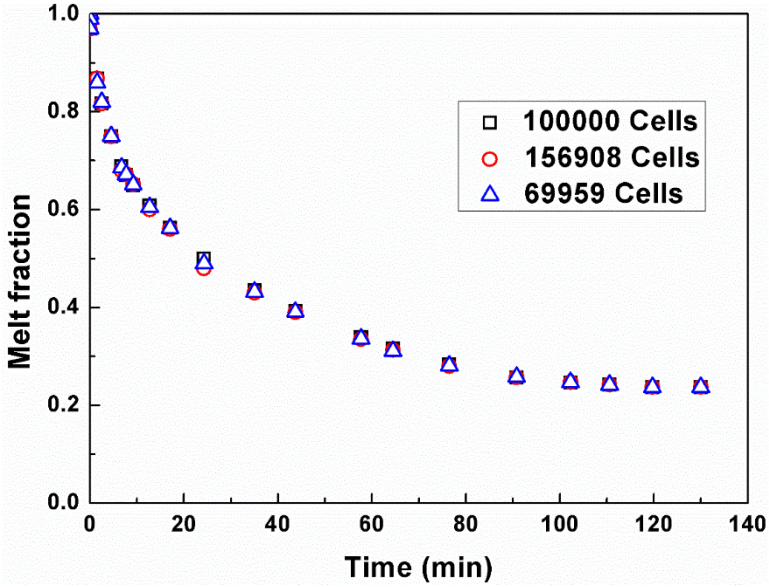


**Fig 3.11: Grid independency for rectangular cavity (solidification at St=0.28)**

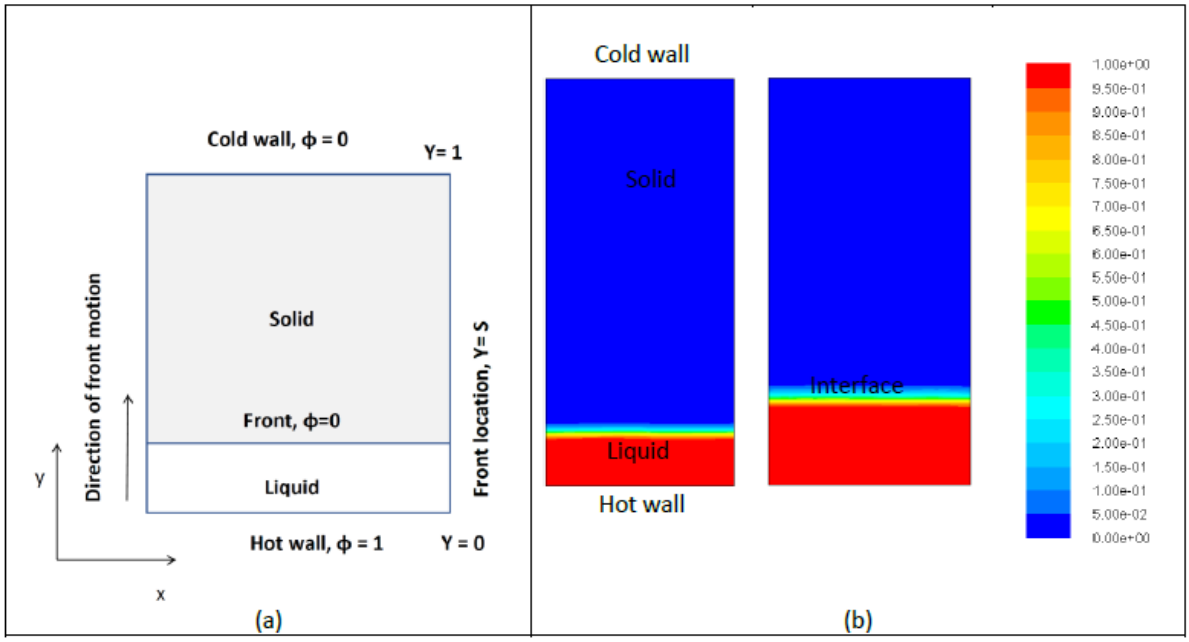


**Fig 3.12: Comparison of (a) standard Neumann melting problem(Chin-Yuan Li 2003) and (b) present numerical model**

**References**

A.R. Archibold, M. M. R., D.Y. Goswami, E.K. Stefanakos (2014). " Analysis of heat transfer and fluid flow during melting inside a spherical container for thermal energy storage." Applied Thermal Engineering 64: 396-407.

Assis, E., Katsman, L., Ziskind, G., and Letan, R (2007). "Numerical and Experimental Study of Melting in a Spherical Shell." Int. J. Heat Mass Transfer 50: 1790–1804.

Chin-Yuan Li, S. V. G., James E Simpson (2003). "Fixed-grid front-tracking algorithm for solidification problems, part I: method and validation." Numerical Heat Transfer, Part B: Fundamentals: An International Journal of Computation and Methodology 43: 117-141.

H. Niyas, S. P., P. Muthukumar (2017). "Performance investigation of a lab scale latent heat storage prototype Numerical results." Energy Conversion Management 135: 188-199.

J.Vogel JF, M. J. (2016). "Naturalconvectioninhightemperature flatplate latent heat thermal energy storage systems." Applied Thermal Engineering 184: 184-196.

Mathura Kumar, D. J. K. (2017). "Influence of Mushy Zone Constant on Thermohydraulics of a PCM." Energy Procedia 109: 314-321.

Mohamed Fadl, P. C. E. (2019). "Numerical investigation of the influence of mushy zone parameter Amush on heat transfer characteristics in vertically and horizontally oriented thermal energy storage systems." Applied Thermal Engineering 151: 90-99.

Simone Arena, E. C., Jaume Gasia, Luisa F. Cabeza, Giorgio Cau (2017). "Numerical simulation of a finned-tube LHTES system: influence of the mushy zone constant on the phase change behaviour." Energy Procedia 126: 517-524.

Y. Kozak, G. Z. (2017). "Novel enthalpy method for modeling of PCM melting accompanied by sinking of the solid phase." International Journal of Heat and Mass Transfer 112: 568–586.

Y. Pahamli, M. J. H., A.A. Ranjbar, R. Bahrampoury (2016). "Analysis of the effect of eccentricity and operational parameters in PCM-filled single-pass shell and tube heat exchangers." Renewable Energy 97: 344-357.

Z.N. Meng, P. Z. (2017). " Experimental and numerical investigation of a tube-in-tank latent thermal energy storage unit using composite PCM." Applied Energy 190: 524–539.

# CHAPTER 4

# STUDY OF MELTING PROCESS IN DIFFERENT CAVITIES

# CHAPTER 4

# STUDY OF MELTING PROCESS IN DIFFERENT CAVITIES

## 4.1 Introduction

The melting process is a very common phenomenon in daily life. Such melting processes are melting of ice, butter, melting of wax during the burning of a candle, melting of metal or alloys during metal casting and welding processes etc. Latent heat energy storage is another application of solid-liquid phase change process. In this process low melting point PCMs are used to store the solar energy or other waste heat by melting and in the next cycle the solidification of PCM fulfils the required energy demand. Therefore, the study of heat and flow analysis during the melting processes is very important, in order to completely understand and control such processes. Viscosity is a property which plays an important role during solid to liquid phase transformation process. The change viscosity and other thermo-physical properties of PCM occur due to heat transfer. Melting not only depends on heat transfer and thermo-physical properties but also depends on shape and material of the cavity. The shape is a controlling parameter of any transport processes and such studies have been discussed in the literature review chapter. A detailed literature review of phase change is reported in Table 2.1. The phase change processes in spherical cavity for paraffin wax with different boundary conditions show that the location of solid-liquid interface is different and also time required for complete phase change are different. In case of spherical cavity, no significant change in shape of solid fraction is observed if the wall boundary condition is uniform through the process (E. Assis 2007; E. Assis 2009; F.L. Tan 2009; M.Z.M. Rizan 2012). The case is different in rectangular cavity. The melting rate and the energy stored in heating, from vertical side, are much higher than that of heating from below or horizontal wall heating, due to enhanced natural convection effect (A.V. Arasu 2012). The rate of phase change in rectangular cavity also depends on the orientation of cavity. Babak and Hamid simulated the melting process of Lauric acid in horizontal rectangular cavity where the heating was supplied from bottom wall and all other

walls were insulated and in case of vertical rectangular cavity the heating was supplied from right wall and all other walls were insulated (Babak Kamkaria 2017). It has been observed that phase change of lauric acid shows melting time is minimum for a horizontal rectangular cavity than vertical rectangular cavity. The effect of thermo-physical properties of PCM also plays an important role during phase change process. The thermo-physical properties of paraffin wax and n octadecane are almost similar, so the phase change process is same for those materials. On the other hand, the phase change of paraffin wax and n octadecane are very much different from that of water. The reason is due to melting the volume of water decreases and the solid phase of water floats on the liquid phase (T.S. Saitoh 1996; T.S. Saitoh 1997; E. Assis 2007; E. Assis 2009; M.Z.M. Rizan 2012). Literature review reveals that melting in different cavities not included the effect of thermo-physical properties of cavity materials. The empirical equations are derived for spherical cavity but not for rectangular cavity. The initial shape of solid also affects the melting process which is not studied by many researchers. In this chapter, the study of melting for different boundary conditions, for different cavity material and for different initial shape like spherical and rectangular cavity are presented.

## 4.2 Melting of phase change material in spherical cavity

The spherical shape is very common and regular where phase change occurred frequently. A large number of works is available where the phase change is studied in a spherical cavity. In this study phase change or melting is studied in 80mm and 60 mm diameter cavity and the details of physical domain are described in the following section.

### 4.2.1 Physical model

A spherical shell with an inner diameter of 80 mm or 60 mm and wall thickness 2 mm is considered. Initially, the spherical shell or cavity is 85% filled with PCM paraffin wax (RT27) at an initial temperature of 300K which is 1 Kelvin less than the solidus temperature. The outer surface temperature of the cavity is kept greater than the liquidus temperature of the PCM. Melting starts at the surface and the moving

boundary moved towards the center. Since the density changes due to phase change, the heavier solid phase sink at bottom of the cavity and the lighter liquid phase has been observed at the top of the container. The thermal conductivity of glass container is taken as 0.81 $Wm^{-1}$ $K^{-1}$for simulation (E. Assis 2007). The properties of the PCM, based on paraffin wax (RT27) as a commercially available material, are given in Table 3.2.

### 4.2.2 Computational procedure

The numerical approach is very important to predict the melting phenomena inside a cavity. During the melting process heat is supplied to the solid which is kept in a cavity. The temperature of PCM becomes constant or varies within a small range of temperature at the time of phase. Therefore, the progress of process is not measurable experimentally. Numerical simulation is the process which analyses the process at each time step. The heat required for melting is same for same mass of PCM but the melting time is not same for various cavity shape and thermal boundary conditions. Numerical simulation is the solution to find the controlling parameters of phase change process. The flow is assumed to be two dimensional and unsteady. It is also assumed that both solid and liquid phases are homogeneous and isotropic. The phase change process is symmetric about the vertical axis therefore; an axisymmetric model is used for the study of melting process. The axisymmetric model reduces computation time. The molten PCM and the air are incompressible Newtonian fluids, and laminar flows are assumed in both the phases. A density-temperature relation is used for air: $\rho = 1.2 \times 10^{-5}T^2 - 0.01134T + 3.4978$ (E. Assis 2007). The PCM is initially at a temperature which is less than the solidus temperature. The study has been performed in cavities of three different thermal diffusivities. The outer surface of cavity is kept around 19$^{o}$C higher than the average melting temperature. The cavity is open to air during the melting process. Properties of PCM are chosen as commercially available paraffin wax (E. Assis 2007). Commercial software Ansys-fluent 16.2 is used for numerical simulation of the melting process.

### 4.2.3 Results and discussion: Melting process in spherical cavity (80 mm diameter) for different cavity materials

The cavity material or thermo-physical properties are very important in heat and flow analysis of melting processes. The thermo-physical properties of cavity affect the rate of heat transfer and control the melting time. The details of melting for three different cavity materials are discussed in this section.

The mathematical model is solved for three different types of spherical cavity materials, they are:

Aluminium cavity with thermal diffusivity (α) as $8.5\times10^{-5}$ $m^2/s$,

Copper cavity with thermal diffusivity (α) as $11.3\times10^{-5}$ $m^2/s$ and

Glass cavity with thermal diffusivity (α) is $3.42\times10^{-7}$ $m^2/s$.

The expression for thermal diffusivity is given by the following equation:

$$\alpha = \frac{k}{\rho C_p} \tag{4.1}$$

These materials are easily available and commonly used for as heating container in lab, domestic and industrial uses. The simulated results obtained from simulation using Ansys-fluent 16.2 for volume of fluid (VOF) model and enthalpy porosity model in the cavity; the coloured contours of solid-liquid front of PCM at various time interval for an unconstrained melting process at outer wall temperature 47°C and initial temperature 27°C are shown in Fig 4.1 and Fig 4.2. The simulation has been performed for three different cavities which are glass, aluminium and copper. Figure 4.1 shows the contours of melt fraction and Fig 4.2 shows the density distribution with time. In Fig 4.1 the blue colour indicates the solid portion and red colour indicates the liquid portion in the cavity. The outer surface of the solid PCM is in contact with the inner wall of the sphere so that heat conduction between the wall and solid PCM dominates. This results in formation of thin liquid layer between solid PCM and wall. With time, the molten zone expands, and the liquid layer grows. In spherical shape of the solid fraction is retained for most of the melting process except towards the end when it loses its spherical shape and becomes flattened or elongated until melting is completed. On the other hand, the denser solid phase is sinking due to gravity as it is not fixed in the cavity. The bouncy force

is included in momentum balance in Eqn. 3.3 to consider the effect of volume change of PCM due to phase change. The density of cell is a function of melt fraction and again melt fraction is a function of temperature. Therefore, the bouncy term shows the effect of thermal bouncy force. The motion of the solid phase is accompanied by the formation of liquid at the melting interface. This liquid is squeezed up through a narrow gap between the melting surface and the wall of the shell, to space above the solid. Therefore, natural convection in combination with sinking of solid portion at the bottom of the container controls the melting process. Both melt fraction and density distribution are similar approximately till 5 min of initiation of the melting process. At around 10 min of initiation of the melting process the shape of solid fraction within the cavity starts changing. The shape of the solid fraction in glass cavity is different from that of aluminium and copper cavities. However, the solid fraction of copper and aluminium cavity are similar. The reason is, with the higher value of thermal diffusivity of the cavity material, the rate of heat transfer from cavity bottom wall to the PCM increases and it melts the PCM immediately and only a small fraction of solid PCM is found at the bottom of the cavity. Figure 4.1 & Fig 4.2 also show that the melting process is slowest in the glass cavity. Thus, the time required for complete melting is inversely proportional to the thermal diffusivity of the cavity materials. The time required for complete melting is almost same for the highest and second highest thermal diffusivity material aluminium and copper respectively and it is almost double in case of glass cavity with lowest thermal diffusivity. Figure 4.2 shows the expansion of volume in the liquid phase by expelling the initial air content within the cavity. The continuity equation given is Eqn. 3.1 is only applied to calculate the volume fraction of PCM and the remaining volume fraction is for air. Therefore, an increase in melt fraction shows an increase in $\alpha_n$ and a decrease in $\alpha_{air}$. Decrease in $\alpha_{air}$ confirms the removal of air from the cavity and increase in PCM height in the cavity. Both Fig 4.1 and Fig 4.2 shows the perfect match of the assumptions of close contact melting with enthalpy-porosity model applied to an open surface cavity. The result presented for melt fraction in Fig 4.1 is obtained by solving the enthalpy-porosity model where air and liquid PCM are not identified separately. The air, liquid PCM and solid PCM are identified

individually in Fig 4.2 using VOF model. The density contour in Fig 4.2 helps to locate the fluid-fluid and fluid-solid interface. Figure 4.3 shows the melt fraction (air +liquid PCM) with time. The melt fraction (air +liquid PCM) is the amount of air and melted wax content in the cavity. It is evident that the melt fraction (air +liquid PCM) within the cavity increases with time and the time required for complete melting is greater for the cavity material having lowest thermal diffusivity. Heat flux is another important parameter in heat transfer study. Volume average heat flux is defined as heat supplied to control volume per unit area. A positive value of heat flux implies heat addition to the control volume and negative value of heat flux implies heat rejection from control volume. Therefore, heat flux is positive on computational domain for melting. Figure 4.4 which represents the variation of heat flux with time shows a sudden decrease in heat flux at the initial stage of melting in spherical aluminium and copper cavity. On the other hand, the change in heat flux is moderate for the glass cavity. In the case of higher thermal diffusivity of the cavity material, initially the temperature gradient between PCM and wall is very high, and the resistance due to conduction is very low, which results in the significantly high rate of heat transfer. In the case of lower thermal diffusivity of the cavity, the temperature gradient is same initially but the resistance to conduction is high compared to higher thermal diffusivity of the cavity and the result is low heat transfer rate. As the thickness of liquid PCM increases the effect thermal bouncy force decreases. The decrease in thermal bouncy force results in lower convection heat transfer and show a falling trend in heat flux with time. In case of copper and aluminium cavity the heat flux curve decreases rapidly than glass cavity due to higher melting rate. Figure 4.5 shows the effect of convection compared to conduction heat transfer. Dimensionless Nusselt number is used to represent the change of mode of heat transfer with time. Nusselt number is the ratio of conduction resistance to convection resistance. Initially, the melting process considered in this study is initiated due to conduction and gradual increase in melt fraction introduces convection heat transfer. Figure 4.5 shows that for aluminium and copper cavity Nusselt numbers are very high which means the conduction resistance is more than convection resistance. The Nusselt number decreases to zero at the end of melting

process as convection heat transfer decreases due to decrease in density change and bouncy effect at the end of melting process. In the case of glass cavity, the Nusselt number decreases gradually with time. Melting in glass cavity is very slow, and the conduction heat transfer controls the process by minimizing the effect of convective heat transfer.

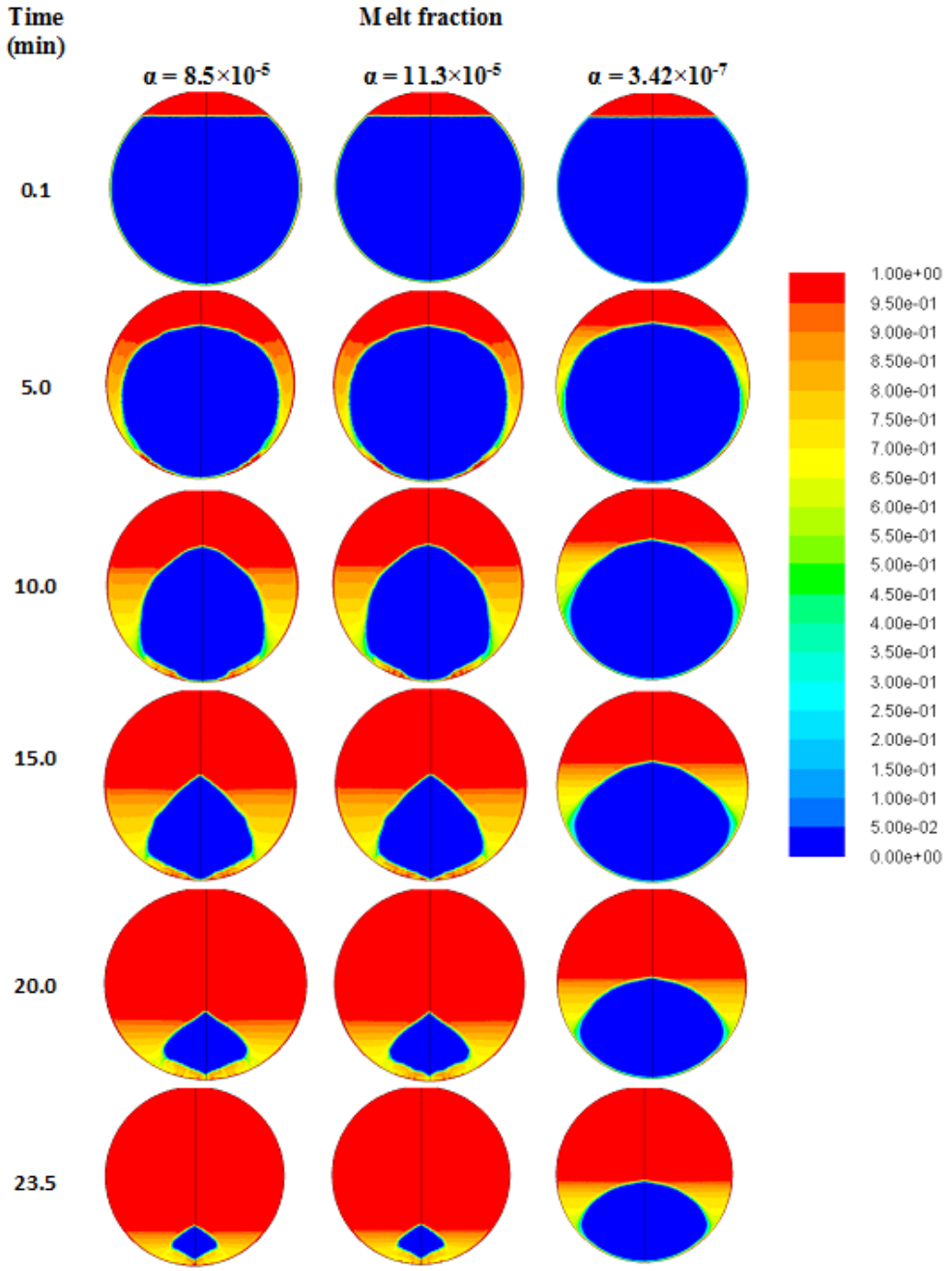


**Fig 4.1: Contours of melt fraction in the cavities for St=0.18 (Debasree Ghosh 2019)**

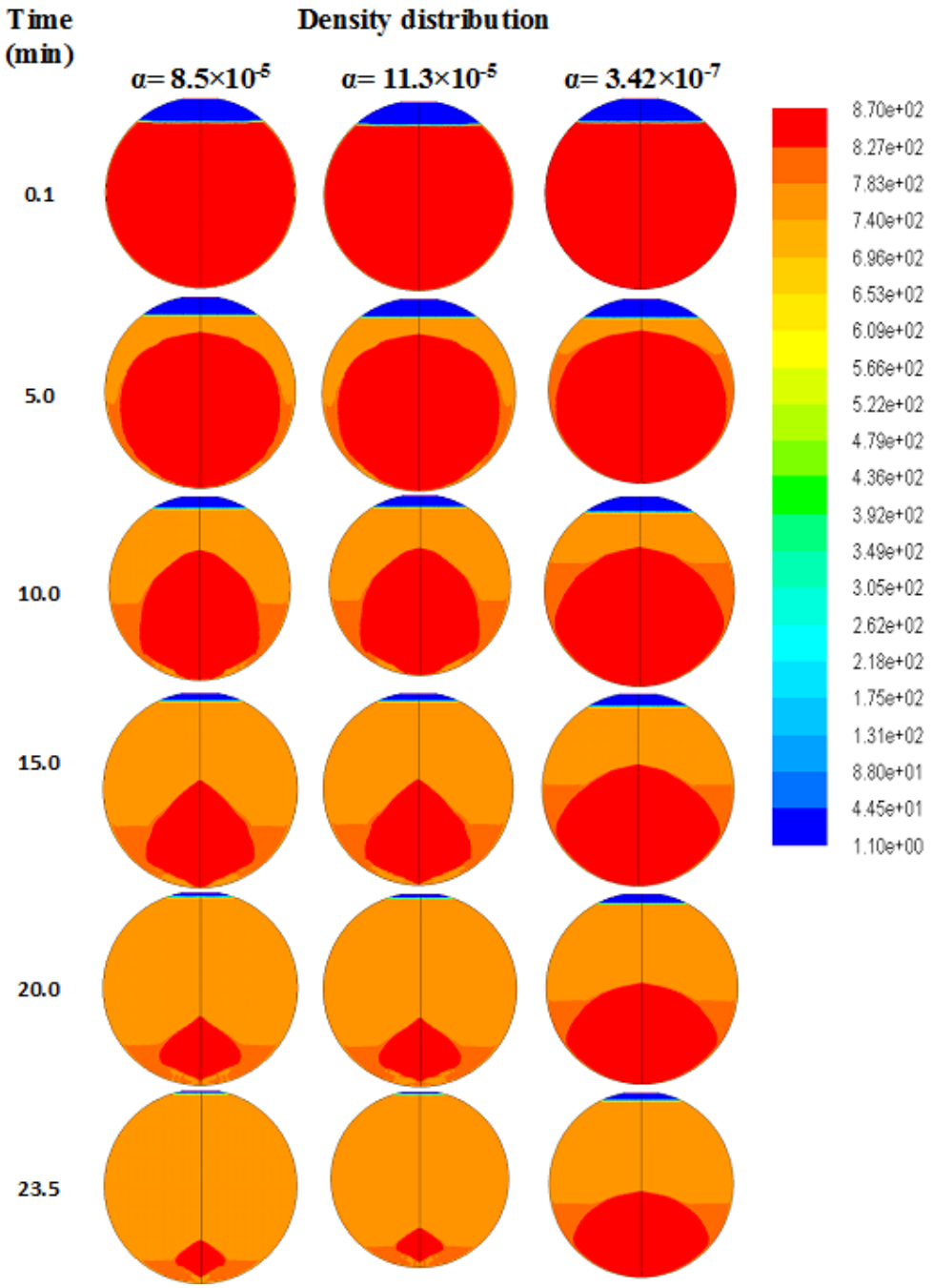


**Fig 4.2: Contours of density in the cavities for St=0.18 (Debasree Ghosh 2019)**

In next section the effect of Stefan number is studied in copper cavity. The copper cavity needs minimum time for melting compared to other cavity materials (aluminium and glass) with same thermal boundary condition.

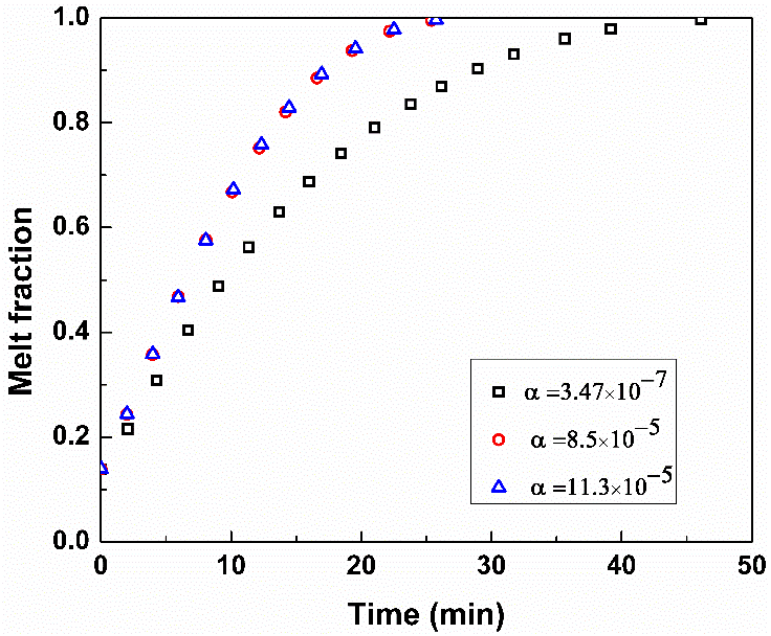


**Fig 4.3: Melt fraction (air +liquid PCM) in cavity for St=0.18 (Debasree Ghosh 2019)**

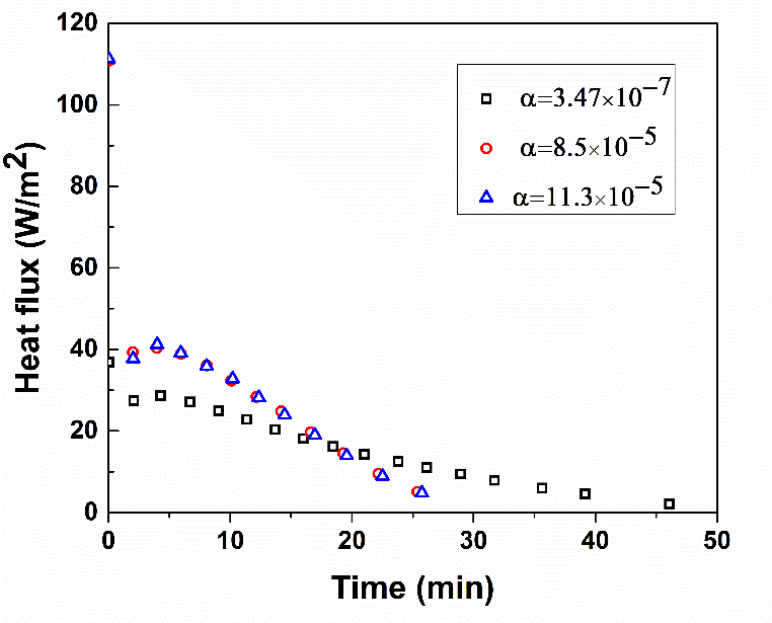


**Fig 4.4: Variation of heat flux with time for St=0.18 (Debasree Ghosh 2019)**

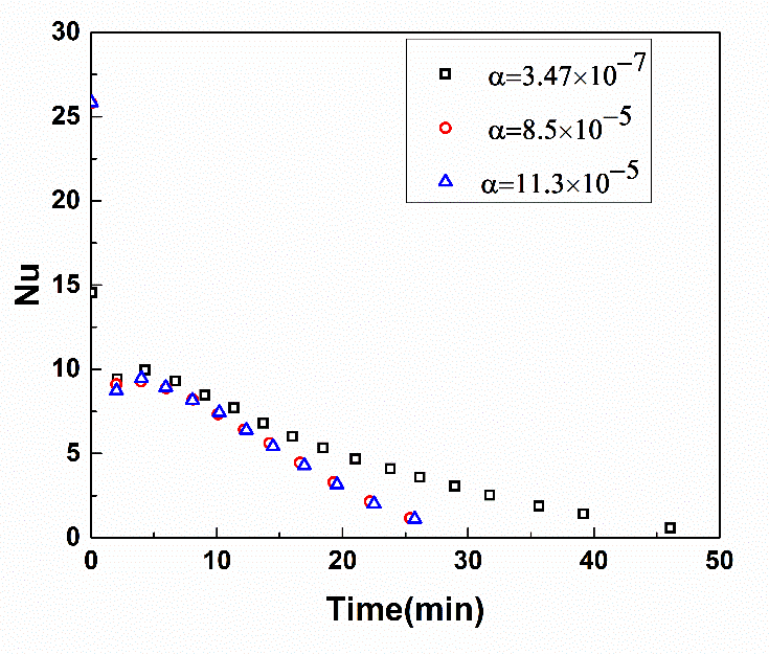


**Fig 4.5: Variation in Nusselt number for St=0.18 (Debasree Ghosh 2019)**

### 4.2.4 Results and discussion: Melting process in spherical cavity (80 mm diameter) for different Stefan numbers

In this section, the effect of cavity wall temperature is studied. To minimize the melting time as well as computational time the process is simulated in copper cavity. Therefore, the melting phenomenon is studied for different Stefan numbers for copper made spherical cavity (80 mm diameter). Stefan number (St), is the ratio of sensible heat and latent heat of the PCM. The surface temperature directly affects the value of Stefan number. The expression for expression for Stefan number is given by Eqn. 4.2.

$$St = C_{pl}(T_w - T_m)/L \quad (4.2)$$

Where $C_{pl}$the specific heat of the liquid PCM, L is the latent heat and $T_m$is the mean melting temperature of PCM and $T_w$is the wall temperature at the surface of the cavity respectively. Paraffin wax (RT27) is having mean melting temperature 302K or $29^oC$ and able to store the heat of low temperature source. Therefore, the temperature difference of cavity and mean melting temperature of PCM is kept below $20^oC$ . The present simulation has been performed at three different Stefan numbers, St=0.13 ($T_w = 42^oC$), St=0.18 ($T_w = 47^oC$) and St=0.28 ($T_w = 57^oC$). As the surface temperature increases and Stefan number increases and the total melting

time decreases. Figure 4.6 shows the variation of the melt fraction (air +liquid PCM) present in the cavity with time. The result shows an increase in volume of fluid with time as melting proceeds. Initial volume fraction of fluid was around 0.15, same as volume fraction of air present in the cavity. As the melting process proceeds the fraction of air is gradually replaced by melted wax. The melted wax is of lesser density and as a result, occupies larger volume. The time required for complete melting is inversely proportional to Stefan numbers which are 22 min, 28 min, and 33 min for Stefan number equals to 0.28, 0.18 and 0.13 respectively as shown in Fig 4.6. Figure 4.7 shows the variation of heat flux with time for different Stefan numbers. Heat flux is highest for the highest Stefan number due to a higher temperature gradient. In case of Stefan number 0.28 the maximum heat flux is 170 $W/m^2$ and for Stefan number 0.13 and 0.18 maximum heat flux are 82 and 111$W/m^2$ respectively. Heat flux decreases with time and becomes zero after completion of the melting process as per the mechanism of heat transfer.

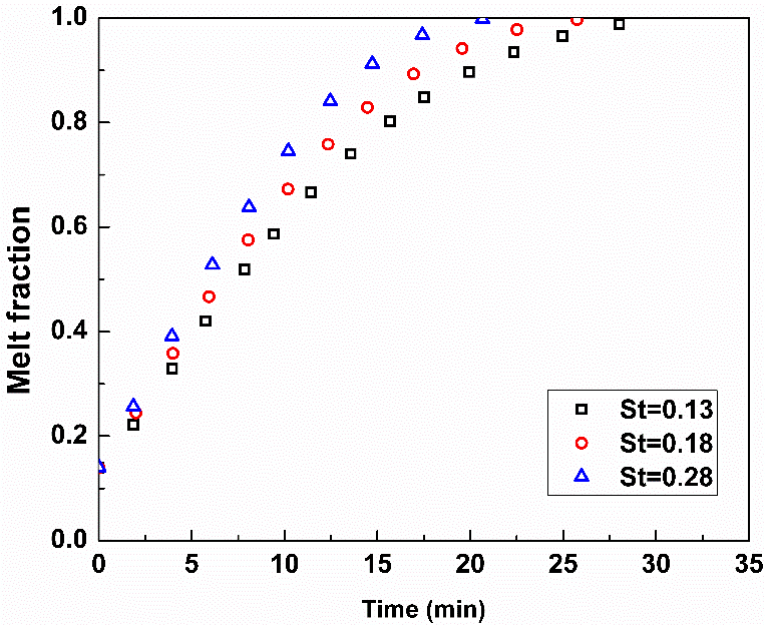


**Fig 4.6: Melt fraction (air +liquid PCM) for different Stefan number in copper cavity (Debasree Ghosh 2019)**

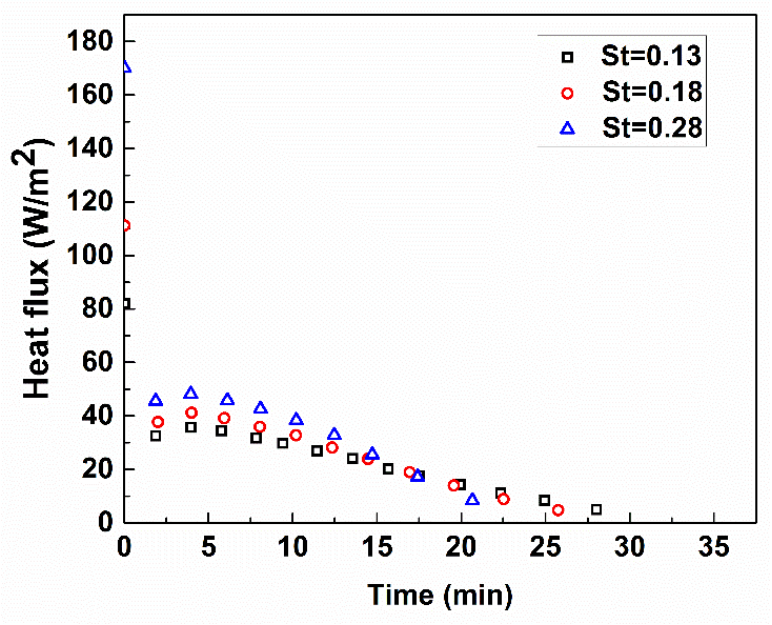


**Fig 4.7: Variation of heat flux for different Stefan number in copper cavity (Debasree Ghosh 2019)**

The maximum velocity during the phase change the process is also investigated. In Fig 4.8 the maximum velocity magnitude of mixture (PCM +air) with time is plotted. Due to presence of air the initially the volume-average maximum velocity inside the cavity is nonzero. Melting process shows at the initiation of process the velocity increases and attain a maximum temperature and then falls approximately to zero after completion of the process. The maximum velocity increases initially due to increase in thermal bouncy force and starts falling with decrease of bouncy force. The maximum velocity is highest in case of highest Stefan number, and reason behind it is the higher rate of melting the effect of convection heat transfer. After around 10 minutes, the change in maximum velocity is almost negligible as shown in Fig 4.8. The reason for higher heat transfer rate in copper cavity is due to bouncy effect and low resistance to conduction and convection heat transfer.

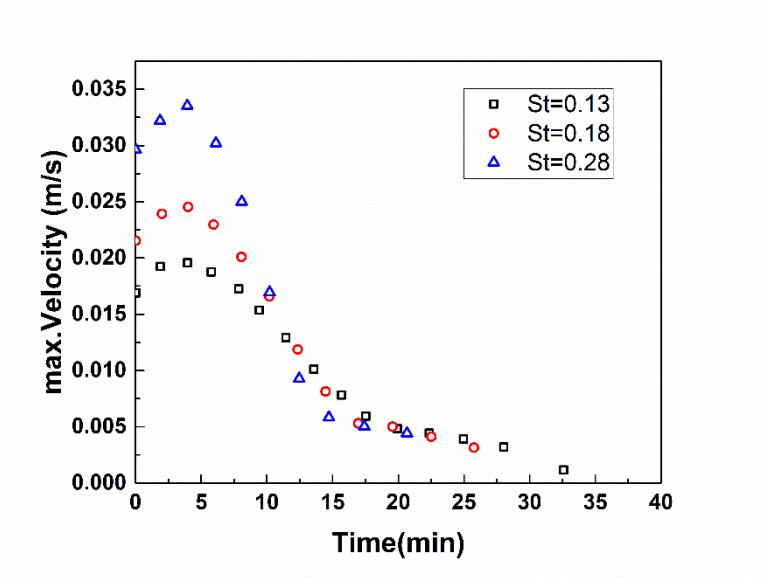


**Fig 4.8: Variation of maximum velocity with time in copper cavity (Debasree Ghosh 2019)**

### 4.2.5 Results and discussion: Effect of rotation of cavity on melting of PCM

Phase change materials (PCMs) are mostly used for latent heat energy storage. During the process of charging or melting of PCM the time required for complete melting is very high. The melting time is high due to lower thermal conductivity of PCM. The time of melting can be minimized by increasing Stefan number or by changing the orientation of cavity. A large number of literature are available using these conditions (B. Binet 2000; J.M.Khodadadi 2001; Sin Kim 2001; E. Assis 2007; J.M. Khodadadi 2007; F.L.Tan 2008; Hamid Ait Adine 2009; Yifei Wang 2016). In section 4.2.3 the effect of thermal diffusivity of cavity material on melting are studied. The results show that the high thermal diffusivity cavity material takes lower time for melting of paraffin wax (RT27). In this section, the rotation of cavity during the phase change process is considered. The rotation of cavity plays an important role in centrifugal casting but, such studies are not usually done for melting processes (P. Maarten Biesheuvel 1998; Su-Ling Lu 2014; Davide Masato 2017). In this study, the rotation effect is introduced without using a stirrer. The stirrer can't be used in unconstrained melting therefore; the rotation is given by rotating the cavity.

The 80mm diameter spherical cavity is taken for the study. The number of nodes and properties of PCM and thermal boundary conditions is the same as taken to study the effect of thermal diffusivity of cavity material. The rotational speeds are considered as 20rad/s and 40rad/s. The cavity material taken for the study is glass and temperature of cavity wall is 320K (St =0.18). Figure 4.9 shows the effect of rotation on melting. It is observed that the melting time remains same throughout the process. The rotational of the cavity is not able to decrease the melting time. In this uncontained melting, the melting start from the wall of the cavity and bouncy force drives the process. On the other hand, the low-density liquid phase is near the cavity wall and high-density solid phase is near the center of the cavity hence, the rotation of cavity wall will not improve the time of melting.

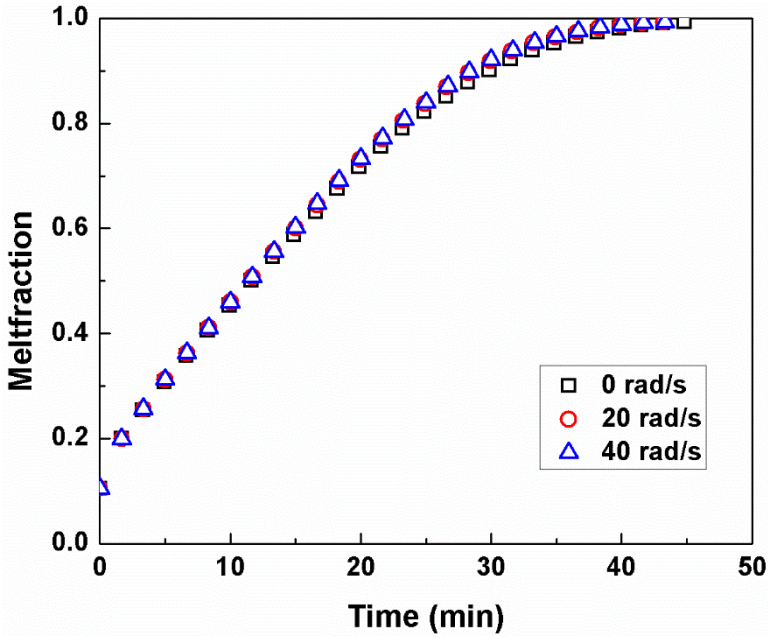


**Fig 4.9: Melt fraction (air +liquid PCM) in a rotating glass cavity for St=0.18**

### 4.2.6 Results and discussion: Melting process in spherical cavity (60 mm diameter) with different Stefan numbers

The similar study is presented for a 60 mm diameter spherical cavity. It is also mentionable that glass cavity is taken for this numerical simulation. The data presented in Fig 4.10 shows that the time required for complete melting is lowest for the highest cavity wall temperature (320K and St=0.18) and it is around 34 min. The time required for same is highest for the lowest cavity wall temperature is

approximately 72 min. For an increase in temperature from 310K to 315K the melting time is reduced by 35% and for increase in temperature from 315K to 320K the melting time is reduced by 25%. Therefore, very high cavity wall temperature may not minimize the melting time very much. The high temperature difference in control volume causes sensible heat transfers and makes the phase change process slower.

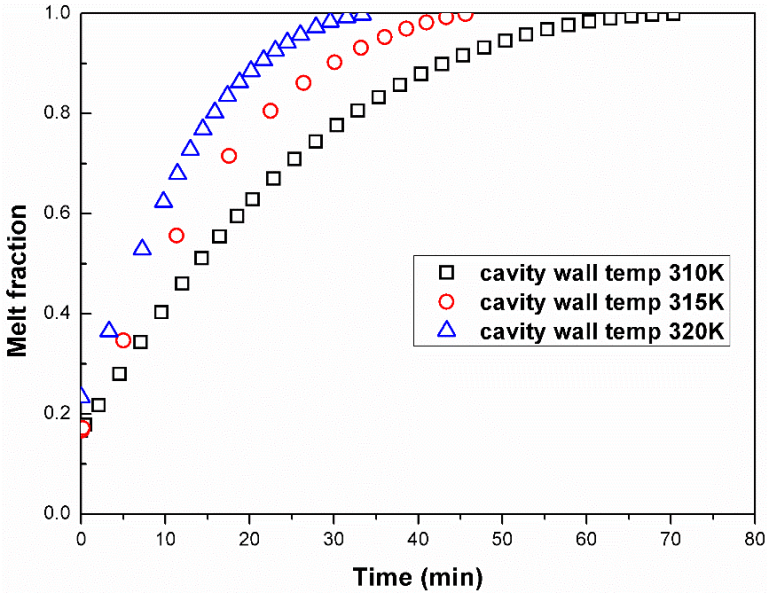


**Fig 4.10: Melt fraction (air +liquid PCM) for different wall temperature in glass cavity**

An important parameter in heat transfer study is heat flux. The following Fig 4.11 shows the variation of volume-average heat flux during melting in 60 mm diameter spherical cavity. The variation of heat flux shows similar variation for high cavity temperature as discussed in melting in in 80mm diameter cavity (Fig 4.7). The nonlinear nature of heat flux variation decreases as the cavity wall temperature decreases and it's almost linear for cavity wall temperature 310K. The reason is, in this case, the conductivity and thermal diffusivity of cavity is very low and for lower cavity wall temperature the temperature gradient is also very low. These lower value of driving force and higher thermal resistance makes the heat transfer or phase change process slower. On the other hand, the volume of cavity is less compared to 80 mm diameter cavity and also the mass of PCM content is lower in 60 mm diameter cavity. The decreasing volume of solid phase PCM reduces the bouncy effect and heat transfer and the phase change process becomes sluggish.

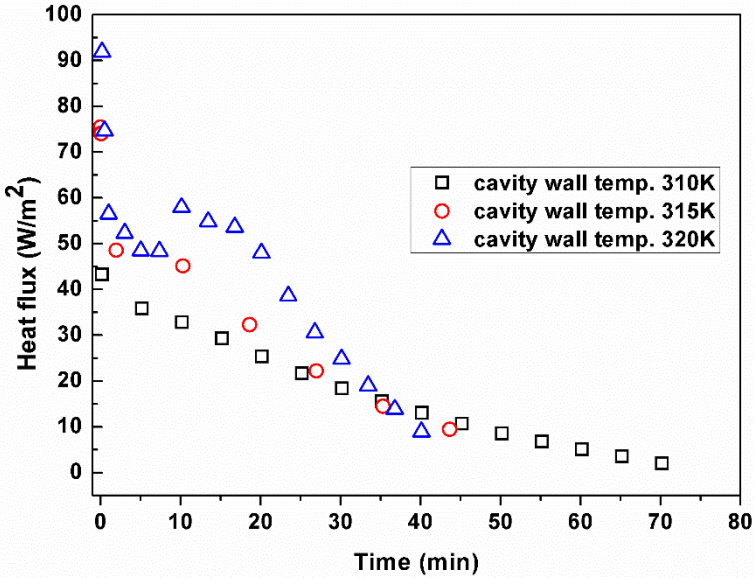


**Fig 4.11: Variation of heat flux for different wall temperature in glass cavity**

### 4.2.7 Conclusion

The simulations of melting in spherical cavity with different cavity materials control the melting time and shape of unmelt solid PCM in the cavity. The melting time is lowest for highest thermal diffusivity cavity material. The melting is also lowest for highest Stefan number. Apart from thermal condition melting time depends on size or volume of cavity or amount of PCM in the cavity. In this study melting time is lowest for highest Stefan number, highest thermal diffusivity cavity material and lowest PCM content. The effect rotation of cavity on melting time is negligible.

## 4.3 Melting of phase change material in rectangular cavity

### 4.3.1 Physical model

In this section, the numerical simulation of melting of paraffin wax (RT27) in a rectangular cavity (80% filled by area) using enthalpy-porosity method (A.D. Brent 1988) is discussed. The size of the rectangular cavity is 50mm×40mm (H×W). The boundary conditions are shown in Fig 3.7(b). Bottom and side edges of the cavity are maintained at a constant temperature which is higher than the mean melting temperature of the material under study. The PCM is sub-cooled and the temperature is 300K. The cavity is open to air and partially filled. Since the cavity is

open to the atmosphere, an ambient condition is maintained at the open edge. The variation of density with temperature is considered for air (E. Assis 2007).

### 4.3.2 Computational procedure

An axisymmetric model is simulated with the volume-of-fluid method. Laminar flow is assumed in the molten PCM. Both PCM and air are assumed to be incompressible Newtonian fluid. The momentum, continuity and energy equations are solved using SIMPLE pressure-velocity coupling scheme. Discretization scheme used are PRESTO for pressure, second-order upwind for momentum, geo-reconstruct for volume fraction, and the second order upwind energy. Commercial software Ansys-fluent 16.2 is used for simulation. The simulation is carried out over a few weeks. The used model and software for this simulation have been already shown to be in good agreement with experimental results for solidification and melting processes, in the various literature(E. Assis 2007; S. Lorente 2014). An axis symmetric model is chosen with 100000 cells. The grid independency test for rectangular cavity is shown in Fig 3.9.

### 4.3.3 Results & discussion: Melting process in rectangular cavity (50mm ×40mm) for different Stefan numbers

These simulations of melting in the partially filled rectangular cavity, incorporated convection heat transfer in the liquid phase, volumetric expansion due to melting, and a specific constant temperature at the boundary wall. The model used to solve the complete unsteady conservation equations, simultaneously for solid PCM, liquid PCM, air-liquid PCM interface and solid-liquid PCM interface. The contours of melt fractions at different times are shown in Fig 4.12. The contours of melt fraction are shown at different time for a mean temperature difference of 28$^{o}$C between mean melting temperature and temperature of the outer wall of the cavity. At this temperature, Stefan number is 0.28. The initial volume-average of the solid fraction is taken as 80% of total height of the cavity. The melting process follows the theory of close contact melting. The bouncy effect drives the sinking of the solid phase in the rectangular cavity. The shape of the solid fraction in rectangular cavity differs

from the shape of the un-melt solid fraction for melting in a spherical cavity due to the aspect ratio of the cavities. Here aspect ratio refers to the ratio of height by width of unmelted solid phase.

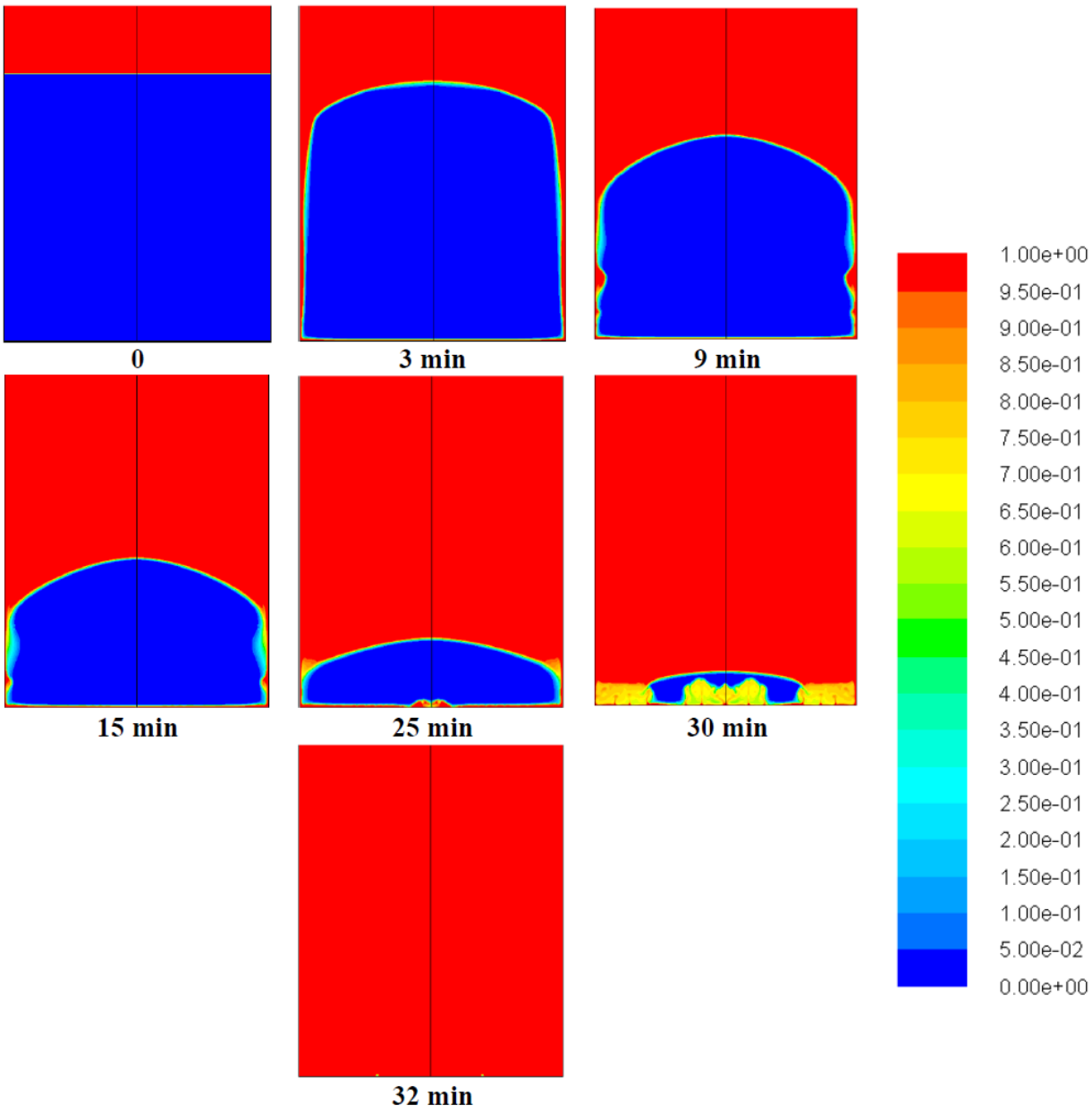


**Fig 4.12: Contours of melt fraction in rectangular cavity**

An increase in a wax label is observed as melting starts, which is shown in Fig 4.13. The decrease in density due to melting causes the rise in wax level.

$$v_{sf} \times \rho_{PCM,solid} = v_{lf} \times \rho_{PCM,liq} \qquad 4.3(a)$$

$$v_{lf} = \frac{v_{sf} \times \rho_{PCM,solid}}{\rho_{PCM,liq}} = \frac{0.8 \times 870}{760} = 0.915 \qquad 4.3(b)$$

Where, $v_{lf}$ and $v_{sf}$ are the final liquid fraction and initial solid fraction of PCM in the cavity. In this study the height of paraffin wax in the cavity is 80% of total height of the cavity and expected volume fraction of liquid after completion of melting is 91.5%. The increase in the rise of the level of PCM is due to volume expansion and change in density due to phase change. The contours of density given in Fig 4.13 show the different phases at a different time. The darkest shed (blue) one represents the presence of air in the cavity and second darkest shed(red) is for solid wax and the light shed (yellow colour) is for liquid phase of wax. The contours show that the amount of air decreases as the melting proceeds. The expansion of liquid phase replaces the air through the open edge of the cavity. The volume-average of the solid fraction of wax with time is shown in Fig 4.14. Initially, the cavity is filled with air and solid PCM. Therefore, the initial melt fraction in the cavity is the fraction of air present in the cavity. As the melting process proceeds the air is replaced by liquid PCM and the transient melting fraction is estimated from the remaining air and liquid PCM in the cavity. On the other hand, the solid fraction contains solid PCM only. Therefore, identification of solid phase is easier compared to that of liquid-air and solid-liquid phases. In VOF model solid fraction gives the measurement of pure phase. Figure 4.14 is more appropriate to estimate the remaining solid fraction of PCM in the cavity. The melting time is high for low Stefan number and low for high Stefan number. The melting process completes when the solid fraction becomes zero. For Stefan number 0.28 the melting time is approximately 32 mins. For Stefan number 0.13 and 0.18 the melting time becomes 41 min and 52min respectively. Figure 4.15 shows the variation of heat flux with time. It shows that at the initial stage heat transfer is controlled by conduction in solid phase and it decreases with decreasing temperature difference of wax and the wall. In the second stage, due to melting, both conduction and natural convection affect the heat transfer process which results in a slight increase in heat transfer coefficient. In the third stage of melting, the heat transfer starts decreasing from a maximum value, as temperature gradient decreases due to phase change. At this stage, the bouncy effect of solid phase decreases as its amount decreases.

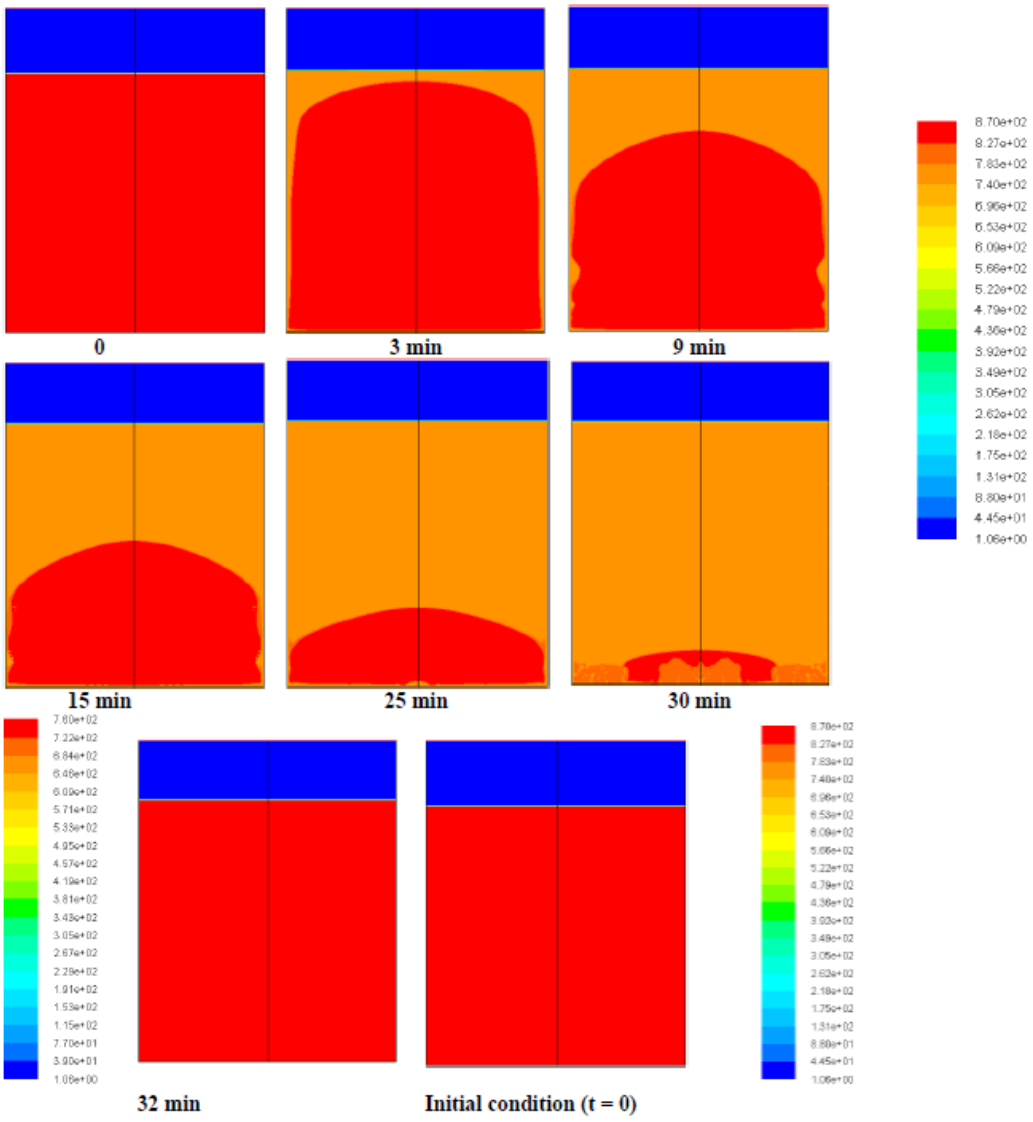


**Fig 4.13: Contours of increasing liquid level in rectangular cavity**

The heat flux is highest for highest Stefan number and lowest for lowest Stefan number. The maximum heat flux for Stefan number 0.28 is approximately 36 W/m$^2$ and for Stefan number 0.18 and 0.13 the values are 22 W/m$^2$ and 18 W/m$^2$ respectively. Figure 4.16 shows the effect of the presence of solid phase on Nussetl number. A decrease in Nusselt number is observed during the melting process, as the amount of solid fraction decreases. After initiation of melting process Nusselt number (Nu) is not significantly varing with Stefan number. Nusselt is defined as follows:

$$Nu = \frac{hl}{k} \qquad (4.4)$$

This implies that in this case the melting process is controlled by natural convection due to density difference. The density of PCM is not depending on the wall temperature of cavity. According to the assumptions taken for study density only vary between solidus to liquidus temperature. Therefore, in absence of any forced convection the Nusselt will not be affected by Stafan number.

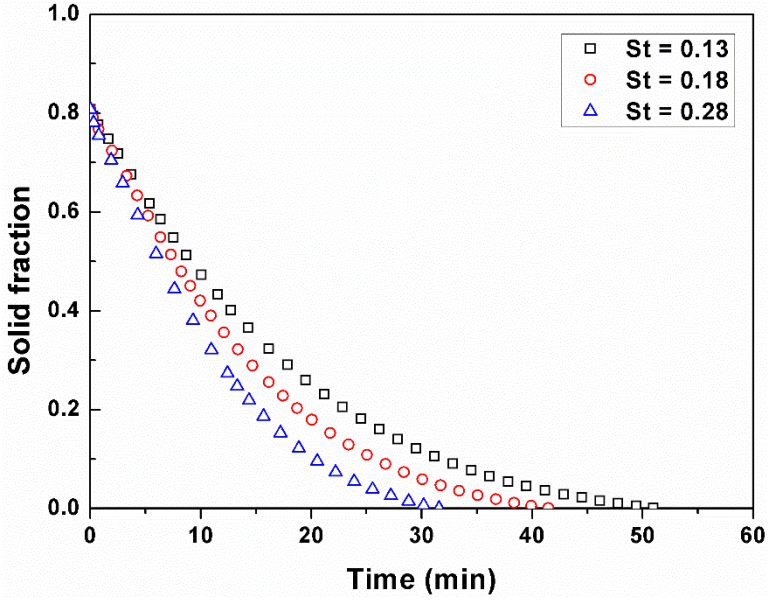


**Fig 4.14: Fraction of unmelted solid wax with time**

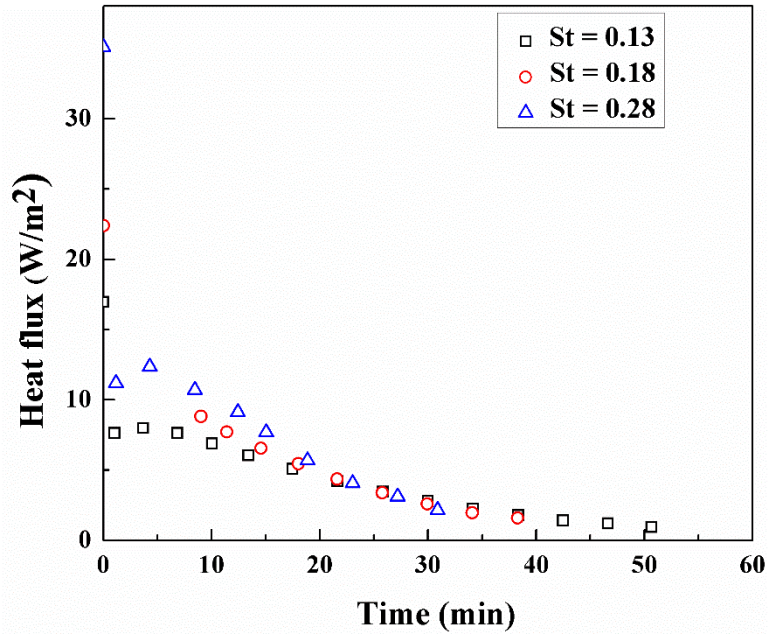


**Fig 4.15: Heat flux with time**

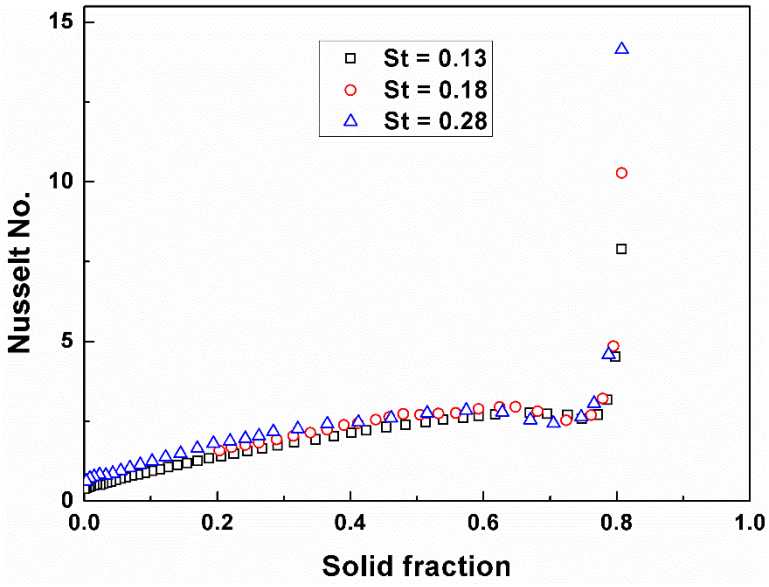


**Fig 4.16: Variation of Nussetl number with solid fraction of wax**

The melting process studied is controlled by conduction and convection processes. In this case, melting process occurs within a cavity and heat transfer is main energy tranfer process. Therefore, the un-melt or solid-fraction (*Sf*) is the function of Grasshof number, Stefan number, Fourier number and Prandtl number. The expression for Stefan number is given in Eqn. 4.2 and for Grasshof number (Gr), Fourier number (Fo) and Prandtl number (Pr) expressions are given below:

$$\left.\begin{aligned} Gr &= \frac{g\beta\Delta T L^3}{\nu^2} \\ Fo &= \frac{\alpha t}{s^2} \\ Pr &= \frac{\mu C_p}{k} \end{aligned}\right] \qquad (4.5)$$

From the parametric study of variation of a solid fraction with dimensionless time for different Stefan numbers, following empirical relation is obtained by minimising the sum of square of errors :

$$Sf = f(St, \mathrm{Fo}) = 0.8(1 - 0.4\, St^{3.6} Fo^{0.58}) \text{ (for St < 1)} \qquad (4.6)$$

Where the coefficients of empirical equations are a function of Grasshof number, Prandtl number of PCM, thermal diffusivity and dimension of the cavity. 0.8 represents the initial solid-fraction of PCM in the cavity. The constant coefficient 0.4

depends on the shape of cavity. The other coefficients 3.6 and 0.58 show the dependency of solid fraction on Stefan number and Fourier number. This empirical equation is valid only for one phase problem with Stefan number less than one. If Stefan number is equal or greater than one the effect of sensible heat transfer will increase than that of latent heat transfer. The above relation is used to calculate the amount of unmelt fraction at any time during the process.

### 4.3.4 Results & discussion: Melting process in rectangular cavity (50mm ×40mm) for different shape of initial PCM

The shape of solid PCM inside the cavity is also varied to check the contours of density and effect on melting. The initial shape taken is shown in Fig 4.17. The figure (Fig 4.17) shown contain different amount of PCM but all are rectangular in shape. In the first case, the solid PCM is in direct contact with sidewall of the cavity. The second case shows a distance or gap between sidewall of cavity and solid PCM and this gap are increased for the third case. The initial solid fractions of PCM are 0.8, 0.35 and 0.24 respectively. The progress of melting is presented through density contours shown in Fig 4.18. In Fig 4.18 the blue colour represents the air phase, red colour represents solid PCM and yellow colour represents the liquid phase. There is an increase in liquid PCM level with time. The shape of solid PCM becomes flatter and it occupies the bottom area of the cavity. Initially, the height of solid PCM is same in medium and minimum wax content. The height of solid PCM decreases with time is more in the minimum wax content cavity than that of the medium wax content cavity. The time required for complete melting is 41 min, 24 min and 19min respectively for three different initial shapes. The total melting time is calculated from Fig 4.19. The important observation is in this case is that the melting time is not proportional to the volume of initial PCM only. It is calculated from Fig 4.19 that for first (max wax content) and second initial shape (medium wax content) the ratio of volume is 2.28 and the melting time ratio is 1.7. For the second (medium wax content) and third (min wax content) initial shape the ratio of volume is 1.46 and the melting time ratio is 1.26. Therefore, the melting time ratio is less though the volume ratio is high for medium and minimum wax content. In such a situation another

factor influences the melting process or decreases the melting rate. In this case, the higher distance or gap between solid PCM and cavity wall for third (min wax content) makes the phase change process slower.

**Fig 4.17: Shape of initial wax content in cavity in rectangular cavity**

### 4.3.5 Conclusion

The study of melting in rectangular cavity shows that the melting time is lowest for the highest Stefan number. The heat flux is large in case of the highest Stefan number due to bouncy driven convection. An empirical equation is also driven to relate solid unmelt fraction in the cavity as a function of Stefan number and Fourier number. It is also shown that melting depends on the distance between the cavity wall and solid phase. The increasing distance shows an increase in melting rate.

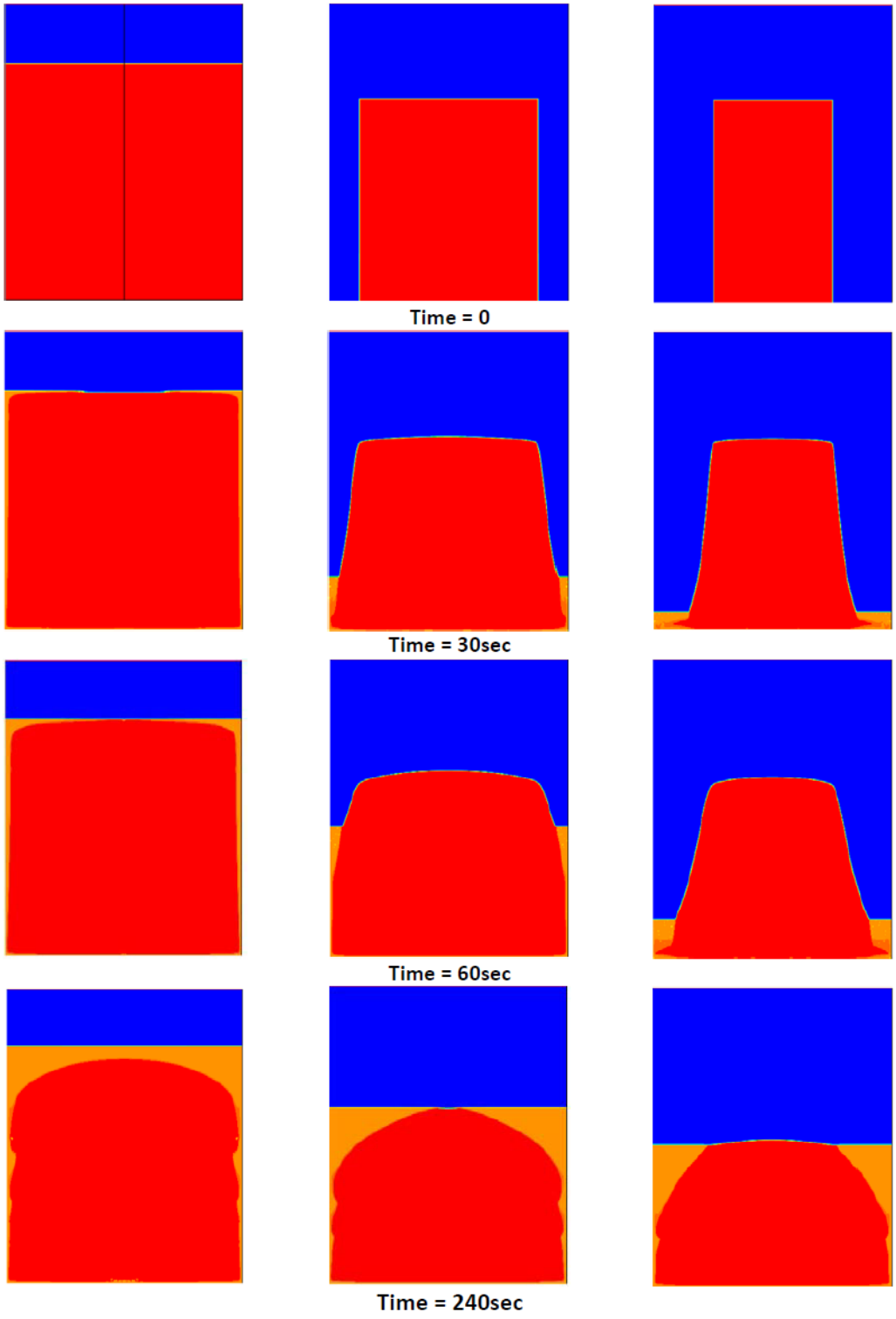


**Fig 4.18: Contour of density for different initial shape of PCM**

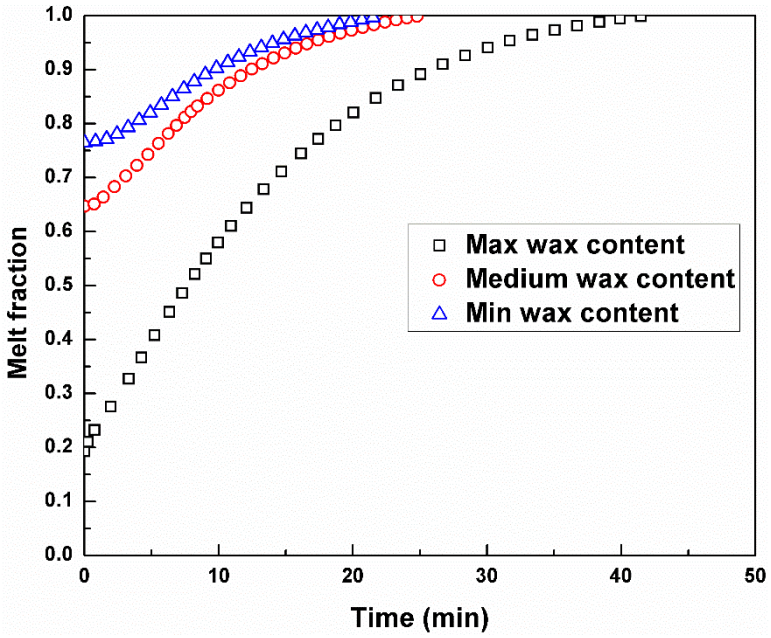


**Fig 4.19: Melt fraction (air +liquid PCM) for time for different initial shape of PCM**

## 4.4 Effect of shape of cavity on melting process

A comparative study of melting is presented to discuss the effect of shape on phase change. The results obtained are presented in Table 4.1. In the first case, the melting in rectangular cavity and spherical cavity are compared. The volume and area of spherical cavities are higher than that of rectangular cavity. The aspect ratio along the direction of fluid flow for rectangular cavity is 1.25 (H/W) higher than spherical cavity. Form the primary knowledge of convection heat transfer it has been seen that with an increase in above mentioned aspect ratio the Nusselt number or convection heat transfer effect is increasing (J.P. Holman). It is also observed that for same area of cavity the convection heat transfer is higher in spherical cavity. Therefore to check the rapidness of melting phase change process for same boundary and operating condition a higher aspect ratio for rectangular cavity is considered compared to spherical cavity. The size of rectangular cavity is 50mm×40mm (H×W) and diameter of spherical cavity is 60mm. Both the cavities are made of glass (k=0.81W/m. K). The height of PCM is 80% of total height in rectangular cavity and 85% of diameter in spherical cavity. The volume considered for different cavities is presented in Table 4.1. The volume and surface area is higher in case of spherical

cavity. The thermal boundary considered is same in both the cavities. The following Fig 4.20 (a) and (b) presents the variation of melt fraction (Liq. PCM +air) for constant cavity wall temperature of 315K and 320K respectively. The initial temperature of PCM is 300K or 1K less than the mean melting temperature. The interesting observation is that though the size of cavity and amount of PCM taken are different but, the time of complete melting is very close. Figure 4.20(a) shows though the initial PCM content is less in rectangular cavity the melt fraction variation with time is similar for 60 mm diameter spherical cavity and rectangular cavity. This concludes melting is faster in spherical cavity. Figure 4.20(b) shows that the initial solid-fraction of PCM in rectangular cavity is 0.8 and that of spherical cavity is 0.85. Since the volume fraction of PCM in rectangular cavity is higher than spherical cavity, the melting process is faster in rectangular cavity. After 24 minutes the difference in melt fraction between rectangular cavity and 80 mm diameter spherical cavity starts decreasing. This decrease in difference in melt fraction implies melting rate becomes slower in rectangular cavity and faster in spherical. On the other hand, for rectangular cavity and 60mm diameter spherical cavity the melt fraction is almost same up to 15 min and after that, the melting is faster in spherical cavity. The mechanism of phase change is close contact melting. In the rectangular cavity, the shape of unmelt shows the contact area between solid PCM and cavity wall decreasing continuously. On the other hand, the contact area between unmelt solid and wall is decreasing very slowly. This very slow change in contact area is continued till the cavity is half filled by unmelt or solid PCM. In both the cavities solid phase is sinking to the bottom of the cavity and takes shape of bottom surface of the cavity. The change of height of solid PCM is lower compared to bottom surface area of the cavity in spherical cavity than rectangular cavity. Therefore, higher contact area between hot wall and solid PCM makes the melting process many faster in spherical cavity. Initially, the melt fraction in rectangular is higher than spherical cavity because the rectangular cavity contains less solid PCM and more air than the spherical cavity. But, the change in melt fraction is higher in spherical cavity. The maximum heat flux at wall for same wall temperature is much lower in rectangular cavity than spherical cavity.

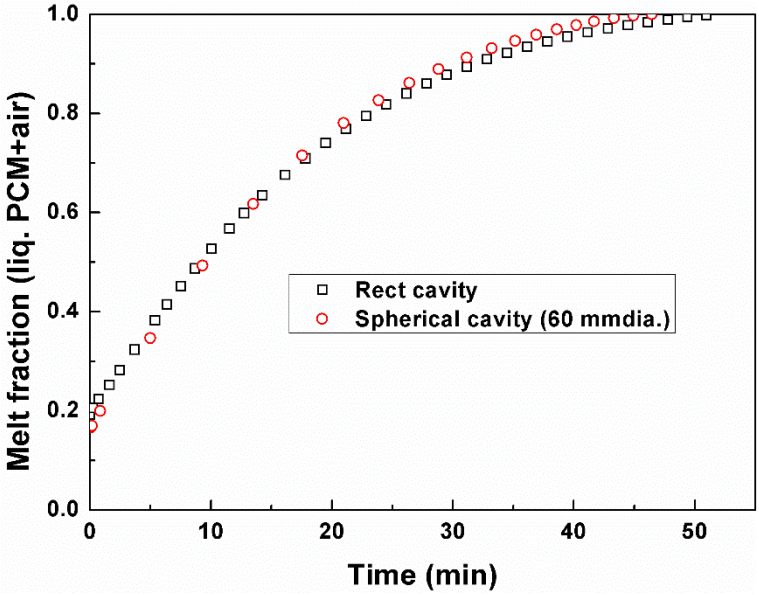


**Fig 4.20(a): Melt fraction in different shape cavities (wall temperature 315K)**

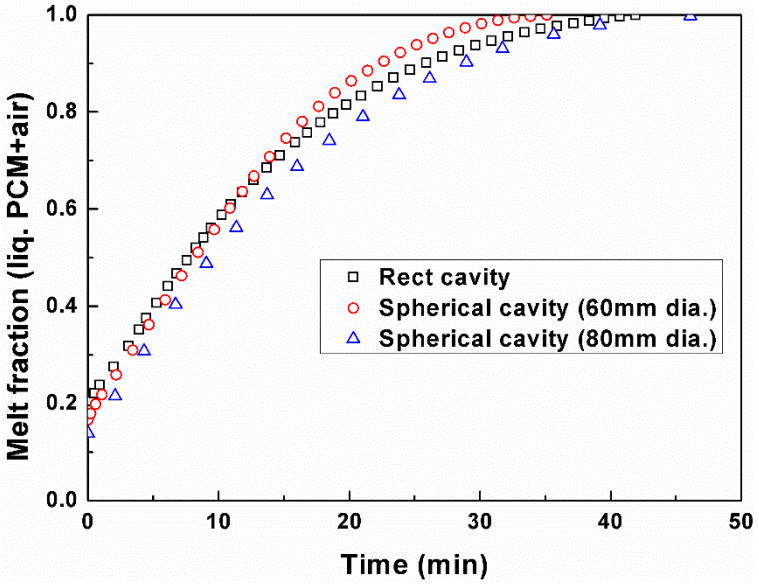


**Fig 4.20(b): Melt fraction in different shape cavities (wall temperature 320K)**

The empirical relation derived to study the effect of cavity wall temperature or Stefan number in order to compare the effect of cavity shape on melting. The derived correlation relates solid-fraction as a function of Stefan number and Fourier number. The derived relation or the coefficients are modified for Stefan number 0.18 for wall

temperature 320K. The parametric study shows that melting time is directly proportional to volume of PCM content ($V$) and inversely proportional to Stefan number ($St$) and area of the cavity ($V$). The relation may be written as follows: $t\infty \frac{V}{St^a.A^b}$

Comparing the melting time in 80mm diameter and 60mm spherical cavity for two different Stefan number the value of constants $a$ and $b$ are calculated. The values are $a = 1.05$ and $b = 0.82$. Similarly for rectangular cavity $a = 0.5$ and $b = 0.58$. Therefore,

For spherical cavity $$t\infty \frac{V}{St^{1.05}.A^{0.82}} \quad (4.7)$$

For rectangular cavity $$t\infty \frac{V}{St^{0.5}.A^{0.58}} \quad (4.8)$$

The above equations conclude that the increase in Stefan number or cavity wall temperature is more effective to minimise the melting time in spherical cavity. Similarly, the increased area decreases the melting time much more in spherical cavity than a rectangular cavity.

**Table 4.1: Effect of shape on melting**

| **Shape of cavity** | **Rectangular (2D)** | | **Spherical (2D)** | | **Spherical (2D)** |
|---|---|---|---|---|---|
| **Size of cavity** | 50mm×40mm (H×W) | | 60mm diameter | | 80 mm diameter |
| **Aspect ratio (H/W)** | 1.25 | | 1 | | 1 |
| **Area of cavity** | 0.0088 $m^2$ | | 0.011304$m^2$ | | 0.02$m^2$ |
| **Cavity material** | Glass | | Glass | | Glass |
| **Height of PCM in the cavity** | 80% of cavity height/40mm | | 85% of cavity height (diameter)/51mm | | 85% of cavity height (diameter)/70mm |
| **Volume (**$m^3$) | 0.0000628 | | 0.000113 | | 0.000268 |
| **Initial average volume fraction of PCM in cavity** | 0.8 | | 0.85 | | 0.85 |
| **Initial temperature of PCM (K)** | 300 | | 300 | | 300 |
| **Cavity wall temperature (K)** | 320 | 315 | 320 | 315 | 320 |
| **Time required for complete melting (min)** | 44 | 52 | 34 | 46 | 47 |
| **Maximum heat flux** ($W/m^2.K$) | 22.337 | 16.94 | 91.9 | 72.2 | 47.1 |
| **Empirical equation for unmelt solid fraction (320K)** | $Sf = 0.8(1 - 0.4\ St^{3.6}\ Fo^{0.58})$ | | $Sf = 0.85(1 - 0.45\ St^{3.6}\ Fo^{0.58})$ | | $Sf = 0.85(1 - 0.5\ St^{3.6}\ Fo^{0.58})$ |

**References**

A.D. Brent, V. R. V., K.J. Reid (1988). "Enthalpy-porosity technique for modeling convection-diffusion phase change: application to the melting of a pure metal." Numerical Heat Transfer **13**: 297-318.

A.V. Arasu, A. S. M. (2012). "Numerical study on melting of paraffin wax with Al2O3 in a square enclosure." International Communications in Heat and Mass Transfer **39**: 8–16.

B. Binet, M. L. (2000). "Melting from heat sources flush mounted on a conducting vertical wall " International Journal of Numerical Methods for Heat & Fluid Flow **10**: 286-307.

Babak Kamkaria, H. J. A. (2017). "Numerical simulation and experimental verification of constrained melting of phase change material in inclined rectangular enclosures." International Communications in Heat and Mass Transfer **88**: 211-219.

Davide Masato, M. S. G. L. (2017). "Prototyping and modeling of the centrifugal casting process for paraffin waxes." Materials and Manufacturing Processes.

Debasree Ghosh , C. G. (2019). "Numerical and experimental investigation of paraffin wax melting in spherical cavity." Heat and Mass Transfer **55**(5): 1427-1137.

E. Assis, G. Z., R. Letan (2009). "Numerical and experimental study of solidification in a spherical shell." Journal of heat transfer **131**: 1-5.

E. Assis, K., L., Ziskind, G., and Letan, R (2007). "Numerical and Experimental Study of Melting in a Spherical Shell." International Journal of Heat and Mass Transfer **50**: 1790-1804.

E. Assis, L. K., G.Ziskind, R.Letan (2007). "Numerical and Experimental Study of Melting in a Spherical Shell." International Journal of Heat and Mass Transfer **50**: 1790–1804.

E. Assis, L. K., G.Ziskind, R.Letan (2007). "Numerical and Experimental Study of Melting in a Spherical Shell." International Journal of Heat and Mass Transfer **50**: 1790–1804.

F.L. Tan, S. F. H., J.M. Khodadadi, L. Fan (2009). "Experimental and computational study of constrained melting of phase change materials (PCM) inside a spherical capsule." International Journal of Heat and Mass Transfer **52**: 3464–3472.

F.L.Tan (2008). "Constrained and unconstrained melting inside a sphere." International Journal of Heat and Mass Transfer **35**: 466–475.

Hamid Ait Adine, H. E. Q. (2009). "Numerical analysis of the thermal behaviour of a shell-and-tube heat storage unit using phase change materials." Applied Mathematical Modelling **33**: 2132-2144.

J.M. Khodadadi, S. F. H. (2007). "Nanoparticle-enhanced phase change materials (NEPCM) with great potential for improved thermal energy storage." International Communications in Heat Mass Transfer **34**: 534-543.

J.M.Khodadadi, Y. Z. (2001). "Effects of buoyancy-driven convection on melting within spherical containers." International Journal of Heat and Mass Transfer **44**: 1605–1618.

J.P. Holman, S. B. Heat transfer, Tata McGraw Hill Publishing company limited.

M.Z.M. Rizan, F. L. T., C.P. Tso (2012). "An experimental study of n-octadecane melting inside a sphere subjected to constant heat rate at surface." International Communications in Heat and Mass Transfer **39**: 1624-1630.

P. Maarten Biesheuvel, A. N., Henk Verweij (1998). "Theory of Batchwise Centrifugal Casting." AIChE **44**(8): 1914-1922.

S. Lorente, A. B., J.L. Niu c (2014). "Phase change heat storage in an enclosure with vertical pipe in the center." International Journal of Heat and Mass Transfer **72**(329-335).

Sin Kim, M. C. K. a. S.-B. L. (2001). "Prediction of Melting Process Driven by Conduction-Convection in a Cavity Heated from the Side." Korean Journal of Chemical Engineering **5**(18): 593-598.

Su-Ling Lu, F.-R. X., Shuang-Jie Zhang, Yong-Wei Mao, Bo Liao (2014). "Simulation study on the centrifugal casting wet-type cylinder liner based on ProCAST." Applied Thermal Engineering **73**: 512-521.

T.S. Saitoh, H. H., K. Yamada (1997). "Theoretical analysis and experiment on combined close-contact and natural convection melting in thermal energy storage spherical capsule." Proc. Energy Conversion Engineering Conference **3 IEEE**: 1656-1661.

T.S. Saitoh, H. K., H. Hoshina (1996). "Theoretical analysis for combined closecontact and natural convection melting in ice storage spherical capsule." Proc. Energy Conversion Engineering Conference **3IEEE**: 2104-2108.

Yifei Wang, L. W., Ningning Xie, Xipeng Lin, Haisheng Chen (2016). "Experimental study on the melting and solidification behavior of erythritol in a vertical shell-and-tube latent heat thermal storage unit." International Journal of Heat and Mass Transfer **99**: 770-781.

# CHAPTER 5

# STUDY OF SOLIDIFICATION PROCESS IN DIFFERENT CAVITIES

# CHAPTER 5

# STUDY OF SOLIDIFICATION PROCESS IN DIFFERENT CAVITIES

## 5.1 Introduction

The solidification is the reverse process of melting. Both melting and solidification involve at least one solid and one liquid phase of phase changing material (PCM). The number of research documented in melting is much higher than that of solidification. This is probably because simulation of melting is little easy to validate experimentally. However, the solidification processes are very common for natural and industrial processes. The solidification process is very important in different casting processes and in discharging period of energy saving processes. Discharging period of energy saving processes refers to the heat discharging period of liquid PCM in latent heat energy storage device. Ghosh and Guha studied the melting of an organic PCM (RT27) under different thermal boundary conditions and for different cavity materials(Debasree Ghosh 2019). In this chapter, the solidification of same PCM (RT27) is studied in spherical cavity. The solidification in spherical and rectangular cavities is also compared. The solidification process depends on the thermo-physical properties of PCM, thermal and flow boundary conditions and size, shape of cavity. The discharging or solidification time is dependent on thermal boundary condition. The thermo-physical properties of PCM changes due to solidification which affects the rate of phase change processes. The change in volume and density restricts the movement of PCM and hence the rate of heat transfer is not uniform throughout the process. In case of high temperature PCM, the cavities sometimes get damaged due to uneven heat loss at different positions of cavity wall. A number of theoretical and experimental works has been done on solidification. The literatures are available for different inclination of cavity. K.A.R. Ismail et al. studied the solidification for different cavity surfaces for only conduction heat transfer and without natural convection(K.A.R. Ismail 2000; K.A.R. Ismail 2014). Y. Hong et al. studied the effect of inverted cavity during the solidification in

rectangular cavity. The thermal behavior is improved by inverting the cavity(Yuxiang Hong 2018). Sharma et al. compared the solidification time of pure copper and copper-water nano-fluid under controlled temperature and concentration (R.K. Sharma 2014). The effect of wall inclination is also shown in this chapter. They also considered that the upper and lower walls of the cavity are insulated. S. Chakraborty et al. simulated the solidification of binary alloy which is solidified or cooled from the top and side wall rectangular cavity is insulated(S. Chakraborty 2003). They used turbulence k-€ model for this study which is also used for other metal alloys(W. Shyy 1992). M.A. Ezan, M. Kalf used Consistent-Update-Technique algorithm for two dimensional simulation of solidification of water in rectangular cavity. During freezing of water, cooling is provided only in one side at a time(M. A. Ezan 2016). M.T. Stickland et al. experimentally studied the solidification of water in a differentially heated cavity. These observations are also limited to upper and lower insulated wall(M.T. Stickland 2007). Literatures show the numerical studies of solidifications are mostly done with conduction only and natural convection is neglected. The solidification processes studied in referred literatures considered different thermal boundary conditions and orientation of cavity. The author found that the mentioned literature did not include the following:

**(i)** The presence of air in the cavity is not considered in melt fraction calculation. The melt fraction is calculated with respect total PCM only. The study of shrinkage of PCM during solidification needs to consider the presence of air.

**(ii)** The comparisons of solidification processes in different cavities are very rare.

In this chapter, the presence of air in the cavity is considered during calculation of melt fraction. The solidification in spherical and rectangular cavities is compared for unconstrained solidification. This numerical study is important to overcome the difficulties involved in transient study of unconstrained solidification processes. An unconstrained solidification process refers to those processes where no measuring devices should touch the phase change material. For example if any thermocouple is

used to the temperature of PCM during the process the movement of liquid phase or solid-liquid interface will be affected. Moreover, if the initial temperature of thermocouple is less than the solidus temperature of PCM the solidification will start from the surface of thermocouple. In unconstrained solidification, the solidification process starts from the inner boundary wall of the cavity. Such solidifications are common for storing frozen foods and for controlling temperature in buildings by using PCM. On the other hand, the experimental study of unconstrained solidification through image analysis is also very difficult if solidification starts from the wall of the cavity. The nontransparent solid phase at cavity wall will make the liquid phase invisible. Therefore, numerical simulation will help to analyze the solidification process. The effect of cavity shape can be compared through such theoretical studies.

## 5.2 Physical model

Fig. 3.7(a) and Fig. 3.7(b) represent the physical domain of the cavities. The cavities are spherical and rectangular in shape. Diameter of spherical cavity is 80mm and rectangular cavity is 50mm in height and 40mm wide. Both the cavities are considered to be made of 2mm thick copper sheet. PCM taken for solidification study is paraffin wax (RT27). The cavities are partially filled and the level of PCM is 80% of total height of cavity. Initial temperature of the PCM is taken as 1K greater than the liquidus temperature of PCM. Outer surface temperature of the cavity is kept at temperature less than the solidus temperature of PCM. The thermo-physical properties of PCM are same as taken for study of melting case as discussed by Ghosh and Guha (Debasree Ghosh 2019). These thermo-physical properties of PCM are given in Table 3.2. In the study of melting process it is observed that melting time is lowest for high thermal diffusivity material copper cavity. Therefore, to reduce the solidification time copper cavity material is considered (Debasree Ghosh 2019). During solidification process a constant temperature is maintained at the cavity wall.

## 5.3 Computational domain

A transient two dimensional flow is assumed within the cavity. The phases within the cavity are isotropic and homogeneous in nature. A symmetric two dimensional model is drawn and quadrilateral meshing is applied to the computational domain. The axisymmetric model in Ansys-fluent 16.2 is chosen for simulation of the phase change process. Since the process is symmetric with respect to the axis of cavity, an axisymmetric model will reduce the computation time. Both PCM and air phases are assumed as Newtonian fluids and the flow is incompressible. A laminar flow type is assumed in both phases. The variation in density of air with temperature is defined by the relation: $\rho = 1.2 \times 10^{-5}T^2 - 0.01134T + 3.4978$(E. Assis 2007; E. Assis 2009). The solidification process of paraffin wax with same operating and boundary conditions are repeated in rectangular cavity. The computational domain are shown is Fig. 3.7(a) and Fig. 3.7(b).

## 5.4 Results and discussion

### 5.4.1 Solidification in spherical cavity

In this study 80mm diameter spherical cavity contains liquid PCM and suddenly the temperature of the cavity wall is decreased. The liquid PCM, which is in contact with cavity wall, starts solidifying. Due to natural convection, the thickness of solid phase formed is higher at the bottom of the cavity. Since the higher density PCM is at bottom of the cavity, bouncy force of solid phase do not have an important role. The contours of melt-fraction, density are shown in Fig. 5.1(a) and static temperature and velocity are shown Fig. 5.1(b). The contours are obtained from the simulation of solidification of paraffin wax (RT27) copper cavity for 274K (St = 0.28) wall temperature. The blue color in density contours shows, that the air is present in the cavity. The volume of air-phase increases due to decrease in volume of high-density solid PCM. The contour of melt-fraction and density show the solidification starts from the low-temperature cavity wall and due to natural convection, the thickness of solid PCM at bottom is higher compared to the upper section of wall. The static temperature is varying uniformly from the inner surface of cavity wall to the solid-

liquid interface. The velocity contour shows the velocity is not significant in solid phase and from 958.75 sec or 15 min onwards no velocity variation is observed in the PCM phase. The difference is melt fraction and temperature contours are noticed at the upper part of cavity which is occupied by air. This is because the temperature of air changes, but air remains in fluid form.

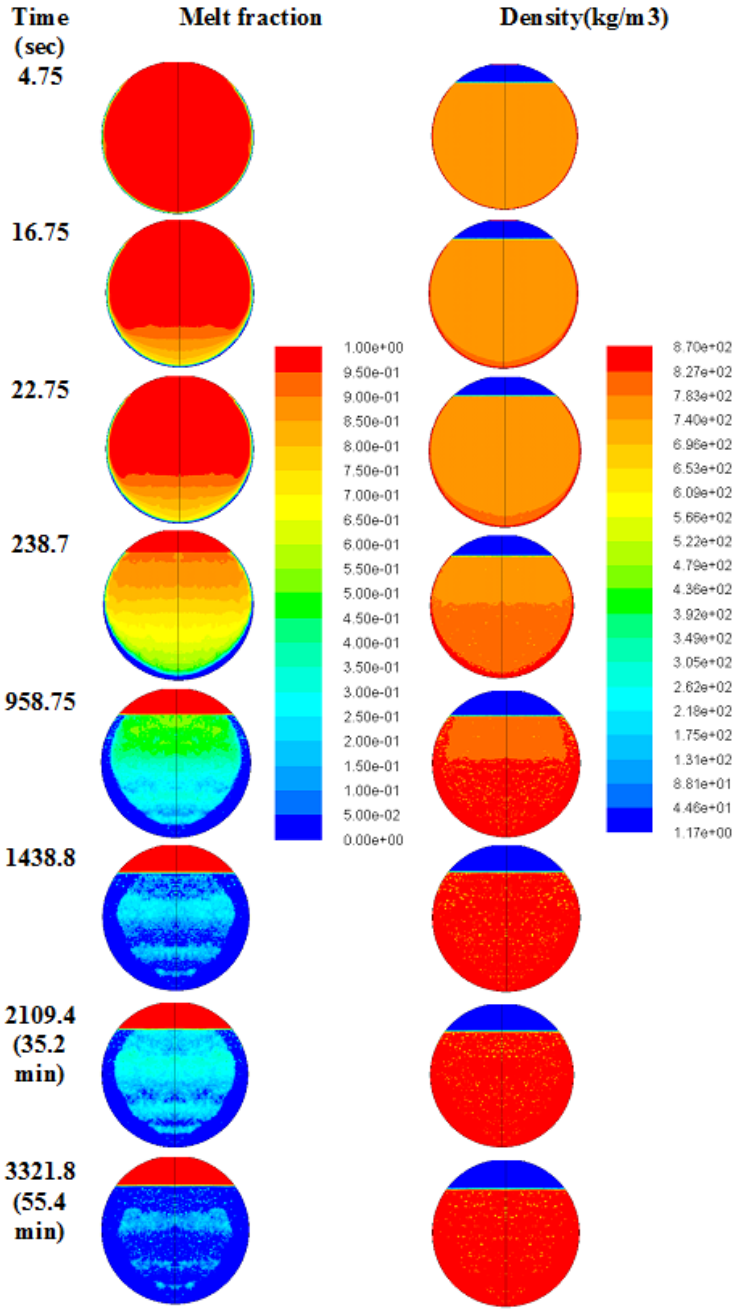


**Fig 5.1(a): Melt fraction and density contours of solidification in spherical cavity**

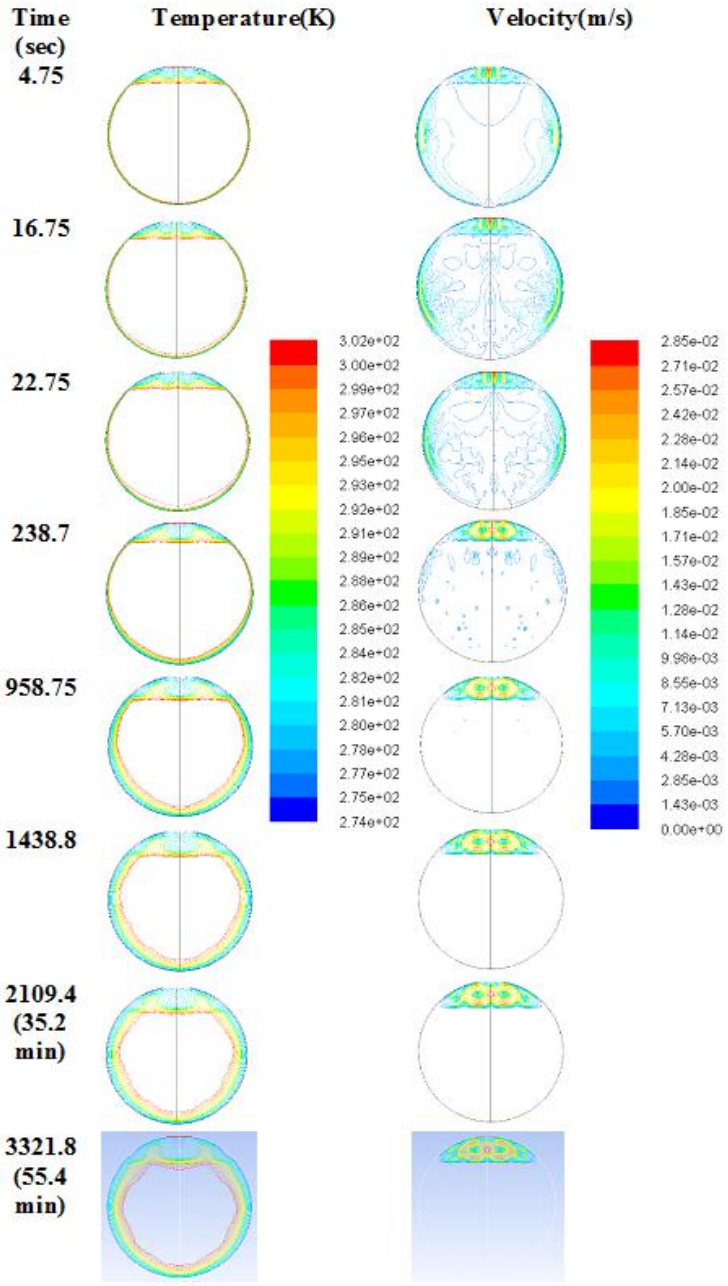


**Fig. 5.1 (b): Temperature and velocity contours of solidification in spherical cavity**

The effect of Stefan number on the solidification time is shown in Fig 5.2. Figure 5.2 shows the solidification time 146 min for Stefan number 0.12 with final melt fraction (air + liquid PCM) 0.35. For Stefan number 0.18 the solidification time is 80 min with final melt fraction (air + liquid PCM) 0.346 and for Stefan number 0.28 the solidification time is 56 min with final melt fraction (air + liquid PCM) 0.28. In this figure, the vertical axis represents the fraction of melt fraction or liquid fraction of the cavity and the liquid or fluid phase includes air also. Therefore, after completion

of solidification process, the cavity contains some air which is the liquid or melt fraction in that cavity. Hence, at the end of phase change process, the melt fraction becomes non zero constant. The initial volume fraction of liquid PCM in spherical cavity is 0.8. Therefore, the final melt fraction in spherical cavity greater than 0.2. The volume solid is less than that of liquid. So, final melt fraction will be greater than initial solid fraction in the cavity. Final melt fraction is the fraction of air content in the cavity after complete solidification. The solidification time is minimum for the maximum Stefan number and maximum for minimum Stefan number. The solidification process is assumed to be complete when the melt fraction (air + liquid PCM) becomes constant with time. The final values of melt fraction (air + liquid PCM) after complete solidification are not same for different Stefan number. The deviation in final melt fraction (air + liquid PCM) is due to trapping of semisolid PCM within the solidified zone. The heat transfer area for conduction decreases radially towards the center of the cavity. Therefore, the liquid phase present at the interior of cavity will not be able to release the heat completely through the thin layer. The lower heat transfer area and the low thermal conductivity of solidified PCM resist the completion solidification process. In case of higher Stefan number 0.28, due to high temperature difference between mean melting temperature and cavity wall temperature, the maximum solidification occurs. On the other hand, for Stefan number 0.12 and 0.18 the solidification process is very small due to the same reason. The initial variation in melt fraction (air +liquid PCM) with time is very small for different Stefan numbers. The melt fractions are same up to approximately 5 min and the corresponding melt fraction is 0.85. For up to 18 min where melt fraction is about 0.45, this variation is significantly less for Stefan number 0.18 and 0.28. Therefore, the solidification processes is initially not affected by Stefan number. The effect of convection heat transfer is dominating the process initially and shows an approximately same variation in melt fraction. After around 0.5 melt fractions, the melt fraction variation is deviating significantly from each other as shown in Fig. 5.2. The increase in solid thickness offers an additional thermal resistance. The heat conduction through solid PCM is lower because of this increasing solid thickness. The low thermal conductivity and slower natural convection decrease the rate of

heat loss at the outer surface of the cavity. As a result of it, the rate of latent heat transfer also decreases at solid-liquid interface. Less heat is conducted through the solidified zone for lower Stefan numbers. Hence, the solidification proceeds with slower rate for low Stefan numbers. It means, longer time is required for solidification of semi-solid material for lower Stefan numbers.

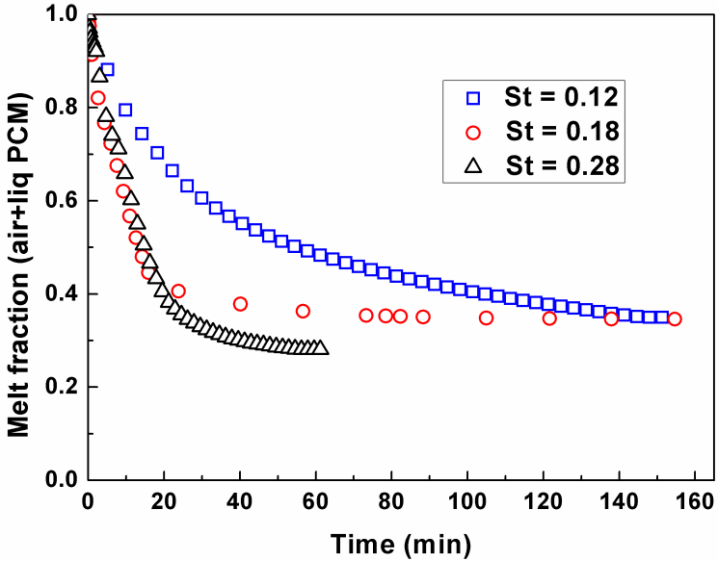


**Fig 5.2: Melt fraction (air + liquid PCM) variation in spherical cavity for different Stefan number**

In Fig 5.3 the heat flux variations with time are shown for different Stefan numbers. The maximum heat flux for Stefan number 0.28 is -180 W/m$^2$, for Stefan number 0.18 is -120 W/m$^2$ and for lowest Stefan number 0.12 is -75 W/m$^2$ approximately. The negative sign in heat flux indicates the heat loss from the cavity. At the time of initiation of solidification process the heat flux is highest for higher Stefan number and then remains unaffected by Stefan number. The average heat flux in the cavity is almost constant after 7 min of initiation of solidification phase change at constant cavity wall temperature. After 18 mins the heat flux is -0.43 W/m$^2$ for Stefan number 0.18 and 0.28 and heat transfer area of conduction controls the process. Since the solidification occurs from the outer wall, the bouncy force affects the motion of liquid PCM. Therefore, PCM forms a non-uniform solidified region, the thickness of which is higher at the bottom of the cavity compared to top of the cavity wall. Therefore, natural convection increases the heat transfer process. Once solidification

starts, the thermal resistance offered by solidified PCM increases rapidly and decreases the effect of natural convection. Hence, the heat flux variations are same for the all three Stefan number. The lower motion or liquid PCM motion makes solidification process slower than melting process for same Stefan number at the boundary of the cavity. Due to natural convection and bouncy force, the unconstrained melting is much faster than the unconstrained solidification process for same Stefan number. Figure 5.4 shows the comparison of solidification and melting in spherical cavity.

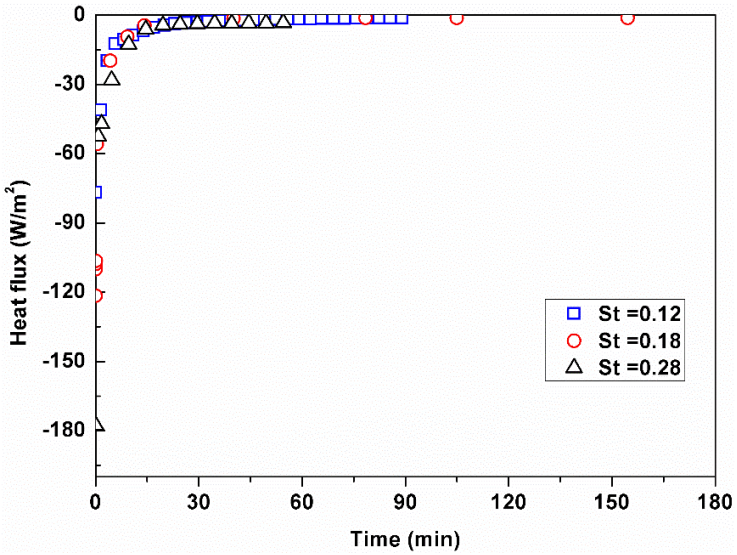


**Fig 5.3: Heat flux variation in spherical cavity for different Stefan number**

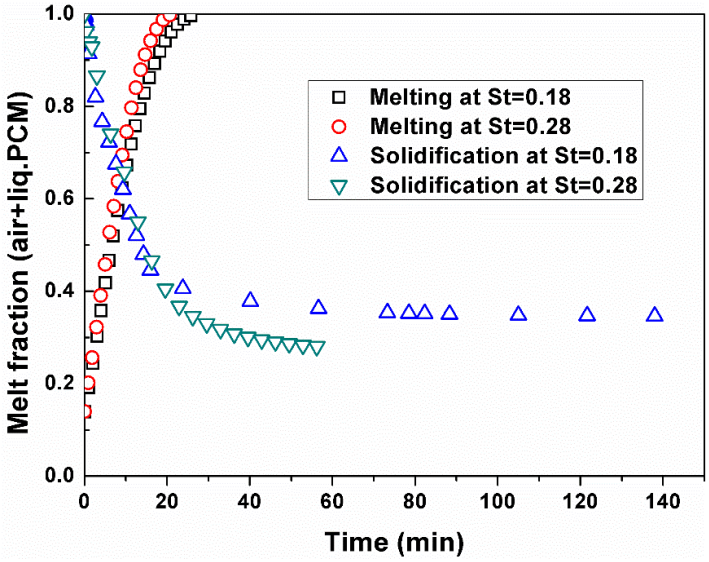


**Fig 5.4: Comparison of melting and solidification in spherical cavity**

### 5.4.2 Solidification in rectangular cavity

The solidification of paraffin wax (RT27) is studied for different Stefan number or wall temperature in rectangular cavity of size 50 mm×40 mm. The temperature of outer wall and bottom wall are kept at lower temperature than the solidus temperature. In this study, the wall temperature are 290K (St =0.12), 284K (St = 0.18) and 274K (St = 0.28) respectively. The level of liquid paraffin wax taken is 80% of height of the cavity. The contours of melt fraction, density at different times are shown in Fig. 5.5(a) and temperature and velocity at different times are shown in Fig. 5.5(b). The density contours of Fig 5.5(a) confirm the shrinkage of volume of PCM. The velocity contour shows the movement of interface only. These are significant in air phase and very small solid-liquid interface. Hence, the process is controlled by conduction heat loss. The decrease in melt fraction with time for different Stefan number is shown in Fig. 5.6. In the Fig. 5.6 the melt fraction refers to the volume fraction of air and liquid PCM present in the cavity. A decreasing trend of melt fraction is observed. The decreasing trend of melt fraction ensures the progress of solidification process. The change in melt fraction is highest for the highest Stefan number (lowest wall temperature, 274K) and lowest for the lowest Stefan number (highest wall temperature, 290K). The times taken for complete solidification are 120 mins, 146 mins and 262 mins for Stefan numbers 0.28, 0.18 and 0.12 respectively. The constant volume of melt fraction with time ensures the completion of solidification process. The final melt fraction in cavity is 0.237. This melt fraction is the volume fraction of air in the cavity. Therefore, the final solid fraction of PCM in cavity is 0.763. The initial PCM volume fraction is 0.8. Therefore, shrinkage of volume due to solidification is observed due to the change in density of PCM. Figure 5.7 shows the variation of heat flux with time for different Stefan number. The negative value of heat flux implies the heat loss from the cavity. Initially the magnitude of heat flux is maximum for highest Stefan number and lowest for the lowest Stefan number. The maximum heat flux for Stefan number 0.28 is -34.88 W/m$^2$, for Stefan number 0.18 is -21.69 W/m$^2$ and for lowest Stefan number 0.12 is -14.8 W/m$^2$. The solidification is simulated for constant wall temperature where the PCM starts solidifying from the cold wall of the cavity. As time goes, the

thickness of solid layers increases at the wall but the layer thickness is not uniform. The decrease in temperature results in an increase in density and introduces the bouncy effect and natural convection. Due to this bouncy effect, the thickness of solid PCM is greater at the bottom of the cavity. The variation in velocity shown in Fig 5.8 is due to different Stefan number is approximately within the range of 0.015 m/s to 0.032 m/s. The volume average maximum velocity exists in the air phase. Therefore, the variation is very low.

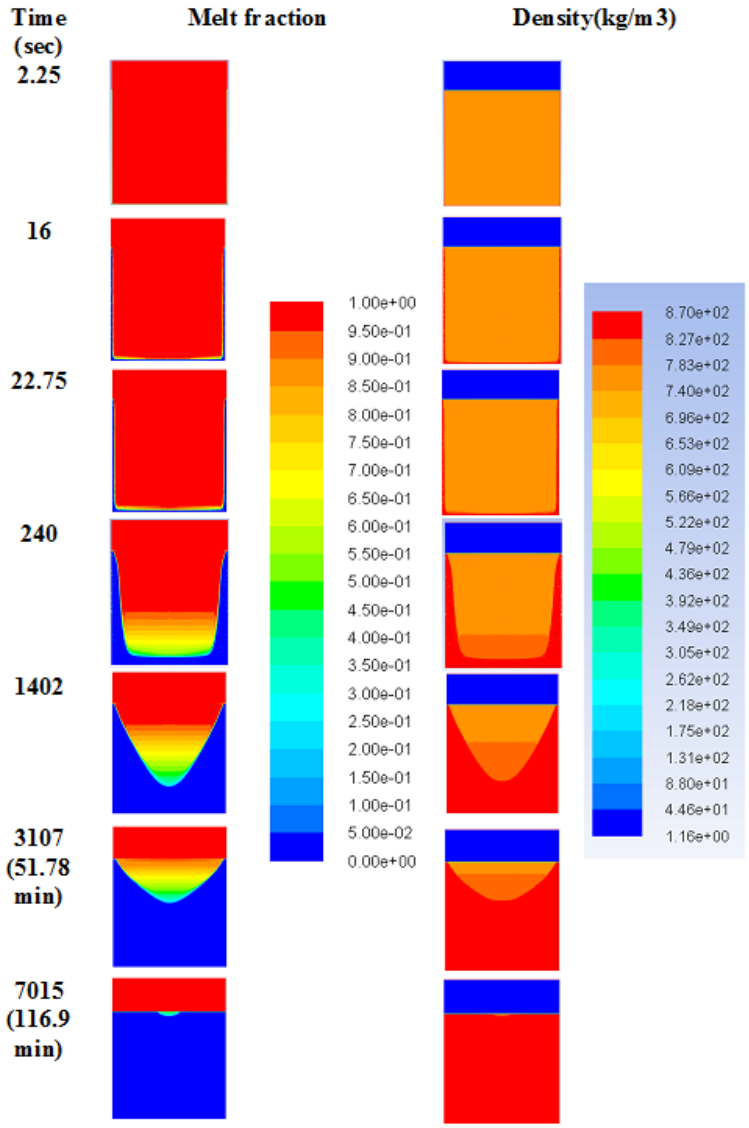


**Fig 5.5(a): Melt fraction and density contours of solidification in rectangular cavity**

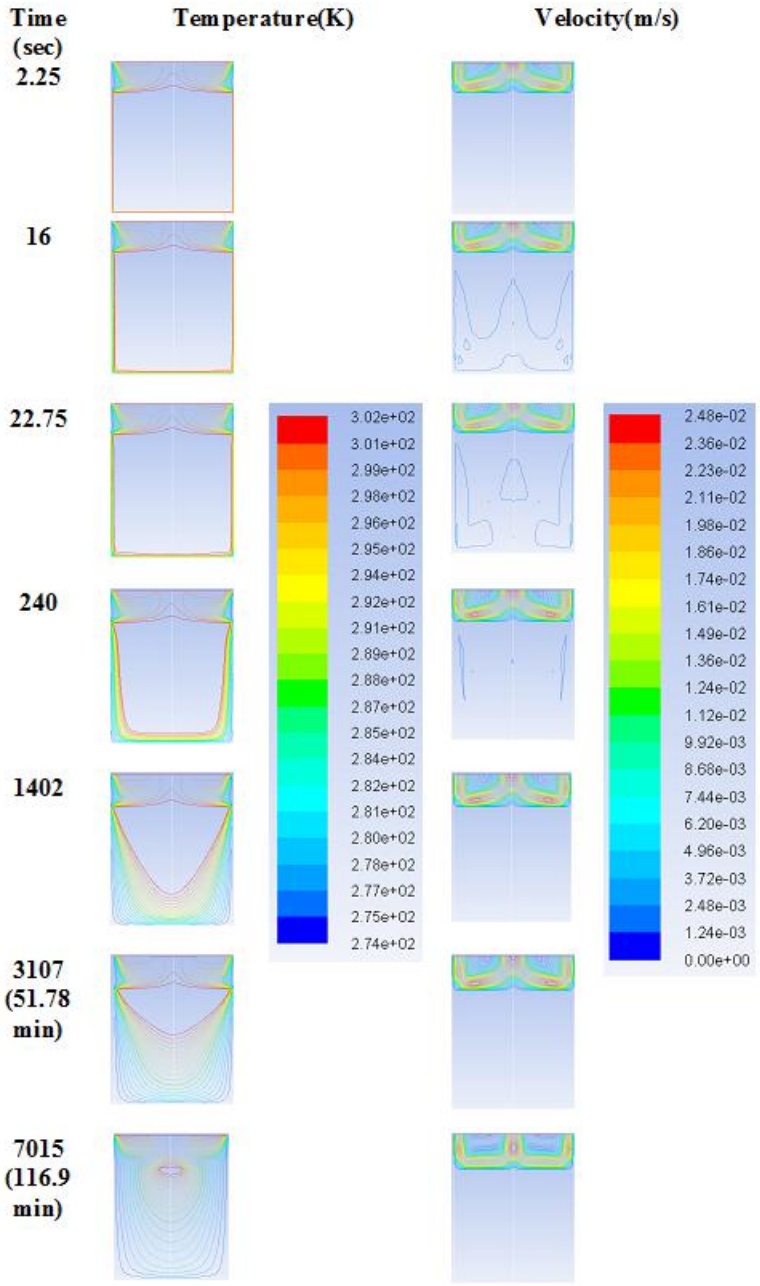


**Fig 5.5(b): Temperature and velocity contours of solidification in rectangular cavity**

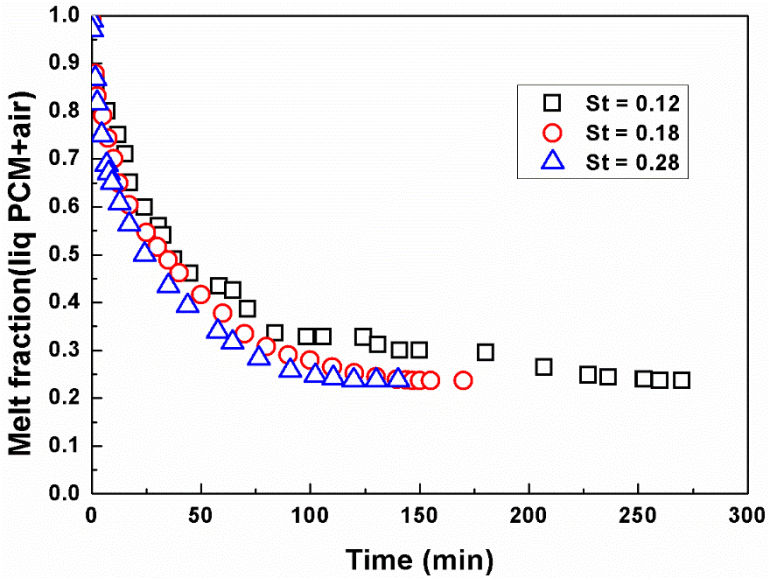


**Fig 5.6: Melt fraction (air +liquid PCM) variation in rectangular cavity for different Stefan number**

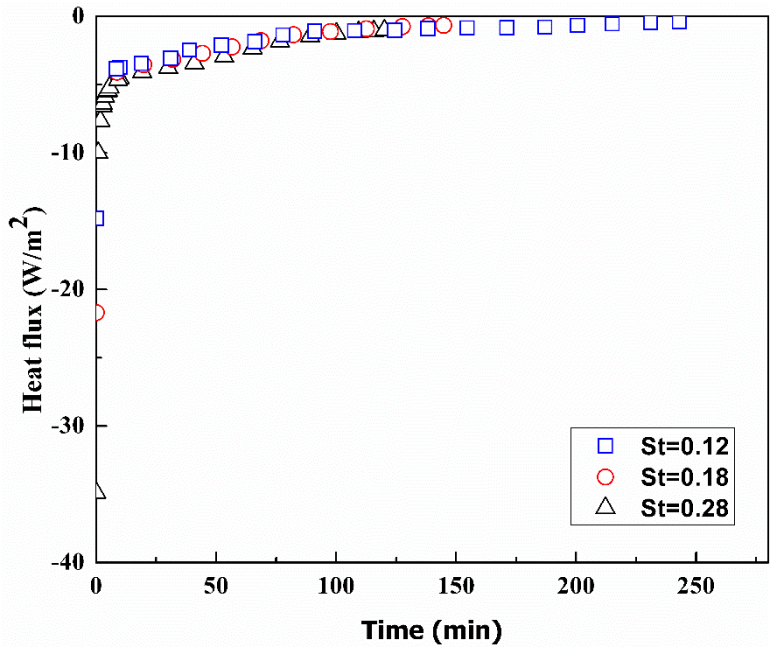


**Fig 5.7: Heat flux variation in rectangular cavity for different Stefan number**

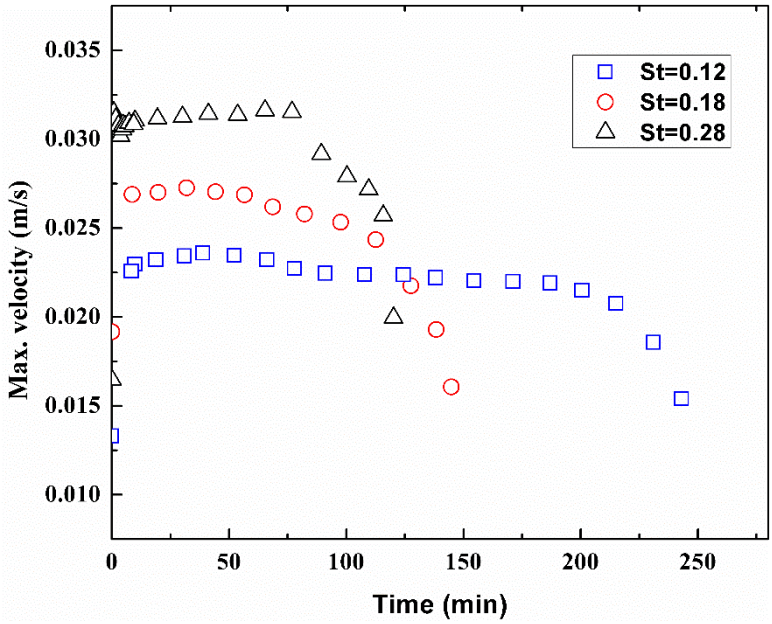


**Fig 5.8: Velocity variation in rectangular cavity for different Stefan number**

### 5.4.3 Effect of shape of cavity on solidification process

The solidifications of paraffin wax (RT 27) are performed in spherical and rectangular cavity. The solidifications are studied in 80mm diameter spherical cavity and 40 mm×50 mm rectangular cavity. The solidification times are compared for same Stefan numbers. It is found that solidification time is much lower in spherical cavity. For Stefan number 0.12 the solidification times are 262 min in rectangular cavity and 146min in spherical cavity. Similarly, for Stefan number 0.18, the solidification times are 146 min and 80 min in rectangular and spherical cavity respectively. The lowest solidification time is for highest Stefan number. In this case, highest Stefan number (St =0.28) solidification time is 120 min, in rectangular cavity and 56 min, in spherical cavity. Figure 5.9 shows the comparison solidification in spherical and melting time for Stefan number 0.28. It shows that, initially solidification depends on Stefan number and after around 0.5 melt fraction the process is affected by shape of the cavity. Figure 5.10 shows the effect of Stefan number on solidification time for rectangular cavity and spherical cavity. The solidification time is higher in rectangular cavity, though the volume and area are less for rectangular cavity. The reason behind this is initial heat flux is much higher at cavity wall of spherical shape. The maximum heat flux for Stefan number 0.28 is -

180 W/m$^2$ for spherical cavity and -34.88 W/m$^2$ for rectangular cavity. Moreover, the area normal to the direction of heat transfer increases at higher rate for spherical cavity than rectangular cavity, which makes the solidification process faster in spherical cavity. The effect of Stefan number on solidification is almost same and the graphs are almost parallel to each other. The solidification process is conduction dominated and hence the flow of PCM due to gravity is less in rectangular cavity compared to spherical cavity. Therefore, effect of surface area of cavity is higher than the effect of Stefan number.

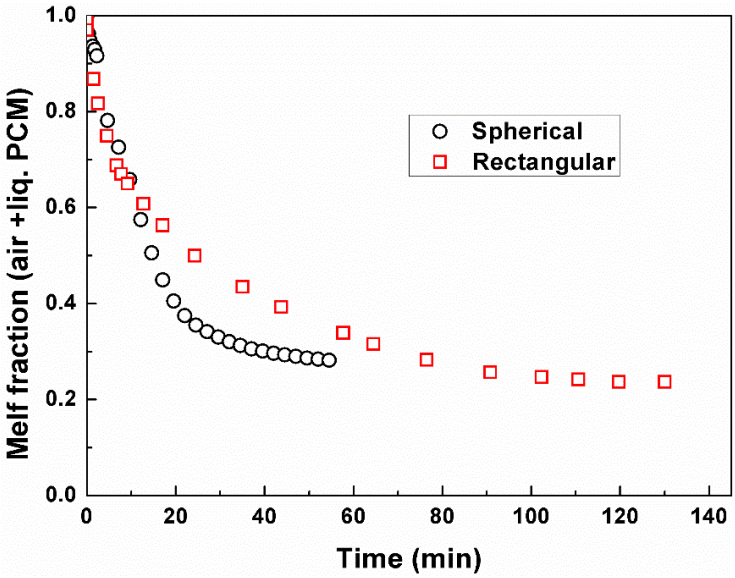


**Fig 5.9: Comparison of solidification in spherical and rectangular cavity (St=0.28)**

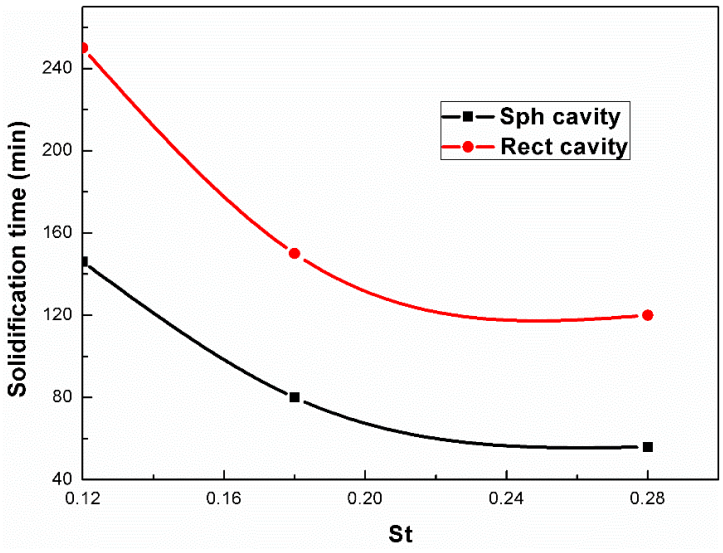


**Fig 5.10: Effect of Stefan number on solidification time**

## 5.5 Conclusion

The numerical simulations of solid-liquid phase change are very important for transient study of the process. The experimental study of solid-liquid phase change, specially concentrates on the boundary conditions and the physical properties of the final solid product. In this chapter the solidification of paraffin wax for different Stefan numbers are studied. The results are shown for rectangular cavity and spherical cavity. The enthalpy-porosity model is used for this study. The model is validated with experimental results of melting process(Debasree Ghosh 2019). The study concludes:

1. The solidification process is faster in spherical cavity than rectangular cavity. This is because the heat flux is lower in rectangular cavity. Moreover in the axisymmetric model, heat transfer occurs in radial direction and the heat transfer area increases along the direction of heat transfer. In spherical cavity this area in higher than the rectangular cavity and makes the solidification process faster in spherical cavity.
2. The solidification is conduction dominated since it starts from the low temperature cavity wall. Therefore, bouncy effect is less during the process.
3. The results obtained are compared with the previous study of melting process and found that solidification and melting time are not equal for spherical cavity(Debasree Ghosh 2019). The low thermal conductivity of solid phase and lower bouncy effect makes the solidification process slower than melting.

Therefore, this type of simulation will help to overcome the limitation of the experimental study of the solidification process. The details of heat and flow analysis will be possible through such numerical simulations.

## References:


A.R. Archibold, M. M. R., D.Y. Goswami, E.K. Stefanakos (2014). "Analysis of heat transfer and fluid flow during melting inside a spherical container for thermal energy storage." Applied Thermal Engineering 64: 396-407.

A.W., D. (2005). Introduction to Computational Fluid dynamics Cambrige University Press.

Debasree Ghosh, C. G. (2019). "Numerical and experimental investigation of paraffin wax melting in spherical cavity." Heat and Mass Transfer 55(5): 1427-1437.

E. Assis, G. Z., R. Letan (2009). "Numerical and experimental study of solidification in a spherical shell." Journal of heat transfer 131: 1-5.

E. Assis, K., L., Ziskind, G., and Letan, R (2007). "Numerical and Experimental Study of Melting in a Spherical Shell." International Journal of Heat and Mass Transfer 50: 1790-1804.

H. Niyas, S. P., P. Muthukumar (2017). "Performance investigation of a lab scale latent heat storage prototype Numerical results." Energy Conversion Management 135: 188-199.

J.Vogel JF, M. J. (2016). "Naturalconvectioninhightemperature flatplate latent heat thermal energy storage systems." Applied Thermal Engineering 184: 184-196.

K.A.R. Ismail, F. A. M. L., R.C.R. Silva, A. B. Jesus, L.C. Paixão (2014). "Experimentally validated two dimensional numerical model for the solidification of PCM along a horizontal long tube." International Journal of Thermal Sciences 75: 184-193.

K.A.R. Ismail, J. R. H. (2000). "Solidification of pcm inside a spherical capsule." Energy Conversion & Management 41: 173-187.

M. A. Ezan, M. K. (2016). "Numerical investigation of transient natural convection heat transfer of freezing water in a square cavity." International Journal of Heat and Fluid Flow 61: 438-448.

M.T. Stickland, T. J. S., J. MacKenzie (2007). "An experimental investigation of natural convection with solidification in a differentially heated cavity." International Journal of Heat and Mass Transfer 50: 36-44.

Mathura Kumar, D. J. K. (2017). "Influence of Mushy Zone Constant on Thermohydraulics of a PCM." Energy Procedia 109: 314-321.

Mohamed Fadl, P. C. E. (2019). "Numerical investigation of the influence of mushy zone parameter Amush on heat transfer characteristics in vertically and horizontally oriented thermal energy storage systems." Applied Thermal Engineering 151: 90-99.

Patankar, S. V. (1980). Numerical Heat Transfer and Fluid Flow. Washington, DC, Hemisphere.

R.K. Sharma, P. G., J.N. Sahu, H.S.C.Metselaar, T.M.I.Mahlia (2014). "Numerical study for enhancement of solidification of phase change materials using trapezoidal cavity." Powder Technology 268: 38–47.

S. Chakraborty, N. C., P. Kumar, P. Dutta (2003). "Studies on turbulent momentum, heat and species transport during binary alloy solidification in a top-cooled rectangular cavity." International Journal of Heat and Mass Transfer 46: 1115-1137.

Simone Arena, E. C., Jaume Gasia, Luisa F. Cabeza, Giorgio Cau (2017). "Numerical simulation of a finned-tube LHTES system: influence of the mushy zone constant on the phase change behaviour." Energy Procedia 126: 517-524.

W. Shyy, Y. P., G.B. Hunter, D.Y. Wei, M.H. Chen (1992). "Modeling of turbulent transport and solidification during continuous ingot casting." International Journal of Heat and Mass Transfer 35: 1229-1245.

Y. Kozak, G. Z. (2017). "Novel enthalpy method for modeling of PCM melting accompanied by sinking of the solid phase." International Journal of Heat and Mass Transfer 112: 568–586.

Y. Pahamli, M. J. H., A.A. Ranjbar, R. Bahrampoury (2016). "Analysis of the effect of eccentricity and operational parameters in PCM-filled single-pass shell and tube heat exchangers." Renewable Energy 97: 344-357.

Yuxiang Hong , W.-B. Y., Si-Min Huang, Juan Dua (2018). "Can the melting behaviors of solid-liquid phase change be improved by inverting the partially thermal-active rectangular cavity?" International Journal of Heat and Mass Transfer 126: 571-578.

Z.N. Meng, P. Z. (2017). " Experimental and numerical investigation of a tube-in-tank latent thermal energy storage unit using composite PCM." Applied Energy 190: 524–539.

# CHAPTER 6

# INDUSTRIAL APPLICATION OF SOLID-LIQUID PHASE CHANGE PROCESSES

# CHAPTER 6

# INDUSTRIAL APPLICATION OF SOLID-LIQUID PHASE CHANGE PROCESSES

## 6.1 The performance study of PCM heat exchanger

### 6.1.1 Introduction

The use of PCM for latent heat storage is an innovative technique to store thermal energy. A small amount of PCM has the potential to store a large amount of thermal energy in the form of latent heat. The limitation of the process is it is a very slow process. The low thermal conductivity of PCMs makes the charging or melting of PCM process sluggish. Therefore to improve the charging process the PCM heat exchangers are used. In heat exchangers, high-temperature fluid (HTF) is flowing through inner or outer tube and after transferring the heat to PCM the HTF exits from the heat exchanger. These types of latent storage units are of different types like direct and indirect type shell and tube heat exchanger, double pipe heat exchanger, plate and packed heat exchanger. The double heat exchanger is most common type PCM heat exchanger because of simple shape and construction. The charging and discharging time depend on many parameters like inlet temperature of HTF, flow rate of HTF, outer surface area of the inner pipe, amount of PCM, thickness of PCM layer and material of heat exchanger. Researchers have studied the performance of PCM heat exchangers experimentally and theoretically to propose appropriate operating and boundary condition to increase the efficiency of PCM heat exchanger. M. Gorzin et al. proposed a system in which the surface area of PCM and HTF is increased to reduce the energy loss (Majid Gorzin 2018). The simulated result shows the time of melting is minimum for 60:40 ratio (weight) of PCM in outer and inner tube respectively. Li et al. theoretically optimized the time of charging by varying the eccentricity and diameter of the inner tube(Saiwei Li 2017). Hamid Ait Adine and Hamid El Qarnia designed a composite PCM heat exchanger having maximum thermal storage efficiency (Hamid Ait Adine 2009). Wang et al. studied the

performance of a vertical shell and tube heat exchanger using erythritol as PCM (Yifei Wang 2016).

The literature shows that the volume of PCM is very less compared to the volume of the tube through which HTF is flowing. Moreover during charging the sensible heat transfer before phase change is also considered. In this study, the volume of PCM taken is very large. This large mass of PCM will store more latent heat. On the other hand, the charging and discharging times also very large due to sensible heat transfer and this large discharging time will not allow PCM to subcool. Therefore, in the next cycle charging time will be less because of negligible sensible heat transfer. In this study, only latent heat transfer is considered. The study also attempts to find some correlation among the controlling parameter of the heat exchanger.

The design or performance analysis of PCM heat exchanger demands correlation among the controlling parameters of phase change process. Correlations make the study simpler. The types of correlation studied in the heat exchanger without phase change are not available for unsteady state PCM heat exchanger. In this study, the temperature and flow rate of HTF is varied for the performance study of PCM heat exchanger. The effect of variation of flow rate and temperature of HTF helped to select an appropriate boundary condition for minimum charging time. The empirical equations are also proposed to correlate melt fraction with Stefan number, flow rate and time.

The commercial software Ansys-Fluent is used to run the governing equation of the enthalpy porosity model. The enthalpy porosity model solved the solidification/melting model in fixed grid domain.

### 6.1.2 Computational domain

A double pipe heat exchanger (HE) is considered for the solidification/melting phase change study. The geometry of the HE contains two concentric pipes and the high-temperature fluid (HTF) is passing through the inner tube. The outer pipe is a closed pipe consists of paraffin wax as phase change material. The outer pipe is having no inlet or outlet like the inner tube. Such a configuration is important to restrict the flow of PCM in the liquid phase. The PCM is used to store the latent heat thermal energy and it is reusable therefore flow out of PCM is not desirable.

Dimensions of the heat exchanger and thermo-physical properties of PCM are given in the following Table 6.1. The details of thermo-physical properties of PCM and HTF are given in Table 6.2. The thermo-physical properties are assumed to be constant, only density changes using Boussinesq approximation. Ansys- Fluent 15.0 is used for simulation of the heat transfer process.

### 6.1.3 Numerical scheme

The process is analyzed for 98281 numbers of triangular cells. The solid model and mesh is shown in Fig 6.1(a) and Fig 6.1(b). The schematic diagram of heat exchanger are also given in Fig 6.2(a) and Fig 6.2(b). The time step taken for the study is 0.1 sec. The discretization schemes used are SIMPLE for pressure-velocity coupling, PRESTO! for pressure, second-order upwind for momentum and energy balance equations respectively. The grid independency of the model is checked. The time step is chosen so that the solution has converged in each step during the process simulation. The results of grid independency are shown in Fig 6.4. Grid independency results are shown for 4 different grid sizes. Grid 1 refers to 98281 numbers of cells, similarly grid 2 is having 94920, grid 3 is having 111072 and grid 4 is having 72030 numbers of cells. The deviation is little high for grid 4. In this section simulation are carried out with grid 1. The mathematical model is validated using the simulated results obtained by M. Gorzin et al.

**Table 6.1: Details of heat exchanger**

| Pipe | ID(m) | OD(m) | Material | Length(m) |
|---|---|---|---|---|
| Inner | 0.07 | 0.072 | copper | 0.9 |
| Outer | 0.14 | 0.144 | | |

**Table: 6.2 Thermo-physical properties of PCMs and HTF**

| Thermo-physical properties | RT((50) (PCM) | Fatty acid (PCM) | Water (HTF) |
|---|---|---|---|
| Density (kg/m$^3$) | 820 | 990 | 998.2 |
| Specific heat (J/kg.K) | 2000 | 2200 | 4182 |
| Thermal conductivity (W/m.K) | 0.2 | 0.44 | 0.6 |
| Viscosity (kg/m.s) | 0.0038 | 0.0078 | 0.001003 |
| Latent heat of solid/liquid phase change (kJ/kg) | 168 | 210 | |
| Solidus temperature (K) | 318 | 326 | |
| Liquidus temperature (K) | 324 | 328 | |
| Thermal expansion coefficient (K$^{-1}$) | 0.006 | 0.006 | |

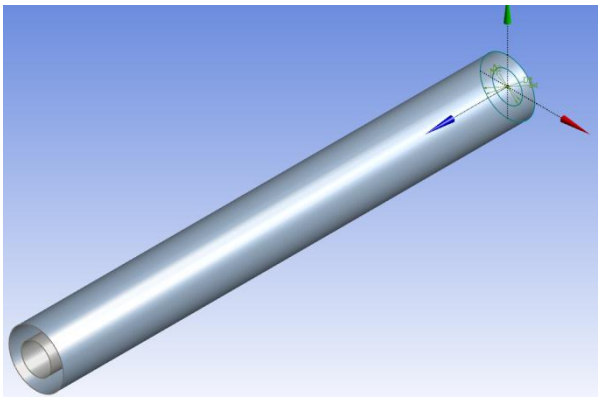

**Fig 6.1(a): 3D drawing of double pipe heat exchanger in Ansys-workbench**

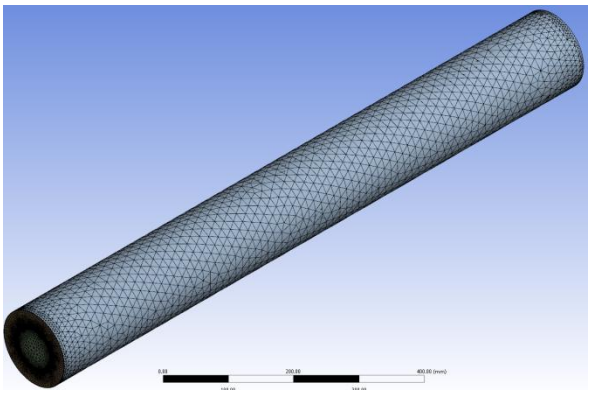

**Fig 6.1(b): Triangular meshing of 3D double pipe heat exchanger**

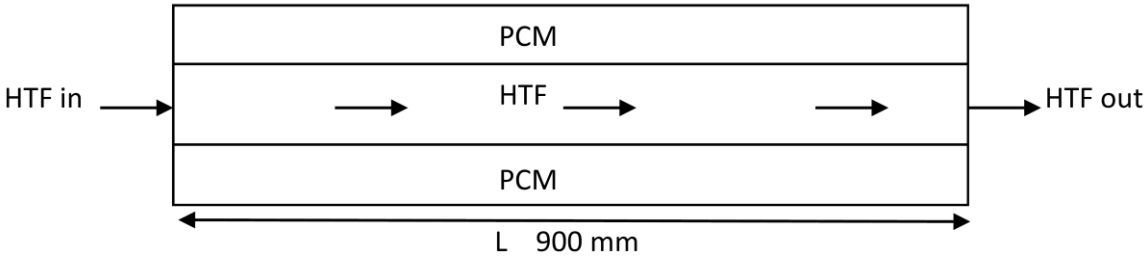


**Fig 6.2(a): Lateral view**

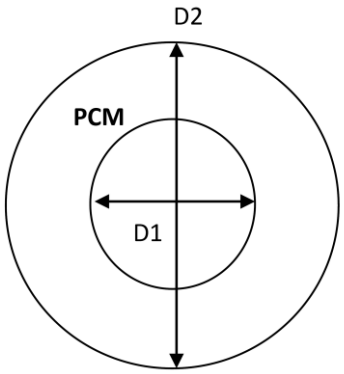


D1 = 70 mm and D2 =140 mm

**Fig 6.2(b): Cross-sectional view**

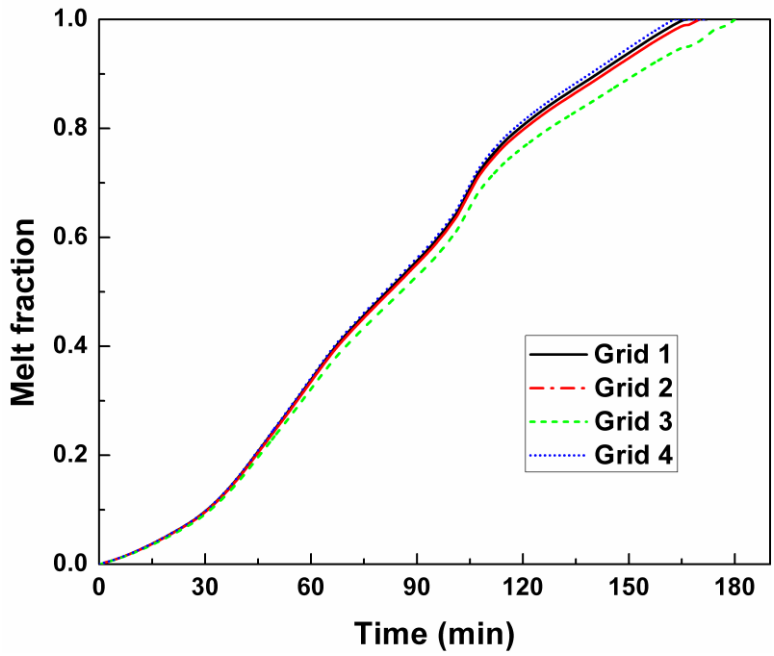


**Fig 6.3: Grid independency of the PCM heat exchanger**

### 6.1.4 Results and discussion: Effect of inlet temperature and flow rate of HTF on charging of PCM in a heat exchanger

The enthalpy model chosen for simulation of proposed work is validated with the model proposed by M. Gorzin et al. (Majid Gorzin 2018). The charging process of PCM is simulated with the same initial and boundary condition proposed by M. Gorzin et al. and the comparison of result is shown in Fig 6.4. At the initiation of charging process, the PCM is at room temperature 298K and the inlet temperature of HTF is 348K and the flow rate is 0.087 kg/s. The deviation between two simulations is very small.

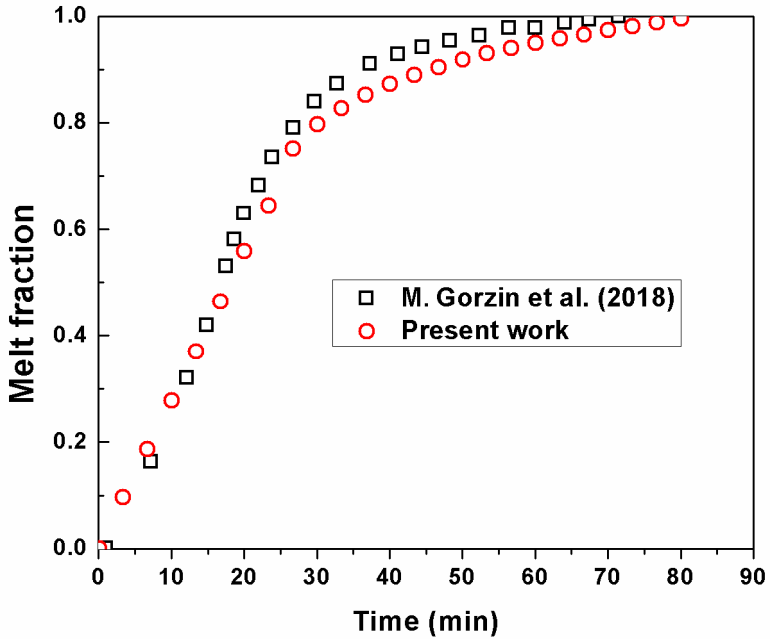


**Fig 6.4: Validation of the numerical model**

In the mentioned PCM heat exchanger HTF fluid is passing through the inner pipe. It is assumed that the PCM is initially at a temperature of 317K or 5K less than the mean melting temperature of PCM. The HTF is flowing through the inner pipe and transferring the heat through conduction to the solid PCM. The PCM receives the heat and after reaching the solidus temperature it starts melting. The temperature of PCM increases uniformly through conduction around the inner pipe. As soon as melting initiated, the density changes and presence of bouncy force shows the non-uniformity around the inner pipe. The formation of liquid phase introduces the movement of liquid PCM due to temperature difference. The source term in

momentum equation of the enthalpy porosity model is used to introduce the movement of liquid phase velocity suppression of solid phase. Therefore, melting results in sinking of solid PCM to the bottom of outer pipe. The solid PCM around the inner pipe melts and comes up to the upper side of outer pipe and solid sinks to the bottom. Due to this natural convection and bouncy effect the rate of melting increases. This bouncy effect is active till the solid PCM in the upper portion of inner tube melts. After that once again the melting rate starts decreasing. The melt fraction contours are shown in Fig 6.5. The uniform phase distribution is observed till 112min for 338K, 30min for 348K and around 25 min for 358K inlet temperature of HTF. In case of inlet temperature 358K the melting process is very fast from 30min to 50 min as shown in Fig 6.5.

The working principle of the heat exchanger revealed that flow rate and inlet temperature of source fluid are very important in order to achieve the desired efficiency. The flow rate of both source and process fluid controls the time of contact of heat transfer. In this study of PCM heat exchanger, PCM is enclosed within the outer pipe and is kept at an initial temperature of 317K or 5K less than mean melting temperature. The source fluid is water in this study. The temperature of source fluid are taken as 358K , 348K, 346K and 338K and inlet flow rate are taken as 0.087kg/s, 0.07kg/s,0.05 kg/s and 0.01kg/s. The melt fractions of PCM at different times are calculated for different temperatures and flow rates. In extreme case i.e. for 358K inlet temperature of water the melt fraction is not affected by flow as shown in Fig 6.6. The graph for inlet temperature 348K of the HTF water is given in Fig 6.7. The time required for complete melting is decreased when the flow rate decreases from 0.087kg/s to 0.07kg/s. In the next stage when temperature of HTF inlet changed to 0.07 kg/s to 0.5kg/s no significant change in melting time is observed and further a decrease in flow rate to 0.01kg/s the melting time of PCM is increased. Therefore, the 0.05kg/s to 0.07kg/s can be the effective flow rate for this configuration of heat exchanger.

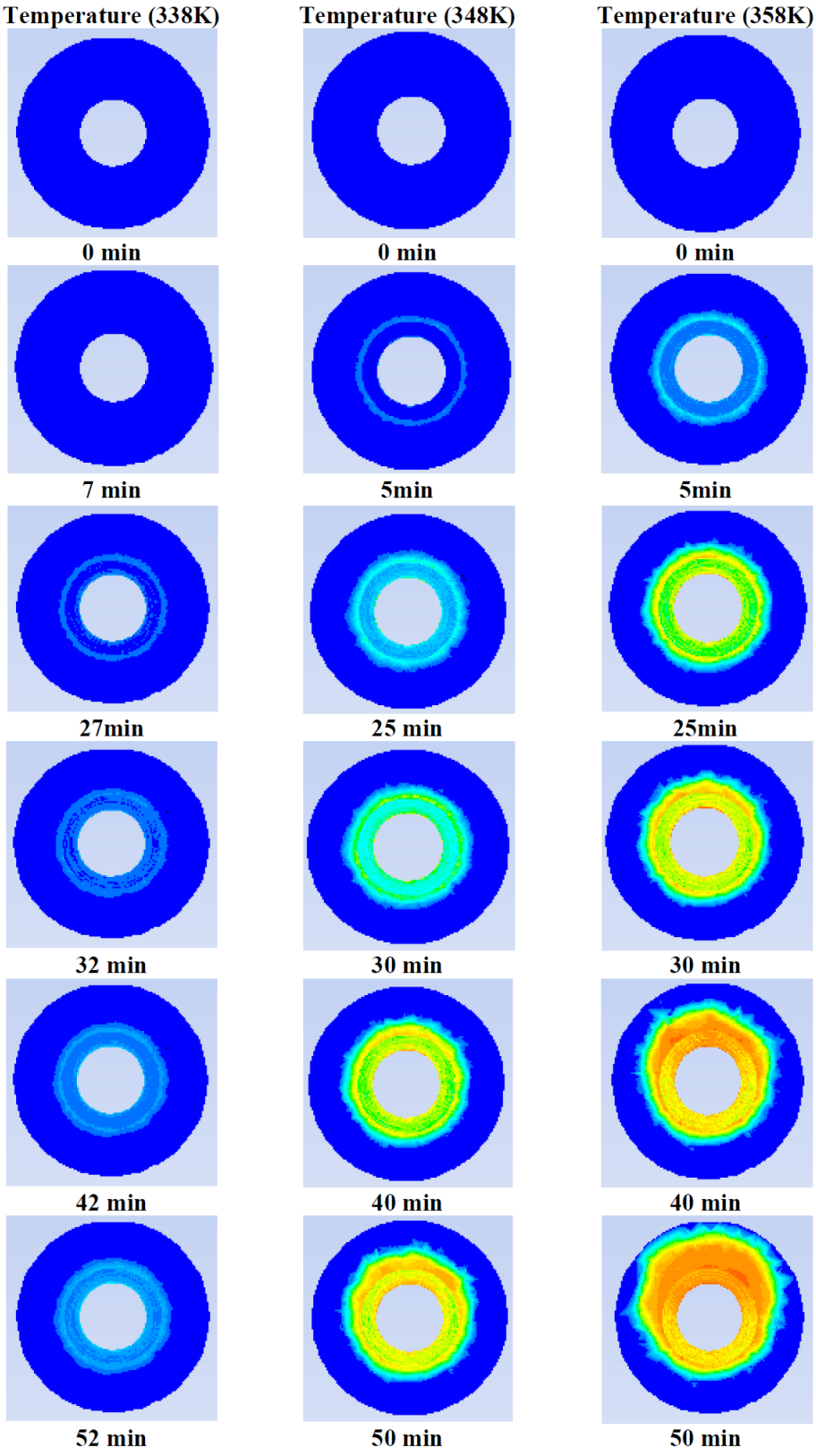


**Fig 6.5: Contour of melt fraction for HTF inlet flow rate 0.05kg/s**

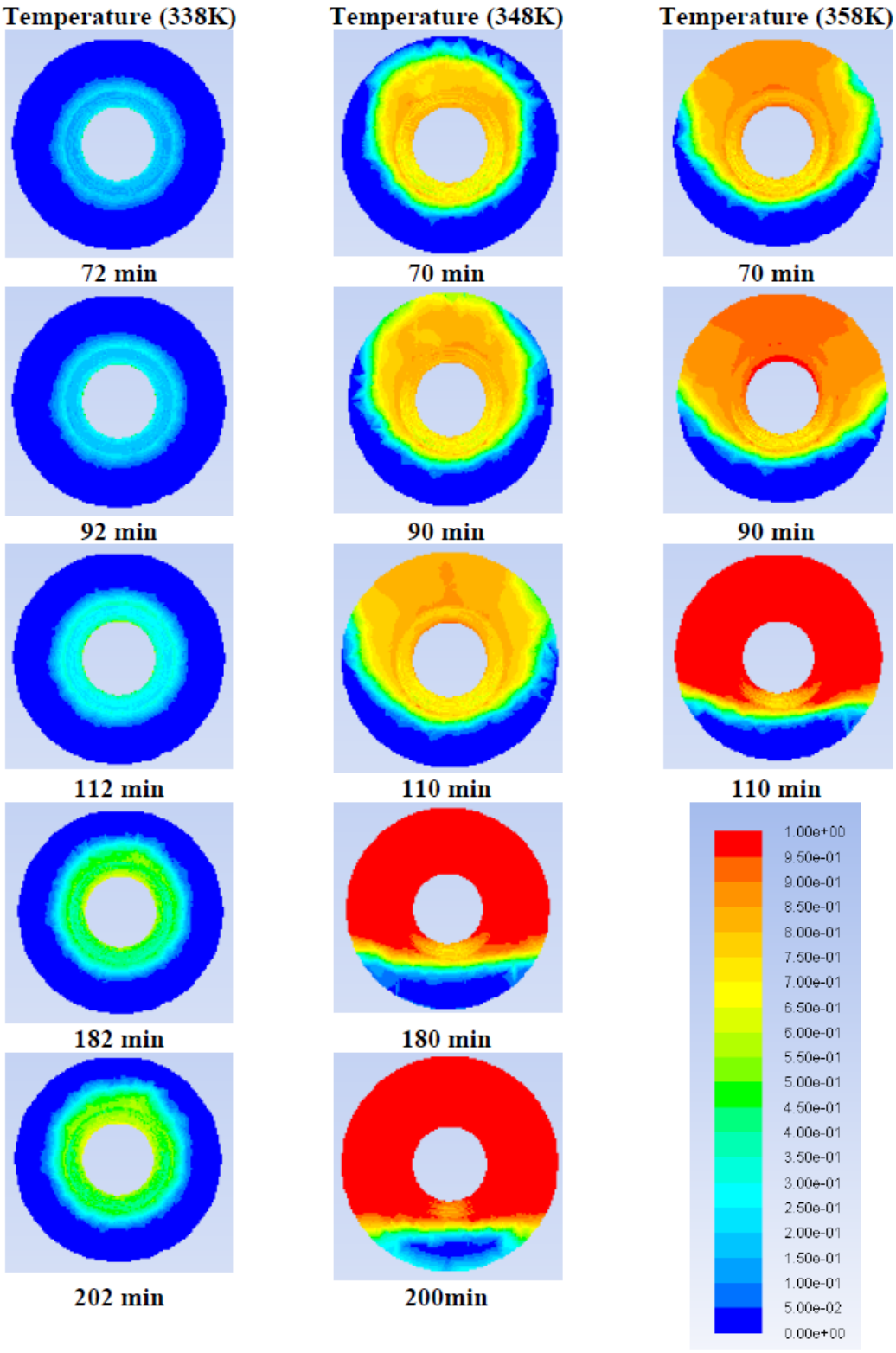


**Fig 6.5: Contour of melt fraction for HTF inlet flow rate 0.05kg/s (continued)**

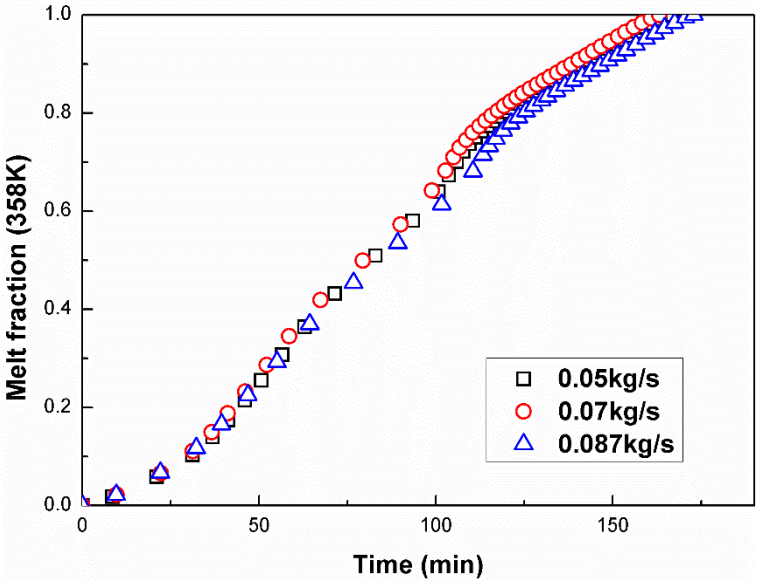


**Fig 6.6: Variation of melt fraction for HTF inlet temperature358K**

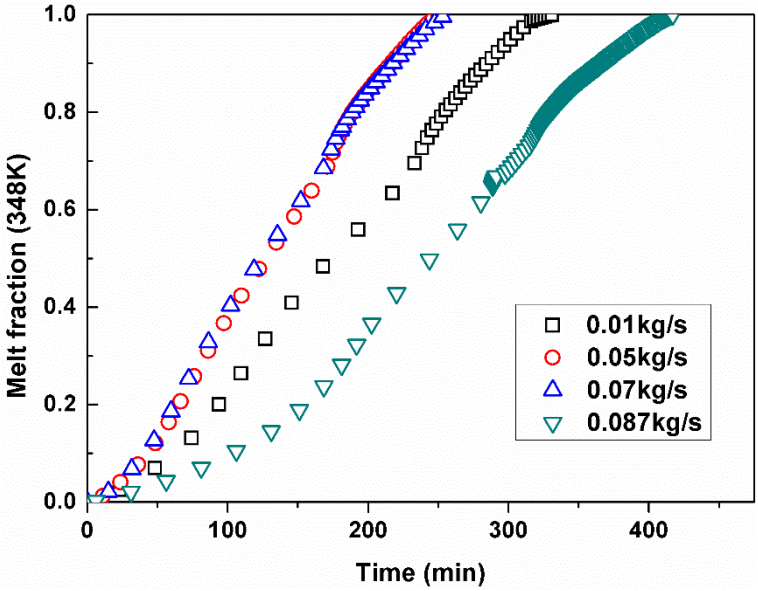


**Fig 6.7: Variation of melt fraction for HTF inlet temperature 348K**

The effect of temperature change is also presented for the different inlet flow rate of HTF in Fig 6.8 and Fig 6.9. The melting time is decreased significantly as inlet temperature of HTF increases from 338K to 358K. It is observed that melting time is very high for both the flow rate for inlet temperature 338K. The melting or charging time is around 300min for inlet HTF temperature 348K and flow rate of 0.087 kg/s. On the other hand for inlet HTF temperature 348K or higher the melting time is less than 200min. This melting time is valid for both the flow rate of HTF. Therefore, the suggested inlet temperature should be more than equal to 348K for this study.

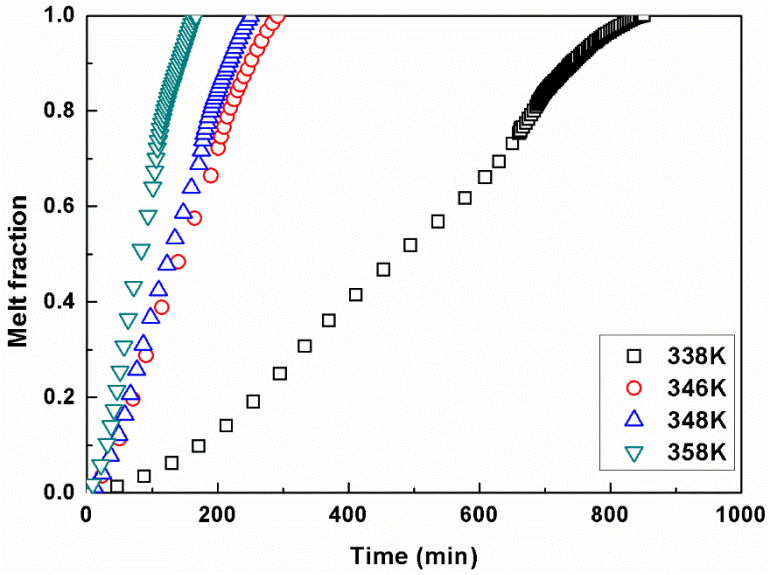


**Fig 6.8: Melt fraction of PCM for inlet flow rate 0.05kg/s of water**

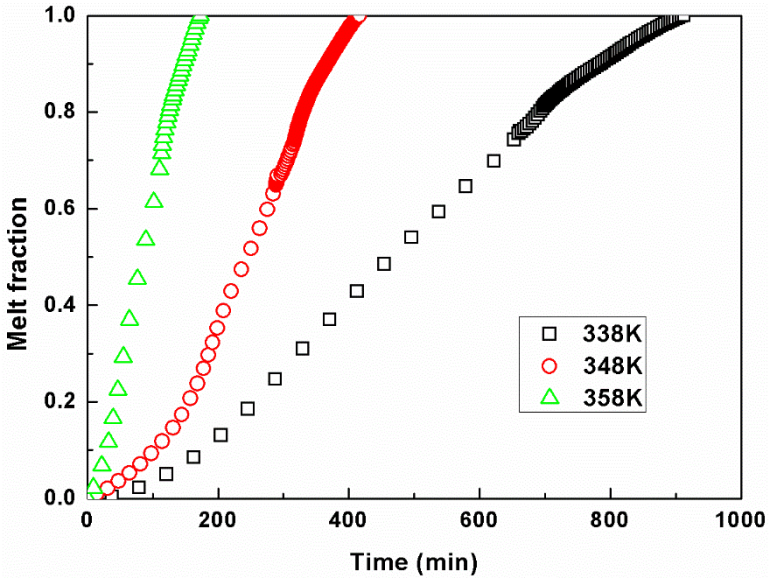


**Fig 6.9: Melt fraction of PCM for inlet flow rate 0.087kg/s of water**

The minimum melting is not the only criterion for designing a PCM heat exchanger. The outlet temperature of HTF should also be studied before making any conclusion about the design of heat exchanger. The outlet temperature of HTF with time is plotted for inlet flow rate of HTF 0.05 kg/s and 0.07 kg/s at two different temperatures 348K and 358K. The temperature difference for are also plotted for the same and shown in Fig 6.10. The outlet temperature dropped from the initial temperature and then starts increasing and reaches the maximum temperature which is little below the initial inlet temperature of HTF. Figure 6.11 shows that the

temperature difference is higher in case of HTF inlet flow rate 0.05 kg/s and temperature 358K. The three different stages of temperature difference are observed in Fig 6.11 for inlet and outlet temperature difference. In the initial stage, temperature difference decreases very fast and in the second stage the temperature difference is almost constant. In the third stage once again temperature difference starts decreasing but with a slower rate than the first stage. The higher temperature difference indicates higher heat transfer to the PCM and results in higher efficiency of PCM heat exchanger. The efficiency of heat exchanger can be defined as the ratio of heat transferred to the PCM and heat lost by the HTF. The efficiency curve for maximum inlet and outlet temperature difference of HTF is presented in Fig 6.12. The maximum temperature difference in HTF implies maximum heat supplied to PCM and expected efficiency is highest among the other boundary conditions. The efficiency at the $n^{th}$ time step is defined as follows:

$$\eta_n = \frac{M \times mf \times L}{m \times C_p \times \sum_{j=1}^{n} \Delta t_j \times (T_{HTF,in} - T_{HTF,out})_j} \quad (6.1)$$

Where M is the mass of PCM in the heat exchanger, m is the mass flow rate of HTF and $\Delta t_j$ is the residence time of HTF in the heat exchanger. Since the sensible heat transfer in PCM is very small compared to latent heat transfer it is neglected in efficiency relation. The efficiency relation is defined assuming that the heat lost from HTF is totally transferred to PCM without any loss. Fig 6.12 shows efficiency increases as phase change occur in and the maximum efficiency is about 30% in this study.

According to the principle of heat transfer for flow through a constant temperature hot/cold pipe the heat transfer coefficient is proportional to Reynolds number assuming other thermo-physical properties of fluid are constant. On the other hand, it is also true that the high Reynolds number causes less time of contact between HTF and PCM hence the heat transfer rate decreases. The detailed parametric study tried to propose an empirical equation to calculate the melt fraction as a function of Reynolds number, Stefan number, and Fourier number. The results obtained from the parametric study are tabulated in Table 6.3 and 6.4**.** The variations of PCM melt

fraction are calculated as a function of Fourier number. For different inlet temperature and flow rate of HTF the power of Fourier number varies from 0.85 to 1.3. For the flow rate range 0.05 to 0.07 kg/s the power of Fourier number decreases and from 0.07 to 0.087kg/s the power of Fourier number increases.

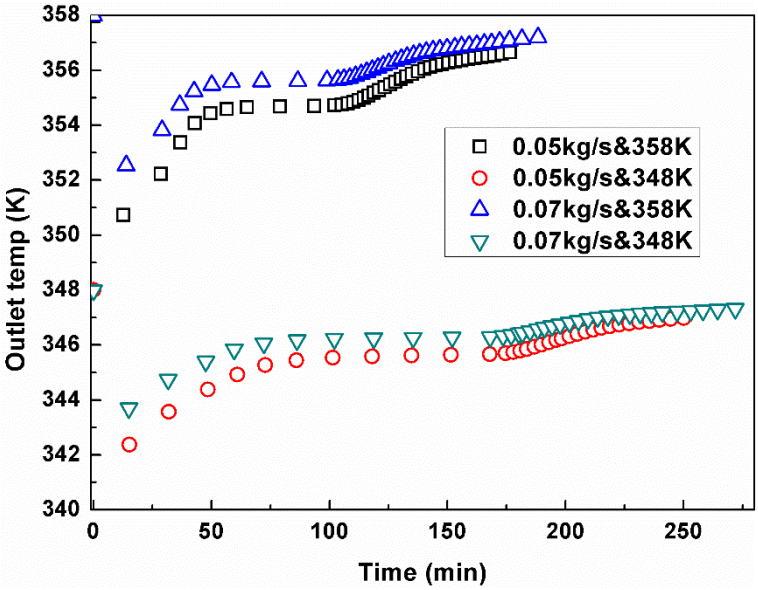


**Fig 6.10: Variation Outlet temperature of HTF**

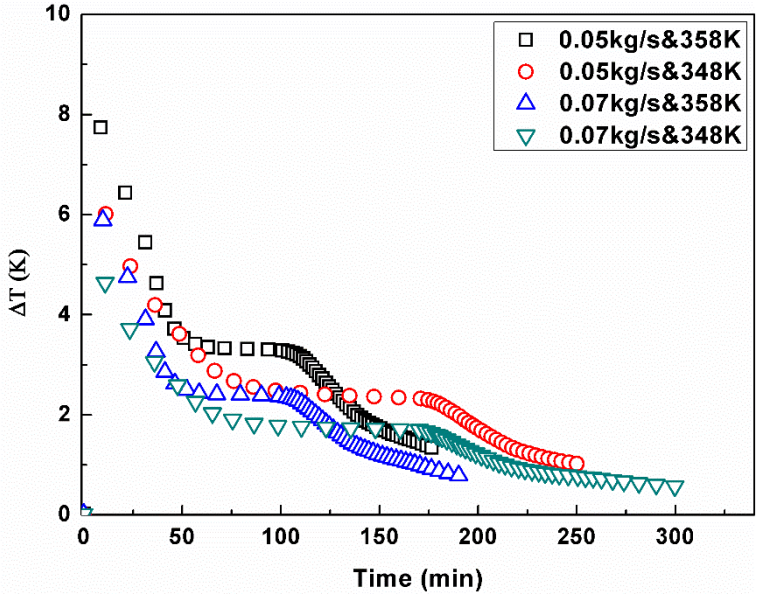


**Fig 6.11: Variation of inlet and Outlet temperature difference of HTF**

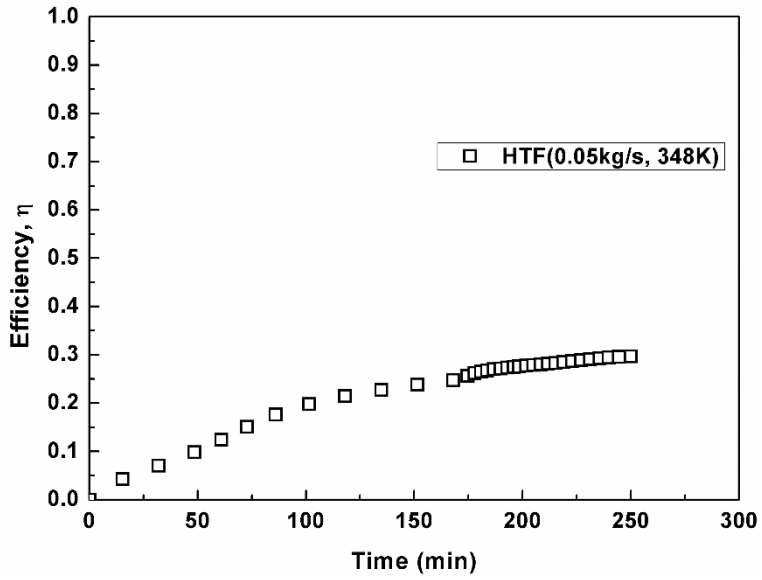


**Fig 6.12: Efficiency of heat exchanger for 0.05kg/s flow rate and 348K temperature of HTF**

The parametric analysis tabulated in following tables show that for flow rate range 0.05 to 0.07 kg/s the dependency on Stefan number and flow rate of HTF are of same degree since the constant terms (26.9 and 27.6) and power of Stefan number (1.7 and 1.8) are almost same. The increase in flow rate of HTF up to 0.087 kg/s shows that the flow-dependent term increased up to 40.44 and the power of Stefan number is increased to 2.4. Therefore, a higher flow rate of HTF affects the charging of PCM significantly. Thus the empirical relation can be proposed as:

$$mf = 27(St)^{1.75}(Fo) \tag{6.2}$$

The above relation is valid for 0.05kg/s to 0.07kg/s flow rate of HTF during charging of paraffin wax (RT50) in a double pipe heat exchanger. For higher flow rate of HTF (0.087kg/s) the relation is given below:

$$mf = 40.44(St)^{2.4}(Fo) \tag{6.3}$$

The developed empirical relations are limited to the dimension of heat exchanger. The melting or charging not only depends on the HTF conditions, but it also depends on the mass or thickness of the PCM taken. The contact surface area of HTF and PCM is another controlling factor of charging process.

**Table 6.3: Melt fraction of PCM as a function of Fourier number**

| Flow rate / Temp | 0.05 kg/s | 0.07 kg/s | 0.087kg/s |
|---|---|---|---|
| 338K (St = 0.235) | $mf = 1.23Fo^{1.3}$ | $mf = 1.85Fo^{0.85}$ | $mf = 1.56Fo^{1.08}$ |
| 348K (St = 0.352) | $mf = 5.87Fo^{1.21}$ | $mf = 4.49Fo^{1.05}$ | $mf = 3.296Fo^{1.3}$ |
| 358K (St =0.469) | $mf = 6.99Fo^{1.05}$ | $mf = 7.028Fo^{1.04}$ | $mf = 6.48Fo^{1.03}$ |

**Table 6.4: melt fraction of PCM as function of Fourier number and Stefan number**

| Flow rate / Temp | 0.05 kg/s | 0.07 kg/s | 0.087kg/s |
|---|---|---|---|
| 338K (St = 0.235) | $mf = 26.9(St)^{1.7}(Fo)^{1.3}$ | $mf = 27.6(St)^{1.8}(Fo)^{0.85}$ | $mf = 40.44(St)^{2.4}(Fo)^{1.08}$ |
| 348K (St = 0.352) | $mf = 26.9(St)^{1.7}(Fo)^{1.21}$ | $mf = 27.6(St)^{1.8}(Fo)^{1.05}$ | $mf = 40.44(St)^{2.4}(Fo)^{1.3}$ |
| 358K (St = 0.469) | $mf = 26.9(St)^{1.7}(Fo)^{1.05}$ | $mf = 27.6(St)^{1.8}(Fo)^{1.04}$ | $mf = 40.44(St)^{2.4}(Fo)^{1.03}$ |

### 6.1.5 Results and discussion: Effect of thermo-physical properties of PCM on the charging of PCM in heat exchanger

In the section 6.1.4 the effect of inlet temperature and flow rate of HTF on the charging process in PCM heat exchanger are studied. The effect of thermal properties of PCM is also studied in this section. The simulation is repeated using fatty acid as PCM. The geometry and mesh size is same as previous geometry. The inlet flow rate and temperature of HTF are taken as 0.05kg/s and 348K respectively. The thermo-physical properties of fatty acid are as follows: density 990Kg/m$^3$, specific heat 2.2kJ/kg. K, thermal conductivity 0.44 W/m. K, latent heat 210kJ/kg, solidus temperature 326K and liquidus temperature 328K. The thermal expansion coefficient remains same for both fatty acid and paraffin wax. Figure 6.13 shows the variation of melt fraction with for two different PCM materials. The time required for complete melting is less for paraffin wax. At the initial stage of the melting or charging process, the melt fraction is slightly higher than the paraffin wax. This is because the initially the process is conduction dominated and the thermal conductivity of fatty acid approximated double than that of paraffin wax. On the

other hand, the Stefan number is 0.22 for fatty acid melting and 0.32 for paraffin wax melting. Stefan number (St) is defined as follows:

$$St = C_p(T_w - T_m)/L \tag{6.4}$$

Where, $C_p$ is the specific heat of PCM, $T_w$ is the temperature of HTF at inlet,$T_m$ is the mean melting temperature of PCM, L is latent heat of PCM. Therefore, the driving force for the process is higher in paraffin wax melting. After around 75% melting of PCM, the difference in melt fraction of two PCMs with time is quite significant. At this stage, the solid PCM is at the bottom of outer pipe of the heat exchanger and natural convection dominates the process instead of conduction process. Therefore, the effect of higher temperature difference and Stefan number make the paraffin wax melting process faster than that of fatty acid. The variation of melt fraction is also compared for the same Stefan number and shown in Fig 6.14. To keep the Stefan number constant the melting of paraffin wax is simulated for HTF inlet temperature 338K and flow rate 0.05kg/sec. Therefore, the study concludes that for the same Stefan number 0.2 (approximately) the time complete melting varies significantly. The time for complete melting is around 300 mins for high thermal conductivity PCM fatty acid and low thermal conductivity PCM the time for complete melting is approximately 800 min. Thus the high thermal conductivity PCM can make the melting or charging process much faster.

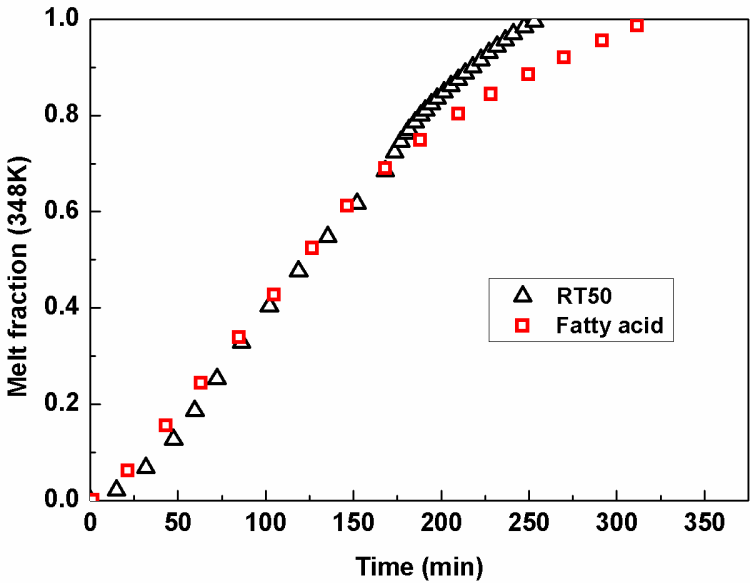


**Fig 6.13: Variation of melt fraction for different PCMs for same boundary conditions**

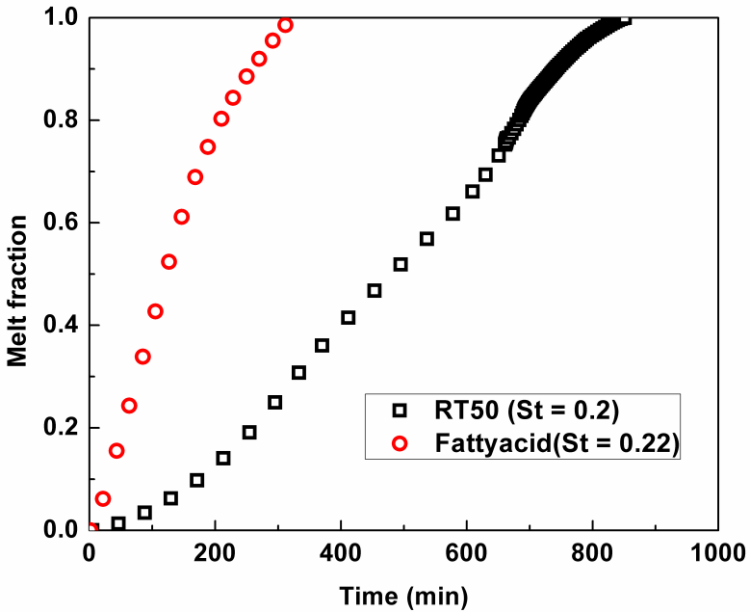


**Fig 6.14: Variation of melt fraction for different PCMs for same Stefan number**

### 6.1.6 Conclusion

In this chapter, the effect of inlet temperature and flow rate on melting or charging of PCM paraffin wax (RT50) in a double pipe heat exchanger is studied. The effects of thermo-physical properties of PCM are also compared. In this case, fatty acid is the RT50 and fatty acid is taken as PCM. The commercial software Ansys-fluent is

used for the study. The fixed grid enthalpy-porosity model used to explain the charging or melting process. The study concludes that

- The melting time is not affected by the inlet temperature of HTF for a high inlet flow rate of HTF.
- The melting or charging time is minimum for a moderate HTF flow rate and inlet temperature.
- Empirical equations show that the melt fraction variation with Stefan number and Fourier numbers are different for different flow regimes.
- The highest difference implies the maximum heat is extracted from the HTF and less heat is lost to the surrounding. The maximum efficiency corresponds to the maximum inlet-outlet temperature of HTF is around 30%.
- The study is limited to this configuration of the PCM heat exchanger. The efficiency of heat exchanger can be improved by increasing the contact surface area of PCM and HTF and by decreasing the amount of PCM.
- The thermal conductivity of PCM and temperature difference between the inlet temperature of HTF and mean melting temperature drives the melting or charging process of PCM.

## 6.2 Study of the casting of pure metals

### 6.2.1 Introduction

Zinc is one of the important non-ferrous metals. It is being used in a variety of industries and products. Pure zinc is predominantly used as a coating material for corrosion resistance. Zinc is also used for many industrial alloys. Zinc in various forms is used in cosmetics, paints, inks, soaps, pharmaceuticals, plastics, electrical equipment, batteries, and textiles. Zinc is also used as a casting material for various metal products. It is therefore important to understand the melting and solidification process of zinc. The numerical and experimental studies on melting and solidification are available for different phase change materials (PCMs) like inorganic, organic PCMs, pure and alloys substances. Some of the PCMs have high phase change temperature and some have a low melting temperature. The

solidification studies are also considered for different casting processes. A large amount of heat is transferred as latent heat in the phase change process which affects the macroscopic behavior of the substance. In this study, the solidification of zinc is simulated using the enthalpy porosity model. The volume of fluid (VOF) is incorporated with the enthalpy porosity model to define the PCM and air interface at the open surface.

Bermudez and Otero compared the solidification of the aluminum slab using direct chill casting and electromagnetic casting processes. The limitation of the proposed numerical model is a fixed grid method(A. Bermudez 2006). Chakraborty studied the solidification of pure substance water using the enthalpy porosity model (Chakraborty 2017). The study considered the variation in specific heat in both the phase and showed a good agreement with the prediction made by Kowalewski and Rebow(Rebow 1999). Bot and Arquis simulated the one dimensional model of deposition and solidification of successive metal layers on a cold surface(Cedric Le Bot 2009). The model used for simulation not considered the convective phenomena because of negligible flow time. Tian et. al studied the effect of cooling rate in polymorph selection during solidification of zinc(Ze-an TIAN 2015). The study showed the effect of polymorph selection is different at a different stage of cooling. Wenyi Hu optimized the casting of AZ31 magnesium slab using the direct chill method with different cooling speeds (Wenyi Hu 2013). Solidification studies are presented for different metals and alloys like Nickel (B.T. Bassler 2003), tin (Hwang 1997), etc. Tomasz and Ewa simulated the solidification of Copper using finite element method. They used a front tracking method to locate the solid-liquid interface(Tomasz Skrzypczak 2012). Similar numerical studies are also presented by several authors with different boundary conditions (Zabaras N 1989; Zabaras N 1990; Zabaras N 1995; Slota 2011). Lewis and Ravindran simulated filling and solidification of molten aluminum in a spiral and spillage wheel type cavity(R. W. Lewis 2000). They used the finite element method with a fixed grid for the solidification study. The fixed grid method is advantageous over the moving grid. The fixed grid considers the total materials as a single phase and for moving grid the control volume is treated as two-phase. In the case of alloys, a number of materials

are present and using moving grid the calculation is complicated. In such a situation, the fixed grid method is more effective. During the casting of metals, the impurities are always present in an optimum amount and fixed grid method is appropriate in such cases. The literature survey shows that there are very few literature available on the solidification of pure metal. The study of phase change for pure metals is important to set a benchmark for alloys. The difference in the thermal behavior of metal and alloys can be studied by performing this type of simulation.

In this section, the authors focused on the fixed grid method for simulation of solidification of pure zinc under different thermal boundary conditions. Volume of fluid (VOF) method is used to describe the interface of air and zinc and the enthalpy porosity model is adapted to locate the solid-liquid interface of the phase changing material. The proposed model is widely applicable to different thermal boundary conditions as well as different inorganic/organic PCMs, high/low phase change temperature materials. The effect of the convection heat transfer coefficient on the solidification process and time are compared. The solidification of zinc and aluminum presented in this section studied the effect of convection heat transfer coefficient on solidification time.

### 6.2.2 Computational Domain and Numerical scheme

Phase-change processes come under the moving boundary problem. The change in density due to cooling and phase change, the velocity suppression occurs which results in an irregular interface. An axisymmetric rectangular cavity has been taken to the study of the solidification process of molten zinc. The size of the cavity is 28mm×78mm. The size of the cavity is very small in order to minimize computation time. The cavity is filled with molten zinc. The schematic diagram of the cavity is shown in Fig 6.15. The initial temperature of molten zinc is 4.5 degrees higher than that of the mean solidification temperature. The study has been performed for different convection heat transfer coefficient. The cavity is exposed to air during the solidification process. The thermo-physical properties of molten zinc are chosen as commercially available zinc. The density of solid zinc is 7134 kg/m$^3$ and 6927 kg/m$^3$ for liquid zinc, specific heat 900.1 J/kg. K, thermal conductivity 164W/m. K,

viscosity is 0.00358 kg/m. s, latent heat 109kJ/kg, solidus temperature is 693K and liquidus temperature is 698K. Ansys-fluent 16.2 is considered for simulation of the casting process. VOF model has been used to describe the zinc-air system with a moving internal surface and no interpenetration of two media (air and zinc). The enthalpy-porosity model is used to identify the solid-liquid interface in the phase change region. The enthalpy-porosity method is used to describe the velocity suppression in the solid phase (Sin Kim 2001). The governing equations of fixed grid enthalpy model are satisfied by of solid and liquid phase of phase changing material. The no-slip boundary condition is maintained at the walls. Axisymmetric, laminar, and incompressible flow within the cavity is assumed during the simulation process. The thermo-physical properties like thermal conductivity, specific heat, the viscosity of zinc are assumed to be constant with temperature. The density of zinc is only varying during the phase transition. The momentum source term is used to describe the movement through the porous medium, at the solid-liquid interface. The value of the mushy zone constant is taken as $10^5$ (A.D. Brent 1988).

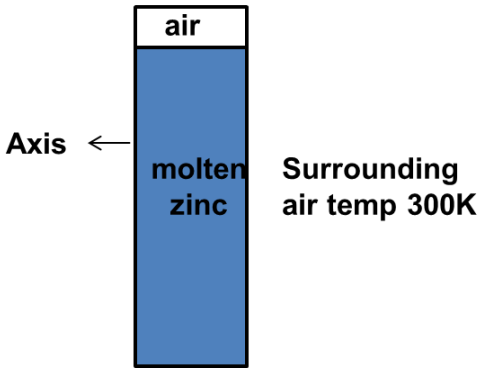


**Fig 6.15: Schematic diagram of the computational domain**

The simulation is repeated with different time step and grid independency is also checked to establish the model. The results are shown for time step 0.001sec and with minimum cells 25056. The details of grid independency study are given in Table 6.5. The convergence criterion is $10^{-3}$for velocity, continuity and $10^{-6}$ for energy. The solutions are converged in every time step. The mathematical model is solved for different convection heat transfer coefficient at the wall boundary.

**Table 6.5: Details of grid independency study**

| Number of nodes | Time step | Time of solidification |
|---|---|---|
| 50040 | 0.001sec | 36 sec |
| 72560 | 0.001sec | 36 sec |
| 25056 | 0.001sec | 36sec |
| 25056 | 0.0001sec | 36 sec |
| 25056 | 0.0005sec | 36 sec |

### 6.2.3 Results and discussion: Effect of thermal boundary condition on solidification of molten zinc

The casting or solidification of pure zinc is studied for different boundary conditions. In this research article solidification of superheated zinc in a rectangular cavity is simulated. The solidus and liquidus temperature of zinc are taken as 420°C and 425°C respectively. The solidification of zinc is a very fast process. The solidification of zinc is studied experimentally. Since the process is very fast except solidification time no other experimental data are recorded. For the experimental study the zinc is melted in a furnace and superheated heated molten zinc is poured into the rectangular cavity. The molten zinc is superheated to avoid the solidification before pouring the metal into the cavity. Figure 6.16 is the image during solidification of zinc in a rectangular cavity. The image is taken using thermal imaging camera FLIR. The red color represents the highest temperature and blue represents the lowest temperature zone. In this figure, heat loss is highest at the upper portion of cavity compared to the bottom portion. The bottom of the cavity is almost insulated as the cavity is kept on an insulating material. The limitation of experimental process is as the process is very fast the temperature change inside the cavity during solidification is not measurable accurately. Therefore, the simulation of solidification process is required for investigation of complete casting process.

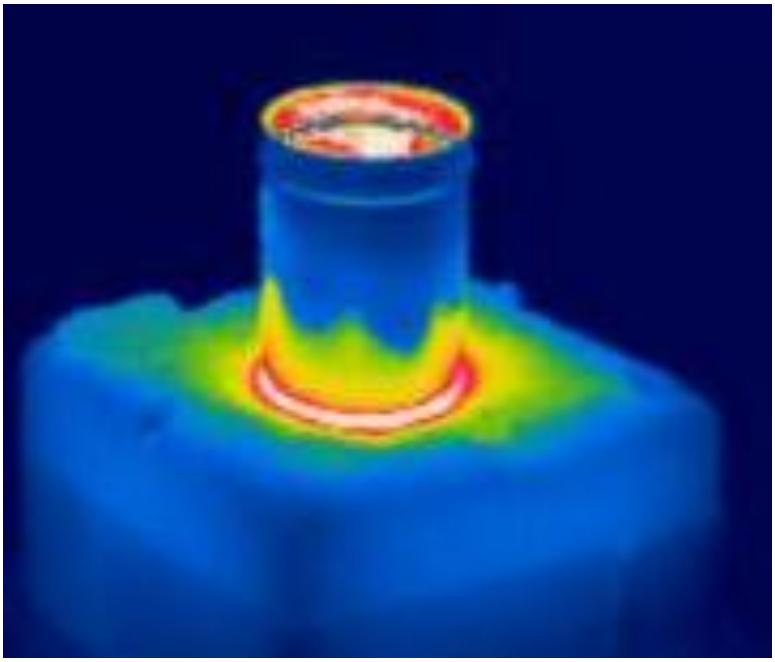

**Fig 6.16: Solidification of zinc in rectangular cavity**

For numerical simulation of solidification process the initial temperature of molten zinc is taken as 427°C (700K). Figure 6.12 shows the solidification time required for zinc under different thermal boundary conditions. These boundary conditions are: (i) solidification with convection heat transfer coefficient (htc) 600 W/m$^2$.K at side and bottom walls, (ii) solidification with convection heat transfer coefficient (htc) 300 W/m$^2$.K at side and bottom walls, (iii) solidification with convection heat transfer coefficient (htc) 600 W/m$^2$.K at side and insulated bottom walls, (iv) solidification with convection heat transfer coefficient (htc) 300 W/m$^2$.K at side and insulated bottom walls, (v) solidification with constant side and insulated bottom wall temperature (300K) and solidification with convection heat transfer coefficient (htc) 200 W/m$^2$.K at side and insulated bottom walls. The solidification time required is minimum for constant side and insulated bottom wall temperature (300K) and it is around 3.5 sec. The solidification time is around 36 sec (maximum) for wall convection heat transfer coefficient 200 W/m$^2$.K with and without bottom insulation. It is observed from Fig 6.17 that the solidification time is not affected by the bottom insulation. The time required for solidification is same for equal side wall convection heat transfer coefficient. The reason behind it is the solidification starts from both the vertical wall and the width of the cavity is less than the height of vertical wall, therefore insulated bottom wall is able to minimize the effect of cold vertical wall. It

is also important to mention that the melt fractions vs. time relation are approximately linear for higher convection heat transfer coefficient.

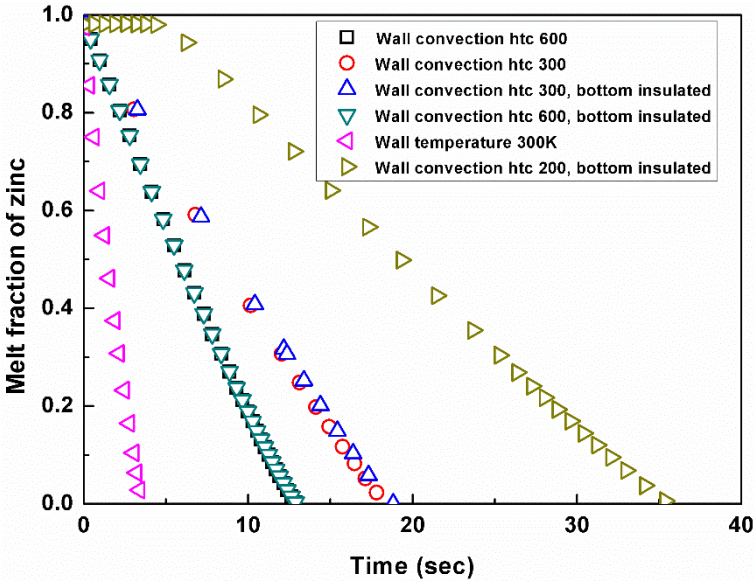


**Fig 6.17: Melt fraction of zinc under different boundary conditions**

The variations of heat flux with time are not similar for all convection boundary condition. Figure 6.18 shows the variation of heat flux. The negative sign of heat flux represents the heat loss from the control volume or cavity. Figure 6.18 concludes that the heat flux from the cavity decreases as solidification proceeds. The trend of heat flux change is almost linear for convection heat transfer coefficient 200 and 300 W/m$^2$.K (with and without bottom insulation) and the trend of heat flux is nonlinear for high heat transfer coefficient 600 W/m$^2$.K (with and without bottom insulation). The slope of heat flux curve is increasing with an increase in heat transfer coefficient and slope becomes variable for higher convection heat transfer coefficient. The contours of melt fraction with time are shown in Fig 6.19. The red color represents a complete liquid phase and blue color represents a complete solid phase. The half cavity is presented in Fig 6.19. The contours are shown for solidification with convection heat transfer coefficient (htc) 200 W/m$^2$.K at side and insulated bottom walls. It is observed that solidification starts at top of side wall due to the effect of cold vertical temperature and atmospheric air present at the open top of the cavity. With time the thickness of solid phase starts increasing from vertical wall. The thickness of solid phase is not uniform over the vertical wall; due to an increase in density of cold metal the thickness of solid zinc is higher in the bottom than that of

top. Towards the end of solidification process, the thickness of the solid phase is minimum at the middle of the cavity and highest the bottom.

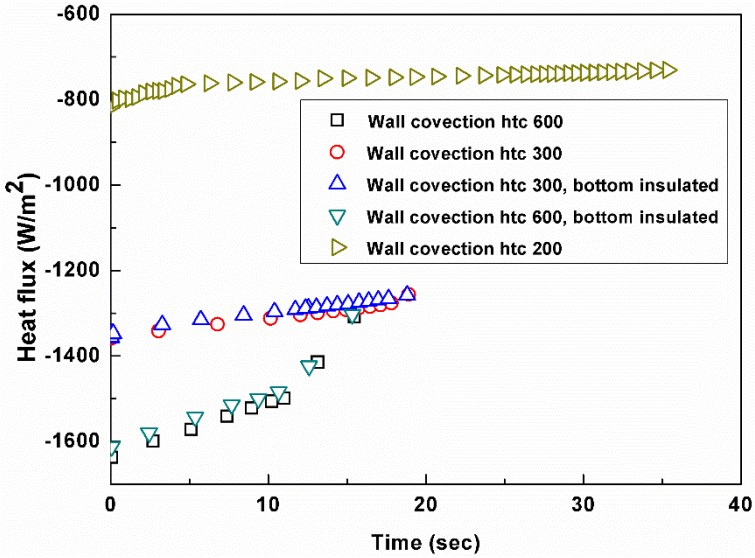


**Fig 6.18: Heat flux variation with time for different wall convection thermal boundary condition**

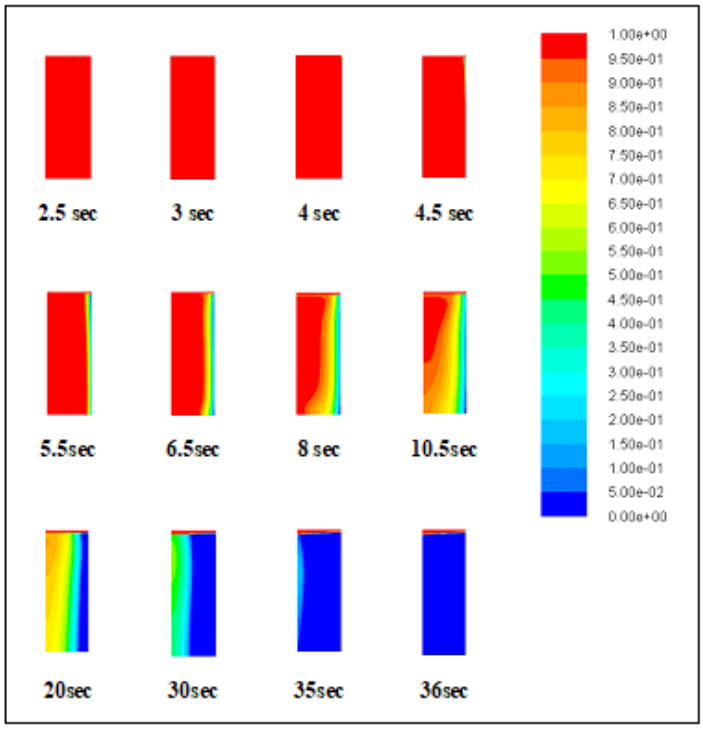


**Fig 6.19: Contour of melt fraction of zinc in half cavity**

### 6.2.4 Results and discussion: The comparison Zinc and aluminum solidification

The effect of thermo-physical properties on solidification is studied in this section. The literature review shows that lower thermal conductivity of phase change material makes the phase change process slower. Figure 6.20 shows that the higher

thermal conductivity materials take less time to solidify. The solidification of Aluminium and zinc under constant cavity temperature is presented in Fig 6.20. The shape of cavity taken is rectangular and the wall temperature is 300K. The thermal conductivity is 202.4 W/m. K for aluminum and 164 W/m. K for zinc and the time of solidification are 2sec and 3.5 sec respectively. The temperature difference between the cavity wall and the mean melting temperature is also higher for aluminum. The higher latent heat value of aluminum is reduces the difference in solidification time between aluminum and zinc. Therefore, the solidification time is inversely proportional to thermal conductivity and specific heat and directly proportional to latent heat. To study the effect of density the density of zinc decreased by ten times and all other properties and boundary conditions are kept constant. The material having density ten times lower than zinc is denoted by M1. The results of simulations are compared and presented in Fig 6.21. Both the curves for melt fraction shown in Fig 6.21 are exactly looking similar. Therefore, the solidification time is not affected due to the change in density of the material.

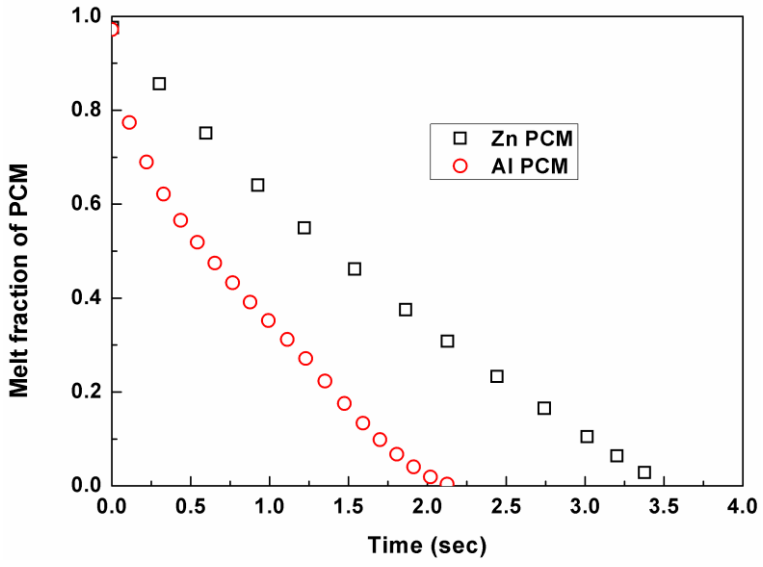


**Fig 6.20: Variation of melt fraction for different materials**

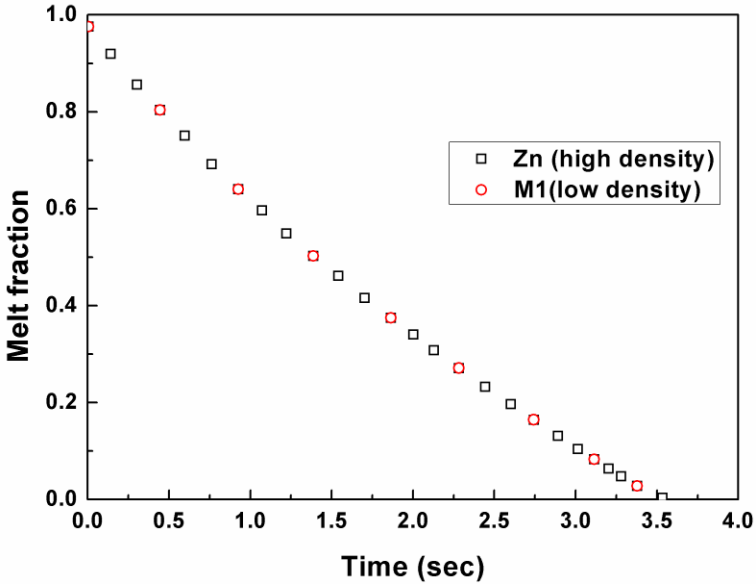


**Fig 6.21: Effect of density change on solidification time**

### 6.2.5 Conclusion

The numerical study helps to identify and analyze each step of a process. Especially for very fast processes, numerical simulations are advantageous. It is a safe and economical way of process investigation. In this section, the solidification of pure zinc is studied for different convection boundary condition. The results show that the solidification process varies. The solidification of any high-temperature PCM is always very fast. The results also show that bottom insulation is not affecting the time of solidification for the same convection heat transfer coefficient (htc). The melting time is highest for the lowest convection heat transfer coefficient htc (200W/m$^2$.K) and minimum for constant cavity wall temperature, 300K. After complete solidification the top surface is not observed to be linear but, a decrease in material level toward the axis of the cavity is noticed. The increase in density due to solidification causes this shrinkage in volume of zinc. The comparison of solidification of molten zinc and aluminum shows that thermal conductivity has higher control on the phase change process than other thermo-physical properties. Such studies can be extended to determine the molecular dynamics of metal. The solidification of metal alloys can also be investigated and compared with pure metal using this fixed grid enthalpy porosity model.

## References:


A. Bermudez, M. V. O. (2006). "An existence result for a two-phase Stefan problem arising in metal casting in metal casting." Mathematical methods in applied sciences 29: 325-350.

A.D. Brent, V. R. V., K.J. Reid (1988). "Enthalpy-porosity technique for modeling convection-diffusion phase change: application to the melting of a pure metal." Numerical Heat Transfer 13: 297-318.

B.T. Bassler, W. H. H., R.J. Bayuzick (2003). "The solidification velocity of pure Nickel." Material Science & Engineering A 342: 80-92.

Cedric Le Bot, E. A. (2009). "Numerical study of the solidification of successive thick metal layers." International Journal of Thermal Sciences 48: 412-420.

Chakraborty, P. R. (2017). "Enthalpy porosity model for melting and solidification of pure-substance with large difference in phase specific heats." International Communication in Heat and Mass Transfer 81: 183-189.

Hamid Ait Adine, H. E. Q. (2009). "Numerical analysis of the thermal behaviour of a shell-and-tube heat storage unit using phase change materials." Applied Mathematical Modelling 33: 2132-2144.

Hwang, K.-Y. (1997). "Effects of density change and natural convection on the solidification process of a pure metal." Journal of Materials Processing Technology 71: 466-476.

Majid Gorzin, M. J. H., Ali A. Ranjbara, Rasool Bahrampoury (2018). "Investigation of PCM charging for the energy saving of domestic hot water system." Applied Thermal Engineering 137: 659-668.

R. W. Lewis, K. R. (2000). "Finite element of metal casting." International Journal for Numerical Methods in Engineering 47: 29-59.

Rebow, T. A. K. M. (1999). "Freezing of water in a differentially heated cubic cavity." International journal of computational fluid dynamics 11: 193-210.

Saiwei Li, Y. C. a. Z. S. (2017). "Numerical simulation and optimization of the melting process of phase change material inside horizontal annulus." Energies 10(1249).

Sin Kim, M. C. K. a. S.-B. L. (2001). "Prediction of Melting Process Driven by Conduction-Convection in a Cavity Heated from the Side." Korean Journal of Chemical Engineering 5(18): 593-598.

Slota, D. (2011). "Restoring boundary conditions in the solidification of pure metals." Computers and Structures 89: 48-54.

Tomasz Skrzypczak, E. W. g.-S. (2012). "Mathematical and numerical model of solidification of pure metals." International Journal of Heat and Mass Transfer 55: 4276-4284.

Wenyi Hu, Q. L., Zhiqiang Zhang, Lei Bao, Jianzhong Cui (2013). "Numerical simulation of DC casting of AZ31 magnesium slab at different casting speeds." Journal of magnesium and Alloys 1: 88-93.

Yifei Wang, L. W., Ningning Xie, Xipeng Lin, Haisheng Chen (2016). "Experimental study on the melting and solidification behavior of erythritol in a vertical shell-and-tube latent heat thermal storage unit." International Journal of Heat and Mass Transfer 99: 770-781.

Zabaras N (1990). "Inverse finite element techniques for the analysis of solidification processes." International Journal for Numerical Methods in Engineering 29: 1569-1587.

Zabaras N, N. T. (1995). "Control of the freezing interface morphology in solidification processes in the presence of natural convection." International Journal for Numerical Methods in Engineering 38: 1555-1578.

Zabaras N, R. Y. (1989). "A deforming finite element method analysis of inverse Stefan problem." International Journal for Numerical Methods in Engineering 28: 295-313.

Ze-an TIAN, L.-l. Z., Yun-fei MO, Yong-chao LIANG, Rang-su LIU (2015). "Cooling rate dependence of polymorph selection during rapid solidification of liquid metal zinc." Transactions of Nonferrous Metals Society of China 25: 4072-4079.

# CHAPTER 7

# CONCLUSION

# CHAPTER 7

# CONCLUSION

## 7.1 Summary of the work

The study proposed a numerical model for the simulation of melting and solidification process. The model is called enthalpy porosity model. A commercial software Ansys-fluent is used for the simulations. The numerical simulation first demands validation of the model. The enthalpy porosity model used for simulation is validated using digital image analysis. The images are obtained from experiment and matched with the contours of simulation. The grid independency of the geometries is also checked. Different time steps are chosen to show the check the limitation of the model.

The melting in spherical cavity with different cavity materials is studied. The effect of Stefan number or cavity wall temperature on melting is studied. A detailed transient heat transfer analysis includes the variation of heat flux, maximum average velocity and melt fraction. The size of spherical cavity is scaled down from 80mm diameter to 60mm diameter and to study the effect on the melting time.

The rectangular cavity is also considered for the study of melting process. The effect of Stefan number on melting time and heat flux are studied. The simulation is repeated for different initial shape of solid PCM in the cavity. The results show the effect on melting process. The comparison of melting in spherical and rectangular cavity is presented.

The solidification process is simulated for different Stefan numbers in spherical and rectangular cavity. The detailed heat transfer analysis with time is presented.
The solidification of high thermal conductivity pure metal is studied for different convection boundary conditions. It also includes the effect of thermo-physical properties of metal on casting or solidification process. The effect of flow rate and temperature of heating fluid or high-temperature fluid is simulated using PCM heat exchanger. PCM heat exchanger is equipment where HTF is flowing through a tube

and the tube is surrounded by a pipe which contains phase change material. The heat from HTF is discharged to PCM and solid PCM liquefies after storing the latent heat. The study is repeated for different temperature and flow rate of HTF.

## 7.2 Conclusions

The major findings of this study can be summarized as:

(i) The properties of the cavity materials play a significant role to describe the nature of phase change process. It affects the shape of solid phase during the melting process. In case of lower thermal diffusivity material glass, the heat flux is less than that of copper and aluminium cavity.

(ii) The aspect ratio (height/breadth) of solid phase is higher in highest thermal diffusivity (Copper) cavity material than glass cavity during transient simulation of melting process. The higher aspect ratio makes an unstable shape which increases the bouncy effect.

(iii) Higher Stefan number shows that the natural convection controls the melting process, as the velocity reaches the maximum value.

(iv) The melting time is proportional to the volume of PCM only for same boundary condition.

(v) The selection of cavity material and boundary conditions of the melting process should be such that it would not affect the stability of the system due to the collapse of un-melted solid phase at the bottom of the cavity. In the case of phase change of energy-storing materials very fast heating or cooling may cause uneven stress distribution. Similarly, the melting of metal before casting process requires a significant amount of heat.

(vi) An empirical relation is developed to estimate solid fraction as a function of dimensionless time (Fo) and Stefan number (St). The relation considers the initial air fraction present in the cavity. The relation is limited to calculate the solid fraction of PCM only. The melt fraction calculated from this relation is mixture of liquid PCM and air which is considered as fluid in this study.

(vii) The rate of phase change or melting does not only depend on volume of initial PCM and cavity wall temperature or Stefan number but depends on the distance between cavity wall and Solid PCM.

(viii) The solidification starts from the wall and solid phase attached to the wall of cavity, the effective heat transfer rate between wall and liquid phase decreases due to low thermal conductivity of solid PCM. Therefore, the solidification time required is much higher than melting time. This implies the melting and solidification processes are not reversible processes.

(ix) The study of charging in PCM heat exchanger concludes that melting time is much effected by inlet temperature of HTF then that of flow rate of HTF. The effectiveness of PCM heat exchanger decreases with increase in flow rate. Empirical equations are also proposed to calculate the melt-fraction with time at different Stefan number in different flow regime.

(x) The PCM with high thermal conductivity and phase change temperature around room temperature is best for energy storage.

(xi) The study of solidification of high thermal conductivity material like pure metals the process is very fast and process variables varies linearly with time.

(xii) The casting or solidification process strongly depends on thermal conductivity of metal and density of metal has negligible control over the phase change processes.

(xiii) The study concludes that the melting time of low thermal conductivity is faster than solidification. On other hand, solidification is very fast for high thermal conductivity and high phase change temperature metals.

## 7.3 Future direction of work

The studies on numerical simulation of flow and heat transfer in melting-solidification problems in different cavities show the phase change process is very sensitive to small changes in operating and boundary conditions. The effect of shape of cavity and thermo-physical properties of PCM is significant. The design of an energy storing system or casting mould needs a detailed study of the process with

various operating and boundary conditions. The extension of such numerical studies will be very helpful for the following studies:

- The simulation of solid-liquid phase processes will be helpful for the selection of proper thermal and flow boundary conditions in different for different casting processes.
- It will also help to select the cavity material for different shape of cavities.
- The storage of food products needs proper storage condition in order to maintain quality and freshness. The simulations of such processes will help to make the process cost-effective.
- In cold countries, such simulation will help to maintain the flow of water without solidification of it.
- Design of the environment-friendly temperature control system needs simulations of solid-liquid phase change process of different organic, inorganic and other materials.

# ANNEXURE

Heat and Mass Transfer (2019) 55:1427–1437
https://doi.org/10.1007/s00231-018-2522-0

ORIGINAL

# Numerical and experimental investigation of paraffin wax melting in spherical cavity

Debasree Ghosh [1] · Chandan Guha [2]

Received: 6 December 2017 / Accepted: 8 November 2018 / Published online: 23 November 2018


## Abstract

Various process parameters influence the melting and solidification phase change process. Studies on the influence of shape of cavity, thermo-physical properties of the phase change material and the boundary conditions, on the phase change process, has been carried out by various researchers worldwide. The effect of the thermal properties of the cavity material on the process is yet to be investigated thoroughly. In this work, melting process of paraffin wax is simulated in a spherical cavity for various cavity materials having different thermal properties and for different boundary conditions. The simulations results are obtained using enthalpy-porosity model for free surface melting process, solved using Ansys-fluent 16.2. Experimental studies were carried out for one type of cavity material. The experimental investigation included visualization of shape of solid fraction which is used to validate the numerical approach of this computational study. The results showed that the materials having higher thermal diffusivity has enhanced melting rate because of increased bouncy effect and convection. It has been found that the higher Stefan number shows the effect of higher natural convection and maximum velocity profile, resulting in enhanced melting process. These simulations are significant for selection of cavity material for different processes like energy storage, melting-solidification of metal in casting and others.

## Symbols

| | |
|---|---|
| $\alpha_n$ | Phase volume fraction of nth fluid |
| $u_i$ | Velocity component in $i^{th}$ direction (m/s) |
| $x_i$ | Cartesian component |
| $t$ | Time (s) |
| $\rho$ | Density of PCM (kg/m$^3$) |
| $\mu$ | Viscosity of PCM (kg.m/s) |
| $C_{pl}$ | Specific heat of liquid pcm (J/kg.K) |
| $p$ | Pressure (N/m$^2$) |
| $g_i$ | Gravitational force (m/s$^2$) |
| $S_i$ | Momentum source (kg/m$^2$.s$^2$) |
| $h$ | Enthalpy (kJ/kg) |
| $k$ | Thermal conductivity (W/m.K) |
| $T$ | Temperature (K) |
| $T_w$ | Wall temperature of the cavity (K) |
| $T_m$ | Mean melting temperature of PCM (K) |
| $C$ | Mushy zone constant |
| $\gamma$ | Liquid fraction |
| $T_s$ | Solidus temperature (K) |
| $T_l$ | Liquids temperature(K) |
| A | Thermal diffusivity (m$^2$/s) |
| St | Stefan number |

✉ Debasree Ghosh
dghosh@bitmesra.ac.in

[1] Department of Chemical Engineering, Birla Institute of Technology, Mesra, Ranchi, India

[2] Department of Chemical Engineering, Jadavpur University, Kolkata, India

## 1 Introduction

Phase-change processes are very common in nature as well as in industrial processes. Phase change materials (PCM) have a great potential to perform as an energy storing element. These PCMs can be used in many applications such as to store pollutant free solar energy, as an alternative heating system and as heat pump etc. PCM based solar thermal systems are also used to minimize such pollutants [1, 2]. Such application of PCM can effectively lead to lesser carbon-di-oxide emission because of reduced use of fossil fuels. Thermal energy can be stored in three distinct ways: sensible heat storage, latent heat storage and thermo-chemical heat storage. Amongst the three ways, the thermo-chemical heat storage is more energetic, but the process is complex due to chemical reactions and adsorption-desorption process. It also requires distinct charging and discharging temperature [3]. On the other hand, latent heat storage is a very simple process with high energy storage

density in a narrow temperature range. In the food and beverage industries and industrial drying processes, sensible heat loss can be minimized, which helps to perform the operation at an optimum temperature [4]. To apply latent heat of phase change process of PCM in industrial application, it is necessary to understand the mechanism of the phase change process of these materials.

Many studies of phase change processes in the spherical cavity have been reported in the literature [5–15]. The phase change process depends on the mechanism of heat transfer. For conduction dominated gravity assisted melting process, the solid phase will not move and in the case of natural convection, the solid phase will sink at the bottom of the cavity [6, 7, 16].

A detailed study on the works carried out on solid/liquid phase change processes is presented in Table 1. It is evident from the Table 1 that the numerical simulations of phase change processes are performed using finite volume method. The Volume of fluid (VOF) method is applied to locate the solid/liquid interface in the cavity and the enthalpy-porosity is applied to define the effect of phase change in momentum balance equation. The phase change processes in the spherical cavity for paraffin wax with different boundary conditions show that the location of the solid/liquid interfaces are different, and the time required for complete phase change is different. In the case of a spherical cavity, no significant change in the shape of the solid fraction is observed if the wall boundary condition is uniform throughout the process [6, 8, 14, 15]. The case is different in a rectangular cavity. The melting rate and the energy stored in heating, from the vertical side are much higher than that of heating from below or horizontal wall heating, due to enhanced natural convection effect [17]. The rate of phase change in the rectangular cavity also depends on the orientation of the cavity. Babak and Hamid [18] simulated the melting process of Lauric acid in the horizontal rectangular cavity where the heating was supplied from the bottom wall and all other walls were insulated and in case of the vertical rectangular cavity the heating was supplied from the right wall and all other walls were insulated. It has been observed that the phase change of Lauric acid shows melting time is minimum for a horizontal rectangular cavity than the vertical rectangular cavity. The effects of thermo-physical properties of PCM also play an important role during the phase change process. The thermo-physical properties of paraffin wax and n octadecane are almost similar, so the phase change process is same for those materials. On the other hand, the phase change of paraffin wax and n octadecane are different from that of water. This is because during melting the volume of water decreases and the solid phase of water floats on the liquid phase [6, 12–15]. The thermo-physical properties liquid metals are very different from water and other organic PCM like paraffin wax and n octadecane. The thermal conductivity of metal is very high, and thermal expansion

**Table 1** Literature survey on melting and solidification phase change processes

| PCM | Shape of cavity | Boundary condition | Cavity material | Model used in simulation | Reference |
|---|---|---|---|---|---|
| Paraffin wax | Spherical | Constant temperature at cavity wall | glass | Enthalpy porosity model for free surface | [6] |
| Paraffin wax | Spherical | Constant temperature at cavity wall and constrained melting | glass | Enthalpy porosity model for free surface | [8] |
| Water | Spherical | Constant cavity wall temperature | | Boundary Fixing Method | [12, 13] |
| Paraffin wax | Spherical | Constant temperature at cavity wall and unconstrained solidification | glass | Enthalpy porosity model for free surface | [14] |
| n octadecane | Spherical | Uniform heat flux at outer shell | Pyrex | Boundary Fixing Method | [15] |
| Paraffin wax + alumina | Square cavity | 1.Heated from bottom side and 2. Vertical side | Not mentioned | Enthalpy porosity model | [17] |
| Lauric acid | Inclined rectangular enclosure | Constrained melting with the right wall of the cavity is set at a constant temperature and the other walls are adiabatic. | Not mentioned | Enthalpy porosity model | [18] |
| Liquid aluminum alloy A356 | Pipe with slope | Cooling slope and no slip boundary condition | Not mentioned | VOF and continuum surface force (CSF) model | [19] |
| Molten salt | Pipe (3D) | Insulated outlet wall and convection heat transfer through the wall | Steel | VOF and continuum surface force (CSF) model | [24] |
| Paraffin wax | Cylinder | Constant temperature at cavity wall and unconstrained solidification | Not mentioned | Enthalpy porosity model for free surface | [25] |
| Polystyrene (Plastic melt) | Cubic | Water cooling channels | Not mentioned | Finite volume method for one fluid model | [26] |

coefficient is very low which results in a decrease in natural convection effect. The higher thermal conductivity is thus an important property for rapid completion of the melting process [17, 19].

Table 1 summarizes the available literatures on different PCM, with different boundary conditions, for different orientation and for different shape of the cavity. However, the thermo-physical properties of cavity material are also important parameters which need to be studied numerically in order to understand the phase change process properly. This study tries to investigate the effect of cavity material on phase change process. In order to investigate the same, the melting process of paraffin wax is simulated in a spherical cavity for various cavity materials having different thermal properties and for different boundary conditions. The experimental investigation included capturing of images of the shape of the solid fraction at different time inetrval which is used to validate the numerical approach of this computational study.

## 2 Experimental procedure

The experiment has been performed in a transparent tank (shown in Fig. 1), filled with distilled water. The level of water is kept constant during the time of experimentation. An electrical heater is used to heat the water and PID (Proportion-Integral-Derivative) controller is used to maintain a constant temperature of the water bath. A spherical shell filled with the solid PCM is placed into the constant temperature water bath. The initial temperature of the phase change material inside the cavity is 300 K (1 K less than the solidus temperature of the PCM) and the experiment continues until the PCM has melted completely. The PCM expands during melting and the increased volume is accommodated by replacing the air through the neck of the cavity. Images obtained during the melting process are recorded by a high-speed digital camera at various stages of the process. These images are analyzed using digital image processing technique and the experimental values of the melt fraction are calculated at various time instants. The results are used for the validation of the numerical approach, as reported in the section 4.1.

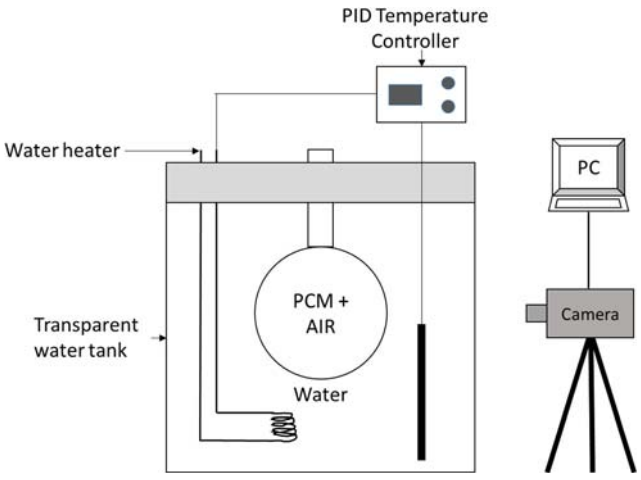


**Fig. 1** Schematic diagram of experimental setup

### 2.1 Physical model

A spherical shell with an inner diameter of 80 mm and wall thickness 2 mm is considered in this study. Initially, the spherical shell or cavity is 85% filled with PCM paraffin wax (RT27) at an initial temperature of 300 K (one Kelvin less than the solidus temperature). The outer surface temperature of the cavity is kept greater than the liquidus temperature of the PCM. Melting starts at the surface and the moving boundary moved towards the center. Since the density changes due to phase change the heavier solid phase sink at bottom of the cavity and lighter liquid phase has been observed at the top of the container. The thermal conductivity of the glass container is taken as 0.81 $W.m^{-1}.k^{-1}$ for simulations [6]. The properties of the PCM, based on paraffin wax (RT27), a commercially available material, are given in Table 2.

### 2.2 Computational procedure

The numerical approach is necessary to predict the melting phenomena inside a cavity. The flow is assumed to be two dimensional and unsteady. It is also assumed that both solid and liquid phases are homogeneous and isotropic. The two-dimensional axisymmetric model is used for the study of the melting process. The axisymmetric model reduces the computation time. The molten PCM and the air are considered to be incompressible Newtonian fluids, and laminar flows are assumed in both the phases. A density-temperature relation is used for air: $\rho = 1.2 \times 10^{-5}\ T^2 – 0.01134\ T + 3.4978$ [6].

### 2.3 Mathematical modelling

Phase-change processes are also called moving boundary problems. The solid-liquid interface or solid liquid boundary continuously changes its shape during phase change. Due to a change in density during heating and phase change, a velocity

**Table 2** Thermo-physical properties of paraffin wax (RT27)

| | |
|---|---|
| Density | 870 kg $m^{-3}$ (solid phase)<br>760 kg $m^{-3}$ (liquid phase) |
| Specific heat | 1800 J $kg^{-1}$ $K^{-1}$ |
| Thermal conductivity | 0.15 W $m^{-1}$ $K^{-1}$ |
| Viscosity | $3.42 \times 10^{-3}$ kg $m^{-1}$ $s^{-1}$ |
| Solidus temperature | 301 K |
| Liquidus temperature | 303 K |
| Latent heat of fusion | 179 kJ $kg^{-1}$ |

field is also generated which results in a non-linear interface. Melting and solidification processes are different from condensation and vaporization. The reason behind it is that the solid phase is static during phase change processes. Whereas in condensation and vaporization both liquid and vapor phase are fluid.

A two-dimensional axisymmetric circular cavity has been chosen in this study of melting process of paraffin wax. The cavity is partially filled (85%) with phase change material (PCM) paraffin wax. The PCM is initially at a temperature which is one degree less than the solidus temperature. The study has been performed in cavities of three different thermal diffusivities. The outer surface of the cavity is kept around 19°C higher than the average melting temperature. The cavity is open to air during the melting process. Properties of PCM are considered as that of a commercially available paraffin wax [6]. Commercial software Ansys-fluent16.2 is used for numerical simulation of the melting process. To describe the PCM-air system with a moving internal surface without interpenetration of two media (air and PCM), volume-of-fluid (VOF) model has been used. VOF model is also successfully applied to vapour/liquid phase change processes in the open cavity [20]. Enthalpy-porosity model is used for the simulation of the melting process in the phase change region. The fixed-grid enthalpy-porosity method requires velocity suppression because at the solid phase velocity is zero. Velocity suppression can be accomplished by the suitable source term in the momentum equation driven to model the two-phase domain as a porous medium [21]. The momentum equation is subjected to no-slip boundary conditions at the walls. The flow is considered to be two-dimensional, laminar, and incompressible. The thermo-physical properties of the materials are constant at solid and liquid phases except for the density of the PCM. The source terms of the momentum equations are used to model the flow through the porous medium, near the solid-liquid interface. The value of the mushy zone constant is taken as $10^5$ [22].

The governing equations are as follows:

Continuity equation:

$$\frac{\partial \alpha_n}{\partial t} + u_i \frac{\partial \alpha_n}{\partial x_i} = 0 \tag{1}$$

Where n is secondary material PCM.

$\alpha_n$ denotes the $n^{th}$ fluid's volume fraction in the computational cell. If $\alpha_n = 0$ the cell does not contain the $n^{th}$ fluid and $\alpha_n = 1$ implies the cell contains only the $n^{th}$ fluid. If $\alpha_n$ lies between zero and one the cell contains a mixture of $n^{th}$ fluid and other fluids. More specifically, the value of $\alpha_n$ is one at solid/liquid PCM interface (n is the PCM) and the value of $\alpha_n$ lies between zero and one at the PCM-air interface. The volume fraction Eq. 1 will not be solved for the primary phase (air); the primary-phase volume fraction will be computed based on the following constraint

$$\alpha_{air} = 1 - \alpha_n \tag{2}$$

Momentum equation:

$$\frac{\partial}{\partial t}(\rho u_i) + \frac{\partial}{\partial x_i}(\rho u_j u_i) = \mu \frac{\partial^2 u_i}{\partial x_j \partial x_j} - \frac{\partial p}{\partial x_j} + \left(\rho - \rho_{ref}\right) g + S_i \tag{3}$$

$\rho_{ref}$ is the density of cell at a reference temperature $T_{ref}$. The density is a function of temperature. During the melting process, with an increase in temperature, melting occurs and density decreases with increasing volume. This density difference causes a bouncy force in the cavity.

Energy balance equation:

$$\frac{\partial}{\partial t}(\rho h) + \frac{\partial}{\partial x_i}(\rho u_i h) = \frac{\partial}{\partial x_i}\left(k \frac{\partial T}{\partial x_i}\right) \tag{4}$$

Where ρ is the density, k is the thermal conductivity, μ is the dynamic viscosity, $S_i$ is the momentum source term, $u_i$ is the velocity component, $x_i$ is a Cartesian coordinate, and h is the specific enthalpy of both the air and PCM respectively in the specified region. The Eq. 3 and Eq. 4 are applicable to air, PCM and their interface. The thermophysical properties like density, thermal conductivity and viscosity are calculated as follows:

$$\left.\begin{aligned} \rho &= \alpha_n \rho_{PCM} + (1-\alpha_n)\rho_{air} \\ k &= \alpha_n k_{PCM} + (1-\alpha_n) k_{air} \\ \mu &= \alpha_n \mu_{PCM} + (1-\alpha_n)\mu_{air} \end{aligned}\right] \tag{5}$$

Where,

$$\left.\begin{aligned} \rho_{PCM} &= \gamma \rho_{PCM,liq} + (1-\gamma)\rho_{PCM,solid} \\ k_{PCM} &= \gamma k_{PCM,liq} + (1-\gamma) k_{PCM,solid} \\ \mu_{PCM} &= \mu_{PCM,liq} \end{aligned}\right] \tag{6}$$

Also, the expression for the change in enthalpy is defined as $h = h_{ref} + \int_{T_{ref}}^{T} C_p dT$ and for phase change, $h = \gamma L$. $h_{ref}$ is enthalpy at a reference temperature $T_{ref}$. L is the specific enthalpy of melting (latent-heat of the material), and $\gamma$ is the liquid fraction during the phase-change which occurs over a range of temperatures and defined by the following relations:

$\gamma$ is defined as follows:

$$\left.\begin{aligned} \gamma &= 0 \; at, T < T_s \\ \gamma &= \frac{T - T_s}{T_l - T_s}, at T_s < T < T_l \\ and\ \gamma &= 1 \; at T > T_l \end{aligned}\right] \tag{7}$$

The porosity function at momentum source term is defined with the help of the Carman-Kozeny equation for flow through porous media and the source is [5, 6]:

$$S_i = -C\frac{(1-\gamma)^2}{\gamma^3+\varepsilon}u_i \tag{8}$$

C in Eq. 8 is called mushy zone constant and the value of C is $10^5$ [6].

The momentum, continuity and energy equations are solved using the SIMPLE pressure-velocity coupling scheme. Discretization scheme used are PRESTO for pressure, second-order upwind for momentum, Geo-reconstruct for volume fraction and second-order upwind energy [23]. The boundary conditions are 1. the temperature of the wall is kept constant and the wall thickness is 2 mm, and 2. the opening of the cavity is at atmospheric pressure condition. The initial temperature of the phase change material kept on 27°C which is 1°C less than the solidus temperature of PCM.

The simulations are repeated for 0.00001 s, 0.0001 s, and 0.001 s time step sizes and the results obtained are similar. The simulations are also repeated with 34,612 and 15,336 numbers of cells to prove the grid independency of the phase change model. In this study, results are shown for the maximum time step of 0.001 s and 22,320 (minimum) numbers of cells. An 80 mm diameter spherical shape glass cavity is chosen for the grid independency study. To minimize the time of simulation a higher Stefan number (St = 0.21) is considered to check the grid independency. Figure 2 shows that the melt fraction is independent of the number of cells. The convergence in each time step has been checked with the convergence criterion of $10^{-3}$ for velocity and continuity and $10^{-6}$ for energy. The mathematical model is solved for three different types of spherical cavity materials; they are:

- Aluminium cavity with thermal diffusivity (α) as $8.5 \times 10^{-5}$ m$^2$/s,
- Copper cavity with thermal diffusivity (α) as $11.3 \times 10^{-5}$ m$^2$/s and.
- Glass cavity with thermal diffusivity (α) as $3.42 \times 10^{-7}$ m$^2$/s.

The simulations are performed for different Stefan numbers, 0.13, 0.18 and 0.28 respectively.

## 3 Results and discussion

### 3.1 Validation of the numerical model

The images are obtained during the experiment of melting of PCM in the spherical cavity (80mm diameter) with water-bath at temperature 47°C. The melt fraction (air and liquid PCM) in the cavity are estimated from the images using digital image analysis technique. The melt fraction (air and liquid PCM) obtained from images were used to validate the numerical method. Melt fraction (air and liquid PCM) with time is shown in Fig. 3. Melt fraction (air and liquid PCM) is an average-volume fraction of fluid in air and paraffin wax mixture. The melt fraction (air and liquid PCM) is calculated using the following relation:

$$melt\ fraction = \gamma_{mix} = (1-\alpha_n) + \alpha_n\gamma_{PCM} \tag{9}$$

The deviation of experimental result from the simulated result at the initial stage of melting is because of the presence of the mushy zone. The estimation of exact melt

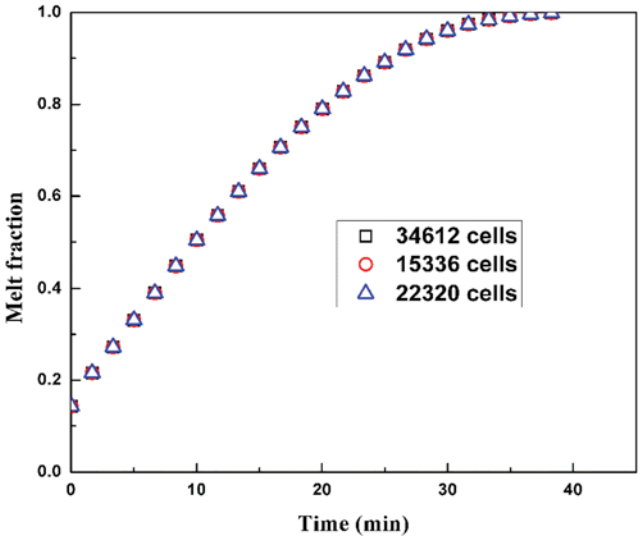


**Fig. 2** Grid independency for the melting process

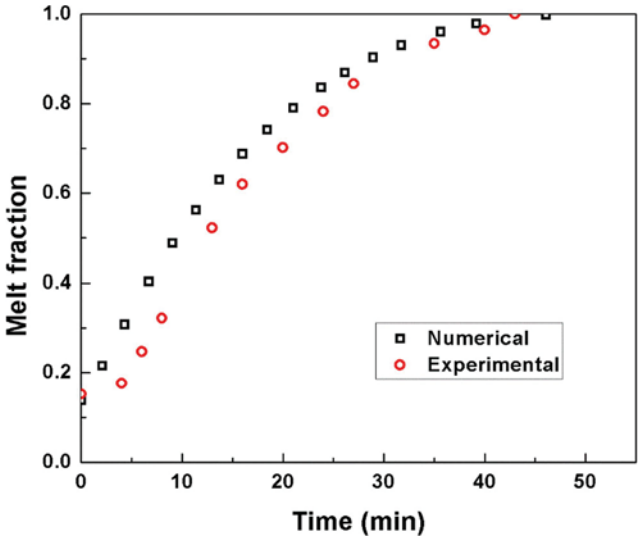


**Fig. 3** Comparison of the experimental and numerical melt fraction (air +liquid PCM)

fraction in the mushy zone using digital image analysis technique is difficult because of similar colour contrast. In digital image analysis, the volume of fluid is estimated from the colour of a different zone. In this case, air and liquid wax are colourless and solid wax is white in colour. During the initial stage of melting, as the volume fraction of liquid is very low in the mushy zone, the colour remains white. Thus, the estimated melt fraction differs slightly from the simulation at the initial stage of the melting process. Figure 4 shows the experimental images and density contours at different instant of time are almost similar. In Fig. 4 the red coloured zone is a complete solid phase and light orange is semi-solid or mushy zone and the yellowcolour is a complete liquid phase. In a digital image processing technique, the complete liquid phase is identified but solid and semi-solid phases are not perfectly distinguishable. In Fig. 4 the interface between the semi-solid region and liquid region of experimental and simulation are comparable. The image validation is very much important for unconstrained melting as no other parameter like temperature inside the cavity, or melt-fraction of PCM are measurable during the continuous process. Due to this reason, the experiments are performed in transparent glass cavity and PCM is also chosen such that the colour of solid and liquid phase are distinguishable. The validated numerical model is applied to simulate the phase change process inside a non-transparent cavity, which are used in practical cases.

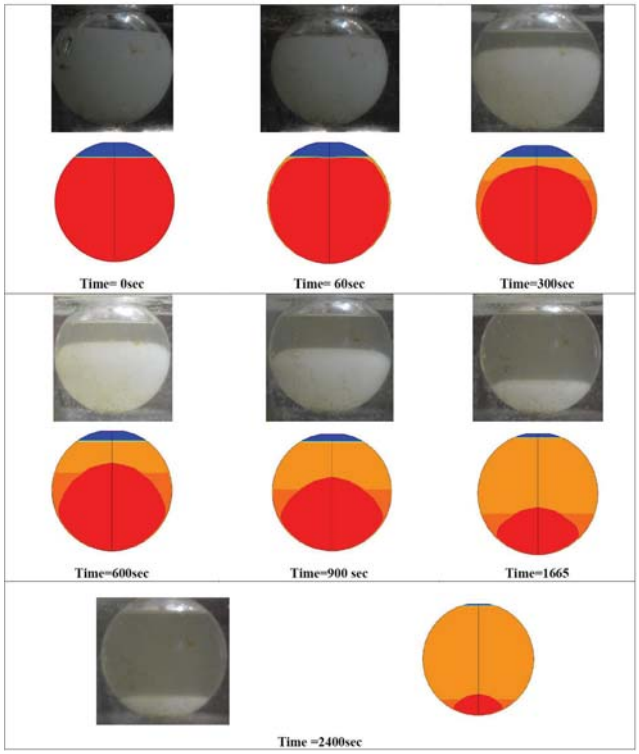


**Fig. 4** Experimental images matched with density contours of simulated result

### 3.2 Results of simulation

The simulated results obtained from simulation using Ansys-fluent 16.2 for volume of fluid (VOF) model and enthalpy porosity model in the cavity; the coloured contours of the solid-liquid front of PCM at the various time interval for the unconstrained melting process at outer wall temperature 47°C and initial temperature 27°Care shown in Figs. 5 and 6. The simulation has been performed for three different cavities which are glass, aluminium and copper. Figure 5 shows the contours of melt fraction and Fig. 6. shows the density distribution with time. In Fig. 5 the blue colour indicates the solid portion and red colour indicates the liquid portion in the cavity. The outer surface of the solid PCM is in contact with the inner wall of the sphere so that heat conduction between the wall and solid PCM dominates. This results in the formation of the thin liquid layer between solid PCM and wall. With time, the molten zone expands, and the liquid layer rises. A spherical shape of the solid fraction is retained for most of the melting process except towards the end when it loses its spherical shape and becomes flattened or elongated until melting is completed. On the other hand, as the solid is denser than the liquid, the solid phase is not fixed, it starts moving downward due to gravity. The bouncy force is included in momentum balance to consider the effect of volume change of PCM due to phase change. The density of cell is a function of melt fraction and again melt fraction is a function of temperature. Therefore, the bouncy term in Eq. 3 shows the effect of thermal bouncy force. The motion of the solid phase is accompanied by the formation of liquid at the melting interface. This liquid is squeezed up through a narrow gap between the melting surface and the wall of the shell, to space above the solid. Therefore, natural convection in combination with the sinking of the solid portion at the bottom ofthe container controls the melting process. Both melt fraction and density distribution are similar approximately till 5 mins of initiation of the melting process. At around 10 mins of initiation of the melting process the shape of the solid fraction within the cavity starts changing. The shape of the solid fraction in the glass cavity is different from that of aluminium and copper cavities than that for glass cavity. However, the solid fraction of copper and aluminium cavity are similar. The reason is, with the higher value of thermal diffusivity of the cavity material, the rate of heat transfers from cavity bottom wall to the PCM increases and it melts the PCM immediately and only a small fraction of solid PCM is found at the bottom of the cavity. Figures 5 and 6 also show that the melting process is slowest in the glass cavity. Thus, the time required for complete meltingis inversely proportional to the thermal diffusivity of the cavity materials. The time required for complete melting is almost the same for the highest and second highest thermal diffusivity material aluminium and copper respectively and it is almost double in case of glass cavity with lowest thermal

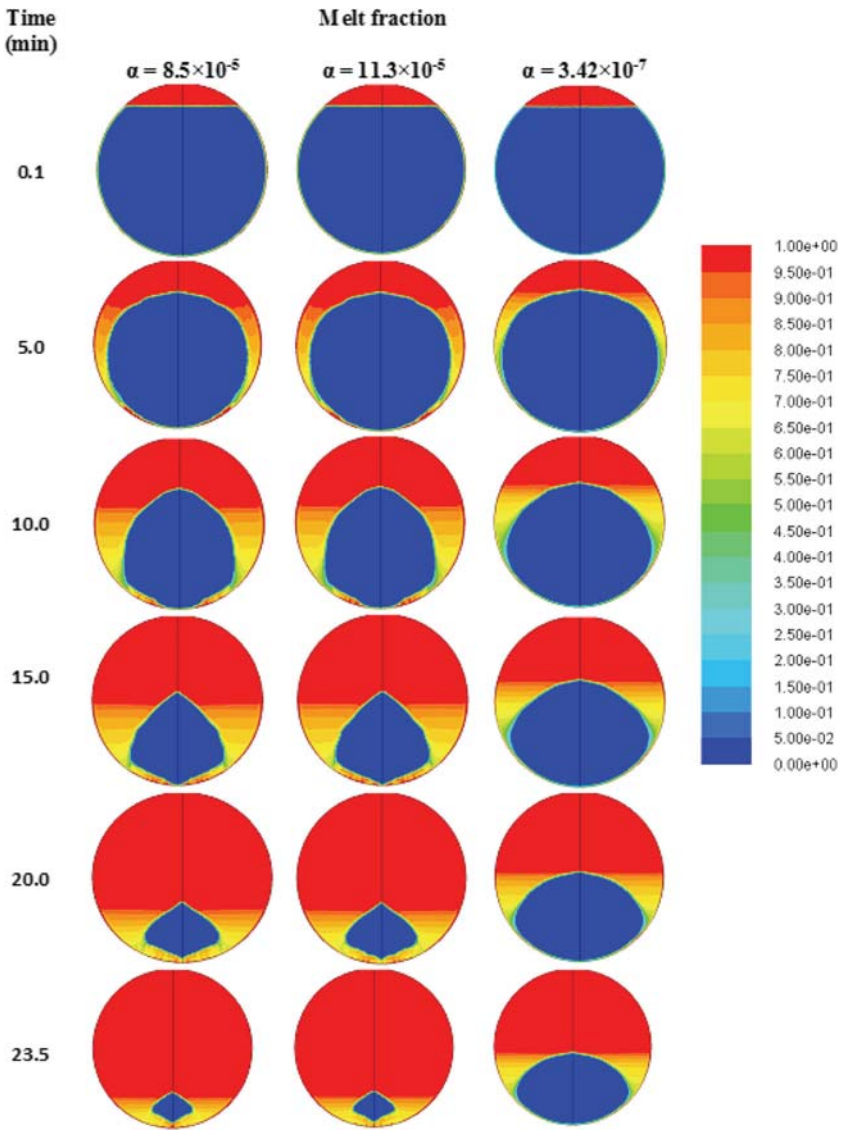


**Fig. 5** Contours of melt fraction in the cavities with different thermal diffusivity for St = 0.18

diffusivity. Figure 6 shows the expansion of volume in the liquid phase by expelling the initial air content within the cavity. The continuity equation given in Eq. 1 is only applied to calculate the volume fraction of PCM and the remaining volume fraction is for air. Therefore, an increase in melt fraction shows an increase in $\alpha_n$ and decrease in $\alpha_{air}$. Decrease in $\alpha_{air}$ confirms the removal of air from the cavity and increase in PCM height in the cavity. Both Figs. 5 and 6 show the perfect match of the assumptions of close contact melting with enthalpy-porosity model applied to an open surface cavity. The result presented for melt fraction in Fig. 5 is obtained by solving the enthalpy-porosity model where air and liquid PCM are not identified separately. The air, liquid PCM and solid PCM are identified individually in the Fig. 6 using VOF model. The density contour of Fig. 6 helps to locate the fluid-fluid and fluid-solid interface.

Figure 7 shows the melt fraction (air + liquid PCM) with time. The melt fraction (air + liquid PCM) is the amount of air and melted wax content in the cavity. It is evident that the melt fraction (air + liquid PCM) within the cavity increases with time and the time required for complete melting is greater for the cavity material having the lowest thermal diffusivity. Heat flux is another important parameter in heat transfer study. Volume average heat flux is defined as heat supplied to control volume per unit area. A positive value of heat flux implies heat addition to the control volume and negative value of heat flux implies heat rejection from control volume. Therefore, the heat flux is positive on the computational domain for melting. Figure 8 represents the variation of heat flux with time, shows a sudden decrease in heat flux at the initial stage of melting in spherical aluminium and copper cavity. On the other hand, the change in heat flux is moderate for the glass cavity. In the case of higher thermal diffusivity of the cavity material, initially the temperature gradient between PCM and wall is very high, and the resistance due to conduction is very low, which results in the significantly high rate of heat transfer. In the case of lower

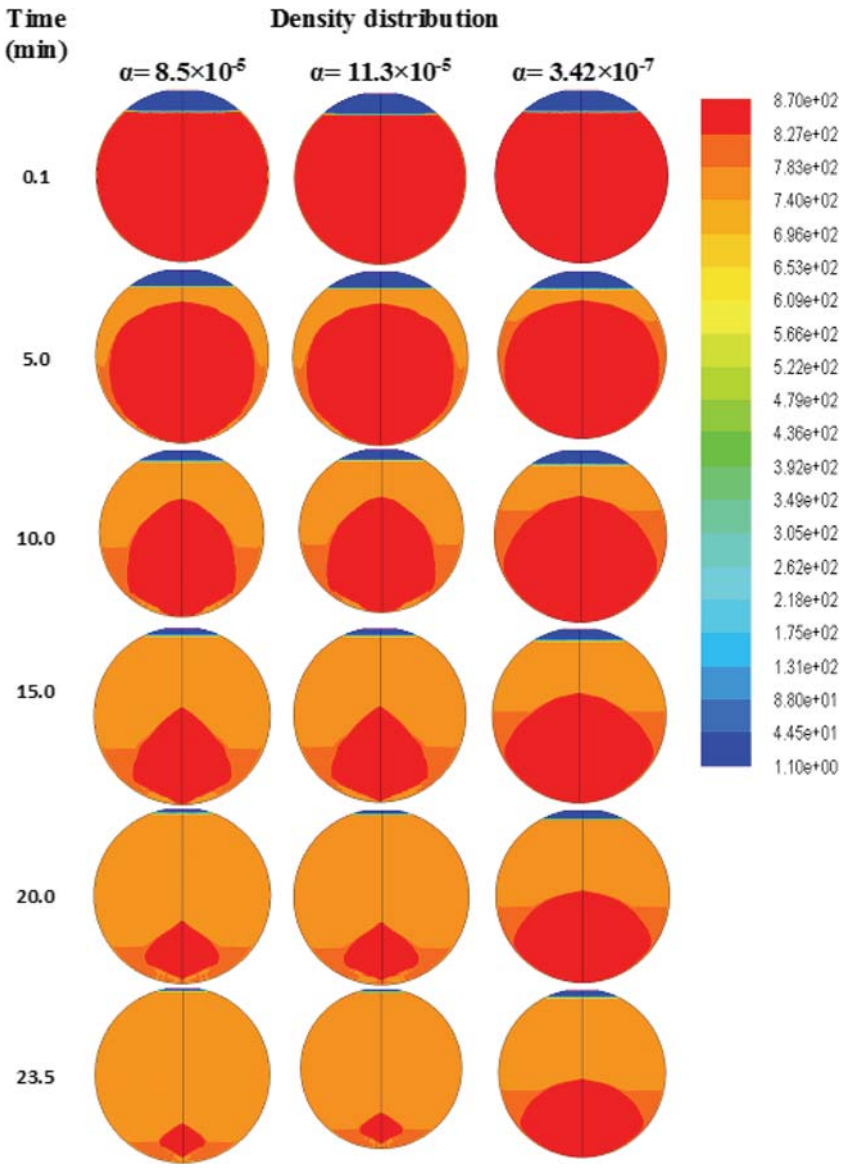


**Fig. 6** Contours of density in the cavities with different thermal diffusivity for St = 0.18

thermal diffusivity of thecavity, the temperature gradient is same initially but the resistance to conduction is high compared to the higher thermal diffusivity of the cavity and the result is low heat transfer rate. As the thickness of liquid PCM increases, the effective thermal bouncy force decreases. The decrease in thermal bouncy force results in lower convection heat transfer and show a falling trend in heat flux with time. In the case of copper and aluminium cavity, the heat flux curve decreases rapidly than glass cavity due to higher melting rate.

Figure 9 shows the effect of convection compared to conduction heat transfer. The dimensionless Nusselt number is used to represent the change of mode of heat transfer with time. Nusselt number is the ratio of conduction resistance to convection resistance. Initially, the melting process considered in this study is initiated due to conduction and gradual increase in melt fraction introduces convection heat transfer. The figure

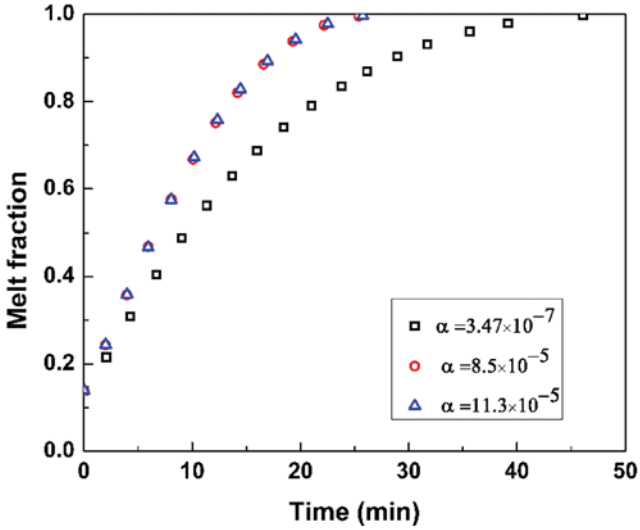


**Fig. 7** Melt fraction (air +liquid PCM) in cavity for St = 0.18

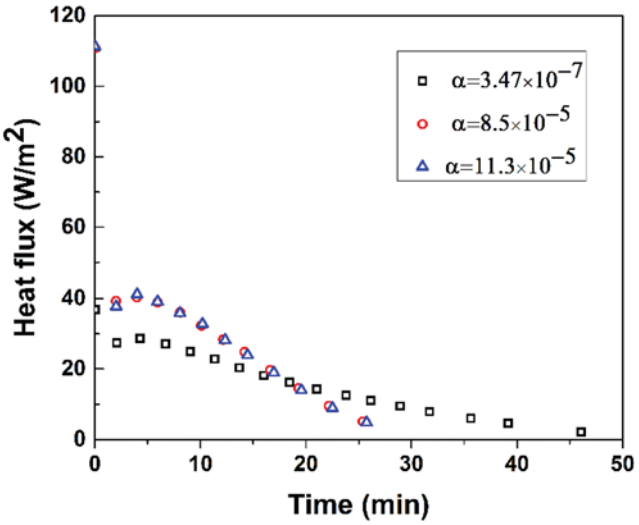


**Fig. 8** Variation of heat flux with time for St = 0.18

shows that for aluminium and copper cavity Nusselt numbers are very high which means the conduction resistance is more than convection resistance. The Nusselt number decreases to zero at the end of the melting process as convection heat transfer decreases due to a decrease in density and bouncy effect at the end of the melting process. In the case of the glass cavity, the Nusselt number decreases gradually with time. Melting in the glass cavity is very slow and the conduction heat transfer controls the process by minimizing the effect of convective heat transfer. It is important to mention that the volume average heat flux is more influenced by thermal diffusivity rather than the Nusselt number. This is because the Nusselt number depends on thermal properties of fluid i.e. PCM and air and not on the thermal properties of the cavity material. Nusselt number variation observed in Fig. 9 is due to the change in melt fraction in the cavity.

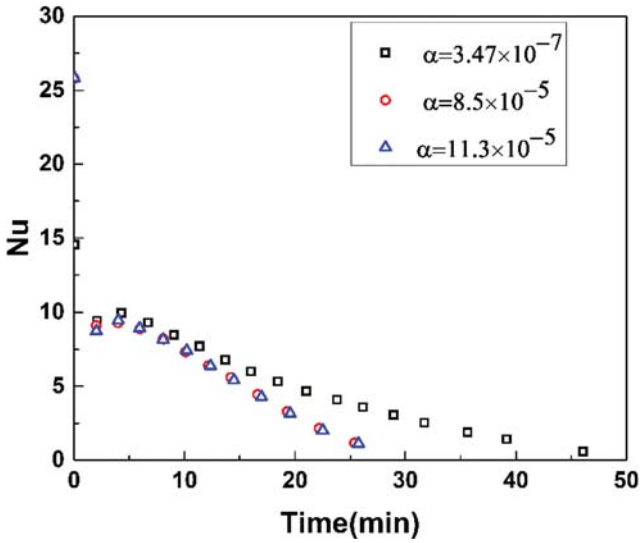


**Fig. 9** Variation in Nusselt number for St = 0.18

The melting phenomenon is also studied for different Stefan numbers for copper made spherical cavity (80 mm diameter). Stefan number (St), is the ratio of sensible heat and latent heat of the PCM. The surface temperature directly affects the value of the Stefan number. The expression for Stefan number is given in Eq. 10.

$$St = C_{pl}(T_w - T_m)/L \tag{10}$$

Where $C_{pl}$ is specific heat of the liquid PCM, L is the latent heat and $T_m$ is the mean melting temperature of PCM and $T_w$is the wall temperature at the surface of the cavity respectively. The present simulation has been performed at three different Stefan numbers, St = 0.13 ($T_w = 42^oC$), St = 0.18 ($T_w = 47^oC$)) and St = 0.28 ($T_w = 57^oC$). As the surface temperature increases and Stefan number increases and the total melting time decreases. Figure 10 shows the variation of the melt fraction (air + liquid PCM) present in the cavity with time. The result shows an increase in volume of fluid with time as melting proceeds. The initial volume fraction of fluid was around 0.15 same as the volume fraction of air present in the cavity. As the melting process proceeds the fraction of air is gradually replaced by melted wax. The melted wax is of lesser density and results in occupying a larger volume. Time required for complete melting is inversely proportional to Stefan numbers which are 22mins, 28mins, and 33mins for Stefan number equals to 0.28, 0.18 and 0.13 respectively as shown in Fig. 10.

Figure 11 shows the variation of heat flux with time for different Stefan numbers. Heat flux is highest for highest Stefan number due to a higher temperature gradient. In the case of Stefan number 0.28 the maximum heat flux is 170 W/m$^2$ and for Stefan, number 0.13 and 0.18 maximum heat flux are 82 and 111 W/m$^2$ respectively. Heat flux decreases with time and becomes zero after completion of the melting process as per the mechanism of heat transfer.

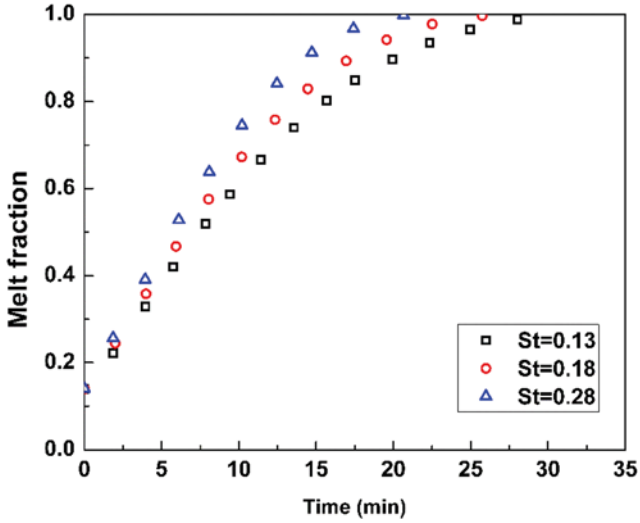


**Fig. 10** Melt fraction (air +liquid PCM) for different Stefan number in copper cavity

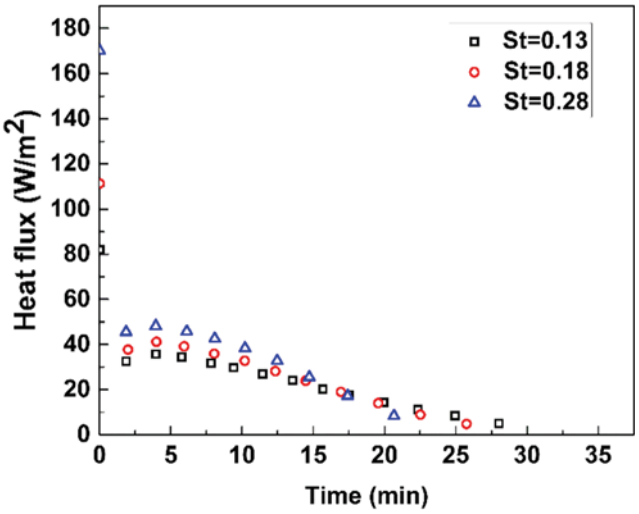


**Fig. 11** Variation of heat flux for different Stefan number in copper cavity

The maximum velocity during the phase change the process is also investigated. In Fig. 12 the maximum velocity magnitude of the mixture (PCM + air) with time is plotted. Due to the presenceofair, the initial maximum velocity inside the cavity is nonzero. Melting process shows at the initiation of the process the velocity increases and attain a maximum temperature and then falls approximately to zero after completion of the process. The maximum velocity increases initially due to the increase in thermal bouncy force and starts falling with a decrease of bouncy force. The maximum velocity is highest in case of highest Stefan number, and the reason behind it is the due to the higher rate of melting the effect of convection heat transfer. After around 10 min, the change in maximum velocity is almost negligible as shown in Fig. 12. The reason for higher heat transfer rate in the copper cavity is due to bouncy effect and low resistance to conduction and convection heat transfer.

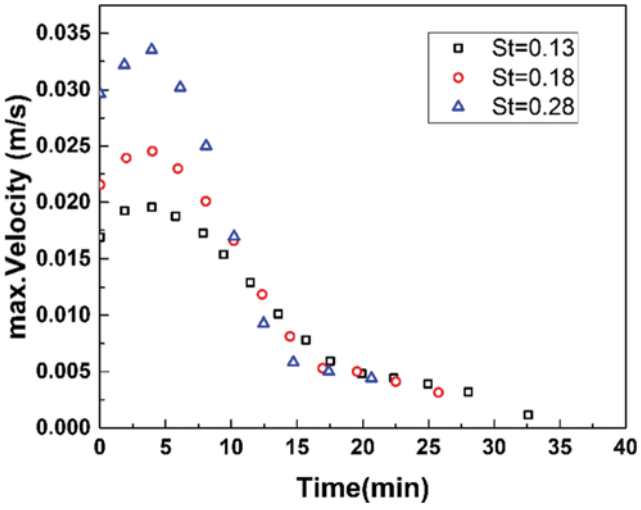


**Fig. 12** Variation of maximum velocity with time in copper cavity

## 4 Conclusion

The numerical study of a phase change process is very important for its visualization especially in unconstrained melting where the dynamic measurement of the parameters is difficult. Digital image analysis technique is the only tool for the validation of the numerical study. For any heat transfer process, the boundary conditions and thermo-physical properties of the cavity and PCM are the most important parameters. In this case of melting in a cavity; the study considered the effect of thermal diffusivity of the cavity material on melting and the effect of cavity wall temperature or Stefan number, on the process. The major findings of this study can be summarized as:

(i) The properties of the cavity materials play a significant role to describe the nature of the phase change process. It affects the shape of the solid phase during the process. In case of lower thermal diffusivity material glass, the heat flux is less than that of copper and aluminium cavity. The higher value of heat flux makes the melting process faster with rapid change in the shape of solid wax during melting.

(ii) The ratio of height and breadth (aspect ratio) of the solid phase is higher in highest thermal diffusivity (Copper) cavity material than glass cavity during a transient simulation of the melting process. The higher aspect ratio makes an unstable shape of the solid which increases the bouncy effect.

(iii) Higher Stefan number in melting shows that the natural convection controls the process, as the velocity reaches the maximum value.

Therefore, the selection of cavity material and boundary conditions of the melting process should be such that it would not affect the stability of the system due to the collapse of unmelted solid phase at the bottom of the cavity. In the case of phase change of energy-storing materials very fast heating or cooling may cause uneven stress distribution but the efficiency of energy storage will increase. On the other hand, during melting of the metal large amount of heat supply is required and cavity material should be chosen such that the thermal diffusivity of metal PCM is less than that of cavity material. The higher thermal diffusivity of cavity material than PCM will increase the life of cavity material. The selection of cavity material is very important when the heat supplied to the PCM by conduction. Hence, these results will help to select the cavity type for various applications. The cavity should be chosen such that it should not be melted or distorted during the process. On the other hand, in case of thermal energy storage, the cavity should be made of a material which can transfer the thermal energy to the PCM very fast. Therefore, the charging of energy storage will be faster in cavity material having higher thermal diffusivity.

## Compliance with ethical standards

**Conflicts of interest** There are no potential conflicts of interest with regard to publication of this paper.

**Human participants and/or animals** Research did not involve Human Participants and/or Animals.

**Consent** Consent to submit has been received explicitly from all co-authors.

**Publisher's Note** Springer Nature remains neutral with regard to jurisdictional claims in published maps and institutional affiliations.

## References


1. Haillot DFE, Gibout S, Bédécarrats J-P (2013) Optimization of solar DHW system including PCM media. Appl Energy 109:470–475
2. Ibáñez MCL, Solé C, Roca J, Nogués M (2006) Modelization of a water tank including a PCM module. Appl Therm Eng 26:1328–1333
3. Zondag HKB, Smeding S, de Boer R, Bakker M (2013) Prototype thermo chemical heat storage with open reactor system. Appl Energy 109:360–365
4. Agyenim FHN, Eames P, Smyth M (2010) A review of materials, heat transfer and phase change problem formulation for latent heat thermal energy storage systems (LHTESS). Renew Sust Energ Rev 14:615–628
5. Ismail JRHq KAR (2000) Solidification of pcm inside a spherical capsule. Energy Conv Manag 41:173–187
6. Assis E, LK GZ, Letan R (2007) Numerical and experimental study of melting in a spherical Shell. Int J Heat Mass Transf 50:1790–1804
7. Tan FL (2008) Constrained and unconstrained melting inside a sphere. Int Commun Heat Mass Trans 35:466–475
8. Tan FL, Hosseinizadeh SF, Khodadadi JM, Fan L (2009) Experimental and computational study of constrained melting of phase change materials (PCM) inside a spherical capsule. Int J Heat Mass Transf 52:3464–3472
9. Hosseinizadeh SF, AARD FLT (2012) Numerical investigations of unconstrained melting of nano-enhanced phase change material (NEPCM) inside a spherical container. Int J Therm Sci 51:77–83
10. Zhao W, AFE AO, Neti S (2013) Heat transfer analysis of encapsulated phase change material for thermal energy storage. Int J Heat Mass Transf 63:323–335
11. Chandrasekaran P, MC VK, Velraj R (2014) Enhanced heat transfer characteristics of water based copper oxide nanofluid PCM in a spherical capsule during solidification for energy efficient cool thermal storage system. Energy 72:636–642
12. Saitoh TS, HK HH (1996) Theoretical analysis for combined closecontact and natural convection melting in ice storage spherical capsule. Proc Energy Conv Eng Conf 3IEEE:2104–2108
13. Saitoh TS, HH KY (1997) Theoretical analysis and experiment on combined close-contact and natural convection melting in thermal energy storage spherical capsule. Proc Energy Conv Eng Conf 3 IEEE:1656–1661
14. Assis E, GZ RL (2009) Numerical and experimental study of solidification in a spherical shell. J Heat Transf 131:1–5
15. Rizan MZM, FLT CPT (2012) An experimental study of n-octadecane melting inside a sphere subjected to constant heat rate at surface. Int Commun Heat Mass Trans 39:1624–1630
16. Hosseinizadeh SF, AARD FLT, Khodadadi JM (2013) Unconstrained melting inside a sphere. Int J Therm Sci 63:55–64
17. Arasu AV, Mujumdar AS (2012) Numerical study on melting of paraffin wax with Al2O3 in a square enclosure. Int Commun Heat Mass Trans 39:8–16
18. Babak Kamkaria HJA (2017) Numerical simulation and experimental verification of constrained melting of phase change material in inclined rectangular enclosures. Int Commun Heat Mass Trans 88:211–219
19. Kund NK, Dutta P (2010) Numerical simulation of solidification of liquid aluminum alloy flowing on cooling slope. Trans Nonferrous Met Soc Chin 20:898–905
20. Zhenyu Liu BS, Yuan J (2012) VOF modelling and analysis of filmwise condensation between vertical parallel plates. Heat Trans Res 43:47–68. https://doi.org/10.1615/HeatTransRes.2012004376
21. Kim S, Kim MC, Lee S-B (2001) Prediction of melting process driven by conduction-convection in a cavity heated from the side. Korean J Chem Eng 18(5):593–598
22. Brent AD, VRV KJR (1988) Enthalpy-porosity technique for modeling convection-diffusion phase change: application to the melting of a pure metal. Num Heat Trans 13:297–318
23. Date AW (2005) Introduction to Computational Fluid dynamics Cambrige University Press